A Novel Approach for the Diagnosis of Human Hepatopancreatobiliary Diseases: *In vivo* Magnetic Resonance Spectroscopy of Bile in One and Two Dimensions

by

Sanaz Mohajeri

A Thesis submitted to the Faculty of Graduate Studies of

The University of Manitoba

in partial fulfillment of the requirements of the degree of

Doctor of Philosophy

Department of Human Anatomy and Cell Science

University of Manitoba

Winnipeg

Sanaz Mohajeri

TABLE OF CONTENTS

List of Abbreviations

1D	One Dimensional
2D	Two Dimensional
ALP	Alkaline Phosphatase
ALT	Alanine Aminotransferase
AMP	Adenosine Monophosphate
AST	Aspartate Aminotransferase
BW	Band width
CA	Cholic Acid
CA125	Carbohydrate Antigen 125
CA19-9	Carbohydrate Antigen 19-9
CBD	Common Bile Duct
CC	Cholangiocarcinoma
CDCA	Chenodeoxycholic Acid
CEA	Carcinoembryonic Antigen
CHESS	Chemical Shift Selective Suppression
Chol-PLs	Choline-containing Phospholipids
CSF	Cerebrospinal fluid
CSI	Chemical Shift Imaging
DIA	Digitized Image Analysis
DOCA	Deoxycholic Acid
DSS	3-(Trimethylsilyl)-1-Propanesulfonic Acid Sodium Salt
ERCP	Endoscopic Retrograde Cholangiopancreatography

FID	Free Induction Decay
FISH	Fluorescent In-situ Hybridization
FOV	Field of View
FWHM	Full Width Half Maximum
FT	Fourier Transformation
GCA	Glycocholic Acid
GCBAs	Glycine-Conjugated Bile Acids
GCDCA	Glycochenodeoxycholic Acid
GDCA	Glycodeoxycholic Acid
Gd	Gadolinium
GGT	Gamma-Glutamyl Transferase
GI	Gastrointestinal
GlcUA	D-Glucuronic acid
GPC	Glycerophosphorylcholine
GPE	Glycerophosphorylethanolamine
HASTE	Half-Fourier Acquisition Single-shot Turbo Spin-echo
HCC	Hepatocellular Carcinoma
HCL	Intra-Hepatocellular Lipid
HPB	Hepatopancreatobiliary
IBD	Inflammatory Bowel Disease
INR	International Normalized Ratio
LCA	Lithocholic Acid
L-COSY	Localized Correlation Spectroscopy

LDH	Lactate Dehydrogenase
MDR3	Multidrug Resistant Protein 3
MRCP	Magnetic Resonance Cholangiopancreatography
MRI	Magnetic Resonance Imaging
MRS	Magnetic Resonance Spectroscopy
Nb	Niobium
NAA	N-Acetyl Aspartate
NAAG	N-Acetyl Aspartyl Glutamate
NMR	Nuclear Magnetic Resonance
NO	Nitric Oxide
NTP	Nucleoside Triphosphates
OLT	Orthotopic Liver Transplantation
PBC	Primary Biliary Cirrhosis
PC	Phosphatidylcholine
PD	Proton Density
PDE	Phosphodiester
PE	Phosphoethanolamine
PFIC	Progressive Familial Intra-hepatic Cholestasis
PhC	Phosphocholine Chloride Calcium Salt Tetrahydrate
Pi	Inorganic Phosphate
PME	Phosphomonoester
PRESS	Point Resolved Spectroscopy
PSC	Primary Sclerosing Cholangitis

PT	Prothrombin Time
PTC	Percutaneous Trans-hepatic Cholangiopancreatography
RBIC	Recurrent Benign Intra-hepatic Cholestasis
RF	Radiofrequency
SD	Standard Deviation
SI	Signal Intensity
STEAM	Stimulated Echo Acquisition Mode
SVS	Single Voxel Spectroscopy
TBAs	Total Bile Acids
TCA	Taurocholic Acid Sodium Salt
TCBAs	Taurine-Conjugated Bile Acids
TCDCA	Taurochenodeoxycholic Acid
TDCA	Taurodeoxycholic Acid
TE	Echo Time
Ti	Titanium
TR	Repetition Time
UDCA	Ursodeoxycholic Acid

Acknowledgments

I'd like to thank my parents for all their support: my mom and my dad who have been with me in all my life. I'd like to thank my husband, Mehdi, who encouraged me to finish this PhD with his love and support.

I'd like to thank my supervisor, Professor Ian CP Smith, for his advice, patience, and help throughout this project. It was a pleasure working for him. I'd like to thank Dr. Tedros Bezabeh, my co-supervisor, for his advice, encouragement, and patience. Thanks to Dr. Omkar Ijare, research associate at National Research Council of Canada for being such a good friend and helping me in each and every step of this research.

Special thanks to my committee members: Dr. Judith Anderson, who helped me a lot during tough times in this PhD, Dr. Thomas Klonisch, who was supportive all the time and finally Dr. Alex MacKey who chose to come to my defense and helped me to learn more about MR physics.

I'd like to thank Dr. Albert Thomas, who advised me in modifying SVS sequence to COSY. Special thanks to our clinical collaborators, Dr. Gerald Minuk, Dr. Jeremy Lipschitz, Dr. Allan Micflikier, and Dr. Iain Krikpatrick for their clinical scientific input.

I'd like to thank Ms. Kim Hawkins, study nurse for screening the subjects and helping me in patient recruitment. I'd like to thank Dr. Scott King and Mike Smith for designing and building the surface coil I used in my experiments. I'd also like to thank all the staff at the National Research Council – Institute for Biodiagnostics, especially Ms. Rena Papadimitropoulos, for helping me in subject recruitment, Dr. Patricia Gervai for teaching me how to operate the 3T MR Scanner, and Mr. Randy Summers for helping me

in the statistical analysis of my data, and everyone at NRC who helped me whenever I needed.

I'd like to thank the Manitoba Health and Research Council (MHRC), and University of Manitoba for their generous support.

Finally, the last but not least thanks goes to my little son, Danial, who fully cooperated during the time I was writing my thesis.

Dedication

With Love to My Mom

List of Tables

List of Figures

ABSTRACT

Bile is a biofluid synthesized by liver and concentrated in the gallbladder. Interference with the bile flow may cause cholestasis. Primary sclerosing cholangitis (PSC) is an inflammatory cholestatic disorder which eventually may result in liver cirrhosis and failure.

The management of PSC is controversial. The only effective treatment for end stage disease is orthotopic liver transplantation (OLT). However, cholangiocarcinoma (CC), which is the major complication of this long-lasting disease, is an absolute contraindication for the surgery. Therefore, early diagnosis of the disease can not only improve the outcome of PSC, but also facilitate the allocation of donated livers to those who can benefit from transplantation. Unfortunately, the diagnosis of CC is challenging. Endoscopic retrograde cholangiopancreatography (ERCP), the gold standard technique, is highly invasive. Non-invasive alternatives such as magnetic resonance cholangiopancreatography (MRCP) have lower accuracy. Therefore, it is essential to develop more accurate and less invasive diagnostic techniques.

Magnetic resonance spectroscopy (MRS) is an evolving technique with potential to detect disease-related metabolic changes. *In vitro* studies have proven the capacity of MRS in the early detection of hepatopancreatobiliary (HPB) disorders based on the metabolic analysis of bile obtained invasively. An *in vivo* alternative has been attempted by others on human bile within the gallbladder. However, due to the poor quality of the acquired spectra, quantification of most major bile metabolites was not possible, except for choline-containing phospholipids (chol-PLs). In the current study, the quality of the *in vivo* 1D spectra has been greatly improved, and we have obtained the first 2D L-COSY

spectra from bile within the gallbladder. Spectral data from healthy controls and PSC patients were compared. Statistically significant differences in the concentrations of chol-PLs, and glycine- and taurine-conjugated bile acids were revealed in the 1D analysis. Our 2D spectra also demonstrated potential for the detection of metabolic differences between the two groups. The success of these studies indicates a strong potential of *in vivo* bile MRS techniques to characterize and diagnose a wide variety of HPB disorders.

CHAPTER 1. INTRODUCTION

1.1 MAGNETIC RESONANCE IMAGING AND SPECTROSCOPY

1.1.1 Magnetic Resonance Imaging (MRI)

Magnetic resonance imaging (MRI) is a relatively modern diagnostic technique which is sensitive to the changes in the amount and characteristics of water in tissues. In our body, 70-90% of different tissues are composed of water. Considering the significant changes in the water content following pathological conditions, a technique which can trace these changes looks very attractive in the eyes of physicians (1).

History

Bloch and at the same time Purcell and Pound described nuclear induction for the first time in 1945. They detected a signal after they applied the radiofrequency energy (RF pulse) with a specific frequency to a sample in a magnetic field. Hahn produced a repeated nuclear magnetic resonance (NMR) signal after a delay by applying a set of RF pulses. This sequence was called spin echo. Finally, NMR became a laboratory spectroscopic technique for determining the structure of complex molecules (1).

In 1959 J. R. Singer at the University of California, Berkeley introduced the first clinical applications of NMR, measuring blood flow. Following the detection of elevated relaxation times in mouse tumor tissue *in vitro* by R. Damadian in 1971, NMR became the foundation of a new imaging modality. Damadian, along with his team, built a super-conducting magnet and acquired the first NMR image from a human body (1).

In 1973 P. Lauterbur suggested application of magnetic field gradients in order to differentiate NMR signals based on the location of their origin tissue. This was the basis of frequency encoding. Selective excitation of image slices was discovered by P.

Mansfield and his team at the University of Nottingham. Finally, R. Ernst and his team in Zurich introduced two dimensional Fourier transform imaging (2D FT). This chain of discoveries introduced a new imaging technology to the world with great contrast sensitivity to differentiate normal tissues from each other and diagnose pathological conditions (1). Unlike X-ray imaging/CT scan, RF waves are non-ionizing and provide a better safety to patients (2).

1.1.2 MRI Hardware

MRI hardware is composed of a magnet, magnetic gradients, an RF system and a computer. Permanent magnets are heavy, and have a very limited application in MRI systems, only up to 0.3 T. Electromagnets are either resistive or superconducting. Resistive magnets are composed of multiple loops of wire with an air core or iron core. They need high power and an advanced water cooling system, and therefore, they are not used in high field systems. Superconducting coils, on the other hand, are the first choice for high field systems. They are composed of loops of wires made of niobium-titanium (Nb-Ti). Liquid helium is used for cooling the magnet. Below 9.5 K, the wires have no resistance to the current (superconducting) and high current flowing in the wires yields a high magnetic field with an acceptable homogeneity. Shimming can increase the homogeneity of the magnetic field. We can shim the magnet passively using metal pieces or actively using shim coils (3). The size of the fringe field is one of the major challenges in using the superconducting magnet. A fringe field may be defined as the magnetic field around the MRI scanner that is not involved in image acquisition. One of the most commonly used solutions is adding another superconducting coil with the opposite magnetic direction to the system outside of the first coil (3). Gradient coils

which are responsible for spatial localization are located in another cylinder inside the cylinder of shim coils (3). The RF system is composed of an RF pulse synthesizer set, transmit amplifiers and receiver amplifiers (3). The computer is composed of an operator's console, a scan computer and an array processor. The operator's console receives information from the user and sends the imaging sequence to the scan computer. The scan computer is responsible for controlling the gradients and the RF system transmits and receives. The array processor is involved in reconstruction of images (3).

1.1.3 The Basic Principles of MRI

Spinning Protons under the Influence of an External Magnetic Field

A moving particle with positive or negative electrical charge creates a magnetic field. The strength of the field depends on the speed and charge distribution of the particle (3). The nucleus of an atom is composed of protons and neutrons. A proton has a very small positive charge; however, because of its fast spin, it can produce a noticeable magnetic field, called a magnetic dipole (2, 3). A neutron doesn't have electrical charge; however because of sub-nuclear charge inhomogeneity, it can produce a magnetic field with lower magnitude and in the opposite direction of the proton magnetic field. The strength and orientation of a magnetic field are represented by a vector called the magnetic moment (2).

If we apply a large external magnetic field (B_0) to the pool of spinning protons, the orientation of the dipoles may change (3). Each proton may assume one of two possible energy states. The protons aligned in the direction of B_0 have a relative low-energy state compared to the protons aligned against the direction of B_0 which have a relative high-energy state (2). However, the net alignment of the protons will be in the direction of

magnetic field and proportional to B_0 (3) (Figure 1.1.3-1). A large pool of spinning protons provided by water and fat in the body helps MRI to provide excellent images using low frequency and energy (3).

Figure 1.1.3-1: Alignment of spins under the influence of the external magnetic field (2). (A), Randomly oriented; (B), Oriented by the field. The number of protons aligned in a parallel direction (low-energy state) to the external magnetic field slightly exceeds the number of protons aligned in the anti-parallel direction (high-energy state).

Bushberg J T, Seibert JA, Leidholdt EM., Boone JM. *The essential physics of medical imaging*. Ed 2, Lippincott, Williams and Wilkins (USA): Philadelphia, PA, 2002, p 377, Fig. 14-3.

The interaction between the external magnetic field and the magnetic field of the proton results in precession of the proton about the axis of B_0 at an angular frequency (Figure 1.1.3-2) represented by the Larmor Equation ($\omega_0 = \gamma B_0$). In this equation ω_0, which represents the Larmor or resonance frequency, is proportional to the strength of the B_0 field. The gyromagnetic ratio or γ is unique for each type of atom (2).

Figure 1.1.3-2: The Interaction between spins and external magnetic field (2).

A, The precessional motion of the proton about the axis of B_0 at an angular frequency represented by the Larmor Equation ($\omega_0 = \gamma B_0$); B, A group of magnetized spins. The net magnetization is represented by the M_0 vector.

Bushberg J T, Seibert JA, Leidholdt EM., Boone JM. *The essential physics of medical imaging*. Ed 2, Lippincott, Williams and Wilkins (USA): Philadelphia, PA, 2002, p 378, Fig. 14-4.

Application of an RF Pulse to the Spins in the B_0 Field

If we apply an RF pulse at the Larmor frequency to the pool of protons in the B_0 field, the energy may be absorbed by spinning protons. The result can be explained both by quantum model and classical model (3).

Based on the quantum model, there is an energy gap between low- and high-energy state spins represented by ΔE. The magnitude of ΔE is proportional to the strength of B_0 field. Following the application of an RF pulse, a number of protons go from a low-energy state to a high-energy state. This number is proportional to the amplitude and duration of the RF pulse (2). According to the classical model, for convenience, we assume the B_0 field is in the direction of the z axis. There are two frames of reference: the laboratory-frame of reference with stationary three dimensional Cartesian coordinates (X-Y-Z) and the rotating-frame of reference (X'-Y'-Z). The magnetization vector (M_0) has two components: longitudinal magnetization or M_z, which is parallel to the external magnetic field, and transverse magnetization which is perpendicular to the B_0 field. When protons absorb the energy of the RF pulse at the Larmor frequency, the magnetization vector deviates from the equilibrium. According to the observer in the laboratory frame, the magnetic moment precesses around Z axis at Larmor frequency. At the same time according to the observer in the rotating frame, the magnetic moment looks stationary (2, 3) (Fig 1.1.3-3). Flip Angle is defined as angular deviation of longitudinal magnetization vector from equilibrium and depends on the duration and amplitude of RF pulse (2, 3)

Figure 1.1.3-3: Application of RF pulse to the spinning protons in the B_0 magnetic field. (2). Left, Laboratory frame; Right, Rotating frame.

Bushberg J T, Seibert JA, Leidholdt EM., Boone JM. *The essential physics of medical imaging*. Ed 2, Lippincott, Williams and Wilkins (USA): Philadelphia, PA, 2002, p 380, Fig. 14-5.

T_2 Relaxation and Signal Decay

Once the RF pulse is terminated, the protons begin to realign with the B_0 field in order to recover the equilibrium. Initially, according to the laboratory- frame observer, the M_{xy} component of the magnetization vector rotates in the transverse plane at the resonance frequency. Therefore, due to the magnetic induction, a receiver coil can detect the signal in this plane. This so called free induction decay (FID) is the NMR signal. However, gradually, the spinning protons dephase and begin to spin at different frequencies. The spin-spin interaction and external magnetic field inhomogeneity are responsible for loss of phase coherence. As a result, the FID decays over time (3, 4).

The spin-spin interaction is related to the proximity of the spins, therefore the dephasing of protons and the signal decay in the solid tissues are much faster than water (2, 4).

The spin-spin interaction which results in dephasing of spins and signal decay is called T_2 relaxation (3). If the flip angle is 90°, the transverse component of magnetization vector can be calculated as follows:

$M_{xy}(t) = M_0 e^{-t/T2}$ (3).

In the real world, the signal decay happens, not only because of the spin-spin interaction, but also due to external magnetic field inhomogeneity. In order to incorporate this factor in the calculation of decaying signal, a new constant, T_2*, is defined (4).

If the flip angle is 90°, $M_{xy}(t) = M_0 e^{-t/T2^*}$ (3).

The T_2 decay constant represents the time period between the maximum amplitude of the transverse signal following excitation and 36.8% of maximum amplitude. This constant is

unique for each tissue (2, 3) (Figure 1.1.3-4, A). T_2* is less than T_2. Therefore in the real world the decay of MR signal is faster compared to the T_2 decay. (4) (Figure 1.1.3-4, B).

Figure 1.1.3-4: The T_2 relaxation curve (2). A, The T_2 constant represents the time when the transverse component of magnetization vector reduces to the ~ 37% of its maximum value; B, In order to consider the effect of magnetic field inhomogeneity in signal decay, T_2* is defined; it always has a lower value compared to T_2.

Bushberg J T, Seibert JA, Leidholdt EM., Boone JM. *The essential physics of medical imaging*. Ed 2, Lippincott, Williams and Wilkins (USA): Philadelphia, PA, 2002, p 386, Fig. 14-12.

T_1 Recovery

Following the termination of the RF pulse, the spins gradually realign with the external magnetic field. Based on the quantum model, this means that from the high-energy state, they go back to the low-energy state. According to the classical model, the energy is released as a result of the exponential recovery of M_z component of magnetization vector back to M_0. Part of this energy is released as thermal energy to the surrounding environment or Lattice. This process is called longitudinal or spin-lattice relaxation (3, 4). The recovery of the longitudinal component is presented by an exponential model.

If the flip angle is 90°, the formula may be simplified as follows:

$M_z(t) = M_0(1- e^{-t/T1})$ (3).

This model is represented by a curve called the T_1 recovery curve (Figure1.1.3-5). T_1,

which is unique to each tissue, describes the time during which 63.2% of longitudinal magnetization is recovered (3-5).

Figure1.1.3-5: T_1 recovery curve. Left, T_1 recovery curve (4); Right, comparison between T_1 recovery curve of fat and water (5).

Left: Hashemi RH, William G, Brandly JR, Lisanti CJ. *MRI: The Basics*, Ed 2, Lippincott, Williams and Wilkins (USA): Philadelphia, PA, 2004, Fig 4-3.

Right: Qayyum A. MR Spectroscopy of the Liver: Principles and Clinical Applications. *Radiographics*, 2009: 29(6): p 1656, Fig 3.

Free Induction Decay (FID)

In a perfect world, the loss of the RF energy to lattice in the absence of gradients produces an NMR signal called a free induction decay. The signal decay is just due to T_1 and T_2 relaxation. However in the real world, the signal loss is faster than the T_2 decay due to inhomogeneity in the main magnetic field, magnetic susceptibility specifically at the air-tissue interfaces, and metal pieces in patient's body (3).

Echo Formation

Using a special pulse sequence to refocus magnetization in the x-y plane, an echo signal will be generated. The time period between the application of the first RF pulse and echo generation is called echo time (TE). Half of this time (TE/2) is used for dephasing of spins and the other half for rephasing (3). There are two types of echoes: spin echoes and gradient echoes. Let's consider spin echoes as an example. After applying a 90 ° RF pulse, the spins dephase and M_0 flips down towards Y axis. After a TE/2 time delay, if we

apply a 180 ° re-focusing RF pulse, the dephased spins rotate 180 ° about the X axis. All the spins rephase after another TE/2 time delay. As a result, a large signal called a spin echo is produced at time TE (2, 3).

1.1.4 Spatial Localization

For spatial localization, we need to make a transient linear change in the strength of the magnetic field from the centre of the magnet to the periphery. This linear change is called a gradient. Simply, in order to gather spatial information, we need gradient coils and gradient pulses applied in orthogonal dimensions (G_x, G_y, G_z). These gradients may be classified based on their functions: the G_z is called the slice-select gradient, the G_x is named the readout or frequency-encoding gradient and the G_y is called the phase-encoding gradient (3, 4).

1.1.5 Slice Selection

As it was explained before, based on the Larmor Equation ($\omega_0 = \gamma B_0$), the resonance frequency varies according to the strength of the magnetic field. Therefore, if we make a transient linear change in the strength of the magnetic field from head to feet, each slice of the body will have its own resonant frequency. In order to excite a specific slice, we need to apply an RF pulse at the resonance frequency of protons at that slice. However, using just one frequency can excite a slice which is infinitely thin. In order to excite a slice with meaningful thickness, we need to apply an RF pulse with a range of frequencies called the band width (BW) (4).

In order to select thinner slices we should either decrease the frequency band width of the RF pulse or increase the slope of the z gradient (slice-select gradient). To increase the

gradient slope, we should increase gradient strength by applying more power. We should apply longer RF pulses to decrease the frequency band width of the RF pulse (3, 4).

We can calculate the frequency band width of RF pulse using slice profile. We can create slice profile in the frequency domain by applying Fourier transform (FT) to the RF pulse in the time domain. The band width can be determined by measuring the full width of the slice profile at half maximum amplitude (FWHM) (3, 4). FT is a mathematical process which can transform the signal from time domain to the frequency domain (3) (Figure 1.1.5-1).

Figure 1.1.5-1: Transforming the RF pulse from time domain to the frequency domain using Fourier transform (4).

Hashemi RH, William G, Brandly JR, Lisanti CJ. *MRI: The Basics*, Ed 2, Lippincott, Williams and Wilkins (USA): Philadelphia, PA, 2004, Fig 10-4.

1.1.6 Frequency Encoding

Slice selection cannot localize each pixel or precisely each voxel (volume element) in the slice. The three dimensional spatial localization needs frequency encoding and phase encoding following slice selection (4).

In order to acquire spatial information from a selected slice along the X axis, we can apply a gradient along this axis. This frequency-encoding gradient should be applied while receiving the echo. Therefore, sometimes it is called readout gradient (4).

Field of View (FOV)

Field of view is determined by gradient strength and receiver band width. In order to achieve a better resolution we may use smaller field of view. This needs a higher gradient

power or a smaller sample band width. Decreasing the band width will increase sampling time and therefore TE and T_2 decay (3).

1.1.7 Phase Encoding

2D FT makes it possible to gather spatial information along the Y axis by applying a phase-encoding gradient along this axis. This gradient is usually applied after the first RF pulse and before the readout gradient (4).

1.1.8 Tissue Contrast and Imaging Parameters

Different tissues have different T_1, T_2, and T_2* values based on their solid properties. This can make the basis for image contrast, even if these values are affected by magnetic field strength (T_1), or imperfection of magnetic field (T_2*) (4). Therefore, by changing parameters of MR sequence we can produce T_1 weighted, T_2 or T_2* weighted, and proton density (PD) images in order to increase the chance of visualization of specific pathology (6). The MR pulse sequence is a set of RF and gradient pulses applied during MRI and spectroscopic studies followed by collecting of information. Among MR sequence parameters, in addition to flip angle, changing the repetition time (TR), and TE , helps us to make the best use of T_1 and T_2 differences between the tissues in order to achieve maximum possible image contrast (3, 4).

As mentioned earlier, TE is the time period between the application of the first RF pulse and echo generation. The repetition time (TR) is the time from the beginning of one pulse sequence until the beginning of the next pulse sequence. The signal intensity (SI) we may receive from each tissue is dependent on the number of mobile protons in that tissue ($M_0 \alpha N(^1H)$), and T_1 and T_2 or T_2* values of the tissue. Based on T_1 recovery formula, if the flip angle is 90°, and t is equal to TR, $M_z(TR) = M_0(1- e^{-TR/T1})$. Based on T_2 decay

formula, If the flip angle is 90°, and t is equal to TE, $M_{xy}(TE) = M_0 e^{-TE/T2.}$ Therefore, we can conclude that: $SI = N (^1H) (1- e^{- TR/T1}) (e^{- TE/T2})$ (4).

If TR goes towards infinity, $1- e^{-- TR/T1}$ will approach 1. Therefore we will have minimum T_1 effect. In practice, if we choose TR between 2000 to 3000 msec or simply TR >= 4-5* T_1 in the field of view, we may eliminate the T_1 effect (4).

If TR is less than T_1 in a tissue, this means the next RF pulse is going to be applied before the full longitudinal magnetization recovery in that tissue. Therefore, a tissue with faster T_1 recovery may generate a larger signal. This can provide an opportunity to differentiate tissues based on T_1 values. In practice, by choosing a TR less than average T_1, we can generate T_1 weighted images. We can eliminate the effect of flip angle by choosing a 90° flip angle, and the effect of T_2 decay by choosing a very short TE (3, 4).

Based on the above formula, the maximum signal is proportional to the number of protons in each voxel. When TE is very short, e^{-TE/T_2} goes towards 1. Therefore, we can minimize the T_2 effect. Theoretically, if TR is infinite or very large, flip angle is 90° and TE is 0, we can create proton density (PD) images. However in the reality, TE cannot be 0. Therefore, we usually have a combination of proton density and T_2 weighted images (3, 4). In practice, in order to create proton density images, we have to choose TRs 5 times longer than T_1 and TEs shorter than 20 msec. In order to create T_2 weighted images, we have to select a long TE, a low flip angle, and a long TR. We can create T_2* weighted images using gradient echo (GRE) sequences, because unlike spin echo sequences, they do not have 180 ° RF pulse to compensate the effect of field inhomogeneity. Usually T_2* decay is not desirable. However, it can be used for detecting the inhomogeneities following bleeding (3).

Figure 1.1.8-1: Comparison between T_1 weighted, T_2 weighted, and proton density (PD) images (6). Left, T_1 weighted image with brighter grey matter and darker cerebrospinal fluid (CSF); Middle, T_2 weighted image with darker grey matter and brighter CSF; Right, PD image with little contrast between gray matter and CSF.

Adapted with permission by Kieran Maher using Graphic Converter from Applied Imaging Technology by Heggie, Liddell & Maher (2000) http://en.wikibooks.org/wiki/File:T1t2PD.jpg

1.1.9 MRI Pulse Sequences

Gradient echo sequences and spin echo sequences are two basic types of MR sequences. A gradient echo sequence is composed of RF pulse(s), slice-select gradient (logical Z channel), phase-encoding gradient (logical Y channel), and frequency-encoding or readout gradient (logical X channel). The spin echo sequences are useful to overcome the T_2* decay problem. They are composed of a 90 ° excitation RF pulse followed by one or two 180 ° refocusing RF pulses. The gradient pulses are arranged accordingly (3).

1.1.10 Contrast Agents

Sometimes the differences between tissues (normal vs abnormal) in proton density and T_1 and T_2 weighted images do not provide enough contrast to diagnose the pathology. The use of contrast agents may help enhance the differences. Gadolinium (Gd), the most common MRI contrast agent, has 7 unpaired electrons. Considering that the magnetic moment of each unpaired electron is 657 times larger than a proton, Gd can provide a huge difference in relaxation times. It is mainly accumulated in extracellular space and vascular beds (3).

1.1.11 K-Space and Fourier Transform (FT)

For each image point, in K-space a complex number is assigned which stores the amplitude and phase information. In order to convert K-space data to an image or spectrum, we should apply a 2D FT. FT can covert time domain data to frequency domain data. The spins precessing faster than the reference frequency will be assigned a positive value in the frequency domain and the ones precessing slower will have a negative value. Considering that the NMR signal is a rotating vector in XY plane, it needs two determinant values: strength or amplitude and a phase (positive versus negative). The FT provides the amplitude and phase of signal at each frequency as a complex number (3).

1.1.12 Basics of NMR Spectroscopy

In order to produce images using MRI, we should acquire enough signal from very small voxels ($1mm^3$) which demands high concentration of the nuclei of interest (for example hydrogen in water and fat). On the other hand, spectroscopy may obtain information from larger voxels. Therefore metabolites with lower concentrations can be detected and in addition to ^{1}H, other less sensitive nuclei such as ^{31}P and ^{13}C may be considered as source of information. As a result, NMR spectroscopy is valuable for the study of metabolites. However, it provides lower sensitivity especially *in vivo* (7).

When a magnetic nucleus is positioned in a magnetic field, it can take one of the few possible orientations (two for hydrogen) with different energy levels. The differences between energy levels (ΔE) may be determined by the size of nuclear magnetic moment and the strength of magnetic field. If we apply an RF pulse at the resonance frequency of the nucleus, the energy level may change ($\Delta E = h\nu$, h is Plank's constant, ν is the

frequency of the pulse). For the each field strength, the resonance frequency depends on the type of nucleus and its specific magnetic moment as well as the atoms surrounding the nucleus in the molecule (chemical shift) (8).

The angular momentum of magnetic nuclei resulting from their spin may be calculated as follows:

$\boldsymbol{I} = [I\,(I+1)]^{1/2}\,\hbar$ where I is the symbol for spin quantum number of nucleus (I = 0, 1/2., 1, 3/2, 2 …) and $\hbar = h/2\pi$. The spin quantum number of a given nucleus depends on the number of unpaired protons and neutrons. When the number of both protons and neutrons are even, I = 0. If both of them are odd, I = 1, 2, 3… If one of them is even and the other one is odd, I = 1/2, 3/2., 5/2…(8).

The magnetic moment of a nucleus is determined by the spin angular momentum ($\mu = \gamma \boldsymbol{I}$) where γ, gyromagnetic ratio, is the characteristic of that nuclei. A given element can have different spins depending on the proton/neutron ratio, e.g. ^{14}N (I =1) and ^{15}N (I = 1/2) (8).

The energy of magnetic moment μ in the magnetic field B is calculated as follows:

$E = -\mu B$. Using the z component of μ we can recalculate the formula: $E = -\mu_z B$.

Considering $\mu = \gamma \boldsymbol{I}$, then $\mu_z = \gamma \boldsymbol{I}_z$.. Moreover $\boldsymbol{I}_z = m\,\hbar$ where m is the magnetic quantum number and can take $2I$ +1 values in integral steps between $+I$ and $-I$. Therefore $E = -m\,\hbar\gamma B$. This means that the $2I$+1 energy levels of spin I nucleus are separated with equal gaps of $\hbar\gamma B$. We can summarize the result as $\Delta E = h\nu = \hbar\gamma B$ and $\hbar = h/2\pi$. Therefore, the resonance frequency can be calculated easily ($\nu = \gamma B/2\pi$) (8).

According to the above formula, the resonance frequency of hydrogen nuclei in a magnetic field of 9.4 T is 400 MHz. Considering that hydrogen is the most abundant nucleus in nature, and the most common nucleus in NMR spectroscopy, the strength of

NMR instruments is usually described by their hydrogen frequency instead of the magnetic field strength (8).

1.1.13 Chemical Shifts

MRI makes use of chemical shifts in a couple of applications such as fat suppression. On the other hand, NMR spectroscopy is able to use chemical shifts as powerful criteria to differentiate each atom in a molecule based on its environment (7). According to the frequency formula ($\nu = \gamma B/2\pi$), the resonance frequency of each nucleus depends on the gyromagnetic ratio of the nucleus and the strength of magnetic field. However, the position of the atom in the molecule can affect the resonance frequency in some degree. This phenomenon, called chemical shift, is due to the effect of local electron distribution on the nucleus. For example, the resonance frequency of ^{1}H and ^{13}C in 9.4 T machine are 400 and 100.6 MHZ respectively, but this frequency may shift a little bit based on the position of the nucleus in the molecule or local electron distribution (8). As an example, let's consider ethanol (Fig1.1.13-1). Ethanol (CH_3CH_2OH) has three types of hydrogen atoms based on their position in the molecule. Using chemical shift information, we can differentiate these three types of hydrogen easily (7).

Figure 1.1.13-1: NMR spectrum of ethanol (7).

NMR spectrum of ethanol: Upper spectrum resembles the signal acquired by Amold et al. in 1951 at 0.7 T machine. Lower spectrum is obtained at 1.5 T. We can differentiate three types of hydrogen: $-CH_3$ (1.22 ppm), $-CH_2-$ (3.7 ppm), and -OH (5.5 ppm) (7).

Boesch C. Molecular aspects of magnetic resonance imaging and spectroscopy. *Mol Aspects Med.* 1999; 20(4-5):p 193, Fig 3.

Chemical shift is the result of so called nuclear shielding. The magnetic field felt by a nucleus in the atom (B) is less than the external magnetic field (B_0). B_0 can induce motion in the circulating electrons which produces a small opposing magnetic field called B'. Therefore, the field experienced by a nucleus in the atom can be calculated as follow: $B = B_0 - B' = B_0 (1- \sigma)$. The proportionality constant σ is called shielding constant. Usually, it is easier to calculate σ based on the resonance frequency as follows:

$\sigma = 10^6 (\nu - \nu_{ref}) / \nu_{ref}$, ν is the resonance frequency of nucleus of interest, and ν_{ref} is the resonance frequency of a reference nucleus. The proportionality constant σ is independent of applied magnetic field. Because of the use of scaling constant 10^6, σ is presented in ppm or parts per million (8). In the molecule the interactions are more complex. B' can be either in the same direction or in the opposite direction of B_0 (8).

In the spectrum plot, usually the σ values increase from right to left. Therefore, the nucleus with maximum shielding is presented at the right end and the nucleus with minimum shielding in the left end (8).

1.1.14 Spin-Spin Coupling

In addition to chemical shifts, spectra can provide us information regarding spin-spin coupling. This chemical phenomenon manifests as split spectral lines. For example, in the ethanol spectrum, $-CH_3$ is presented as a triplet (3 lines with 1:2:1 magnitude ratio separated with equal spaces), and $-CH_2-$ as a quartet (4 lines with 1:3:3:1 magnitude ratio separated with equal spaces) (8, 9).

Spin-spin coupling is due to the effect of spin orientations of nuclei in the neighboring groups on the magnetic fields of nuclei in the group of interest. Simply, in the above

example, the three hydrogen atoms of methyl group may have four different spin orientations with four different energy levels. Each spin orientation may affect the external magnetic field experienced by hydrogen atoms in the methylene group by either strengthening or opposing it. Following the interaction with these four magnetic fields, the resonance frequency of methylene hydrogen atoms split into four resonance frequencies. The area of each peak is proportional to the number of possible spin arrangements for each interacting energy level (1:3:3:1 for methylene group in this example). Similarly, the two protons of methylene group may have three different orientations. Following the interaction with these three energy levels, the resonance frequency of methyl protons split into three resonance frequencies with relative peak area of 1:2:1 (9).

1.1.15 Volume Localization and *In vivo* Spectroscopy

Magnetic resonance spectroscopy provides chemical information about the structure of molecules and is useful for the detection of small amounts of metabolites. Spectra can provide useful information regarding chemical shifts (based on position of peaks compared to a reference peak), spin- spin coupling (according to the number of lines in each peak) and the relative concentration of metabolites (based on the relative area under each peak) (1, 8, and 9).

Spectra can be acquired both *in vitro* from fluid or tissue samples and *in vivo*. *In vivo* spectroscopy combines spectroscopy and MRI. It presents spectroscopic chemical shift information along with MRI spatial information (1, 7).

Volume localization is a key factor for *in vivo* spectroscopy. In the absence of volume localization, we may acquire signal from the whole body. The use of transmit / receive

surface coils can restrict the signal acquisition to a particular sensitive volume. However, the sensitive volume may not represent the anatomical structure of interest (7).

A more modern solution for this problem is the application of gradients similar to those used in the imaging sequences. Gradients are incorporated in the structure of two major *in vivo* MRS pulse sequences: single voxel localized spectroscopic (SVS) sequences and multi voxel chemical shift imaging (CSI) sequences. Single voxel techniques apply slice-select gradients in order to select a single voxel. CSI techniques, on the other hand, apply both slice-select and phase-encoding gradients. However, considering the interference of readout gradients with chemical shift information, they cannot be applied during data collection. Instead, Information regarding the third spatial dimension is collected by application of two or three phase-encoding gradients in different spatial dimensions (7).

1.1.16 Single Voxel Localization Techniques

Two popular spectroscopic single voxel localization techniques are stimulated echo acquisition mode (STEAM) and point resolved spectroscopy (PRESS) (Figure 1.1.16-1). The STEAM pulse sequence is composed of three 90° RF pulses along with one orthogonal gradient for each RF pulse. This pulse sequence generates echoes. Among them, stimulated echo provides the spectroscopy signal (1). After the first RF pulse, the dephased protons are turned by the second RF pulse. The first spin echo is generated by refocusing of transverse components. The third RF pulse can turn longitudinal components to the transverse plane. Stimulated echo is produced by refocusing these components. Therefore, the amplitude of stimulated echo depends on T_2 relaxation between the first and second pulse, and T_1 relaxation between second and third pulse. The time between first and second pulse and the time between the last pulse and stimulated

echo are equal to TE/2. The time between second and third RF pulse is called mixing time (1). STEAM is the preferred spectroscopic sequence for detection of metabolites with short T_2 relaxation times and homo-nuclear coupled groups because it makes possible the use of very short TEs (<20 msec). It also offers a better water suppression. However, compared to PRESS, it produces less signal intensity (9).

PRESS pulse sequence is composed of a 90° excitation RF pulse followed by two 180° refocusing RF pulses. The time between the excitation pulse and the first refocusing pulse as well as the time between the last refocusing pulse and signal acquisition are equal to TE/4. The time between two refocusing pulses is equal to TE/2. An orthogonal slice-select gradient is considered for each RF pulse in order to provide spatial information. According to the design, this pulse sequence can generate a spin echo and refocus it again by third RF pulse (1, 9).

PRESS sequence can offer a better signal intensity and signal-to-noise-ratio (SNR) compared to STEAM. However it cannot acquire data using short TEs. Originally, the minimum possible TE was 144 msec, because short TE can result in considerable signal loss due to short relaxation times. However, newer versions of the PRESS sequence can use echo times as short as 30 msec (1, 9).

Figure 1.1.16-1: Comparison between STEAM and PRESS single voxel spectroscopic pulse sequences (1). RF line represents the applied RF pulses; $G_{z,}$ $G_{y,}$ and G_x represent three orthogonal gradients. Top: The STEAM pulse sequence is composed of three selective 90° RF pulses along with one slice-select orthogonal gradient for each RF pulse.

Bottom: The PRESS pulse sequence is composed of a 90° excitation RF pulse followed by two 180° refocusing RF pulses. The spatial information is provided using an orthogonal slice-select gradient for each RF pulse.

McRobbie DW, Moore EA, Graves MJ, Prince MR. *MRI from picture to proton.* Ed 2, Cambridge University Press (UK): Cambridge, 2006, p 311, Fig 15-4.

McRobbie DW, Moore EA, Graves MJ, Prince MR. *MRI from picture to proton.* Ed 2, Cambridge University Press (UK): Cambridge, 2006, p 314, Fig 15-6.

1.1.17 Two Dimensional Magnetic Resonance Spectroscopy

Two dimensional magnetic resonance spectroscopy (2D MRS) is a technique which can extend one dimensional spectral data into two different frequency dimensions. As a result, the overlapping peaks may appear separately and further conformational information may be collected (10).

The 2D pulse sequence is composed of a preparation time with one or more excitation RF pulses, followed by a t_1 evolution time or t_1 delay, then a mixing time which includes one or more RF pulses and finally a t_2 detection time followed by FID acquisition (10, 11).

Therefore, the simplest 2D pulse sequence is composed of two 90° RF pulses separated by a t_1 delay time. The FID is collected after time t_2 which is a function of t_1 (Figure 1.1.17-1). Repeated acquisitions with incremented t_1 values can provide us a spectrum of resonances according to t_1 evolution time (8, 10).

Figure 1.1.17-1: A simple 2D pulse sequence (10). The 2D pulse sequence is composed of a preparation time with one or more excitation RF pulses ($90°_x$), followed by a t_1 evolution time or t_1 delay, then a mixing time (Δ) which includes one or more RF pulses ($90°_x$, $90°_{-x}$) and finally a t_2 detection time followed by FID acquisition.

Bax A, Lerner L. Two-Dimensional Nuclear Magnetic Resonance Spectroscopy. *Science*. 1986: 23; 232(4753): p 962, Fig2.

The 2D MRS is usually presented as a frequency (F_1) vs. frequency (F_2) contour plot similar to a topographical map. In the 2D spectrum, the structure of molecule is presented by two types of multiplets: diagonal-peak multiplets which have the same F_1 and F_2 frequency on the coordinates and cross-peak multiplets which have different F_1 and F_2 coordinates (11). F_1 and F_2 values indicate the chemical shift of the interacting nuclei. There are different types of 2D spectra. Nuclear overhauser effect spectroscopy (NOSEY) and correlated spectroscopy (COSY) are commonly used in spectroscopy (8).

Figure 1.1.17-2: The schematic 2D COSY spectrum of a hypothetical molecule with two coupled protons (A at chemical shift of δ_A, and X at chemical shift of δ_X) (11).

Keeler J. Basic concepts for two-dimensional NMR. http://www-keeler.ch.cam.ac.uk/lectures/2d_a4.pdf, p 3-1

1.1.18 Summary

In 1D spectroscopy, among different spectroscopic parameters, TR, and TE are the ones which should be adjusted routinely in the clinic. By increasing TR we can eliminate T_1 effect. Usually in TR>10 seconds the spectrum is fully relaxed. Therefore, we can have maximum signal recovery. However, this can increase the scanning time. Decreasing TE can decrease T_2 signal loss. Therefore, especially lipid peaks can appear in the spectrum. Unfortunately, based on the current technology, in PRESS sequence, in most platforms we cannot have TE< 30 msec. Usually TE< 15-20 msec is desirable to detect the majority of lipid signals (1, 9).

2D spectroscopy is useful to detect the overlapping signals which cannot be resolved in 1D spectroscopy (10). Moreover, it has potential to diagnosis the pathologies based on presence or absence of a signal, in some cases. As a result, by improving the quality, and decreasing, the scanning time, it may become a useful technique in the clinic in the future.

1.2 HEPATOPANCREATOBILIARY DISORDERS & NMR SPECTROSCOPY

1.2.1 Hepatopancreatobiliary System

The hepatopancreatobiliary (HPB) system is composed of liver, pancreas, gallbladder, and biliary and pancreatic ducts. The liver is a large solid intraperitoneal organ positioned in the right upper quadrant. It is attached to the diaphragm, peritoneum, great vessels, and upper gastrointestinal organs by a number of ligaments. The dual blood supply is composed of 20% oxygen-rich blood provided by the hepatic artery and 80% oxygen-poor, nutrient-rich blood provided by the portal vein. The portal vein carries blood from gastrointestinal (GI) organs to the liver. Therefore the liver can filter the nutrient-rich blood coming from the GI system. (12-17). The liver performs a variety of metabolic, excretory and secretory functions which can be classified in a few major categories: synthesis of serum proteins including albumin and coagulation factors, synthesis and secretion of bile, metabolism of nutrients such as glucose, solubilization, transport and storage and finally conjugation, detoxification and excretion of lipid-soluble waste products and toxic chemicals in the bile or urine, such as bilirubin and drugs (13, 17).

Lobules, the structural units of the liver, are hexagonal organizations of hepatocytes extended from portal areas in the periphery to the central vein in the centre (13, 17).

Bile is produced by hepatocytes in the hepatic lobules and stored in the gallbladder. The gallbladder is a pear shaped organ located in the visceral surface of the liver. The biliary tree begins from small canaliculi and continues as small bile ductules, interlobular bile ducts, and septal bile ducts to the right and left hepatic ducts and finally the common hepatic duct. After receiving the cystic duct from the gallbladder, the common hepatic duct continues as common bile duct (CBD). The CBD and pancreatic duct join together

and enter the second part of the duodenum via the ampulla of Vater. The sphincter of Oddi regulates the delivery of bile and pancreatic juice to the duodenum (12, 13, 17).

The electrolyte composition of hepatic bile is very similar to that of plasma (3–4 g/dL). The major organic components of bile which are transported to the canaliculi by active secretion include bile acids (80%), conjugated bilirubin, choline-containing phospholipids (chol-PLs), and unesterified cholesterol. In the normal canalicular bile, the ratio of bile acids:phosphatidylcholine:cholesterol is 10:3:1 which is suitable for formation of mixed micelles of phosphatidylcholine (PC) with the bile acids and cholesterol. Any changes in this ratio may initiate the precipitation of cholesterol and formation of gallstones (13, 17).

While the bile passes through the biliary tree, its composition changes. Cholangiocytes actively transport glucose and amino acids back to the circulation in order to inhibit bacterial overgrowth in the gallbladder. The apical membrane of the cholangiocytes contains an enzyme called gamma-glutamyl transpeptidase (GGT) which can hydrolyze glutathione to amino acids in order to facilitate the transport of amino acids (13). In the gallbladder, the majority of inorganic anions, chloride and bicarbonate, get reabsorbed through the epithelium; however, the higher rate of water reabsorption increases the bile solute concentration to 10–15 g/dL (17).

Bile acids are the major component of the bile. They play a significant role in biliary excretion of cholesterol, digestion of lipids, absorption of lipids from the intestine including lipid-soluble vitamins, maintaining normal bile flow, and helping water and salt transport in the colon. Cholic acid and chenodeoxycholic acid (CDCA) are the primary bile acids synthesized from cholesterol in the liver. Following conjugation with glycine

or taurine (the ratio of glycine conjugated bile acids (GCBAs): taurine conjugated bile acids (TCBAs) is 3:1), these bile acids are secreted into the bile. Secondary bile acids, such as deoxycholate and lithocholate and ursodeoxycholic acid (UDCA) are produced by the metabolic reaction of bacteria in the colon from primary bile acids (17).

The pancreas is a retroperitoneal gland composed of both exocrine and endocrine parts. The exocrine pancreas produces the most powerful digestive enzymes for the digestion of carbohydrates, proteins and lipids. The enzymes are finally secreted through the main pancreatic duct or accessory pancreatic duct. The main pancreatic duct joins the CBD and delivers the enzymes to the duodenum at the ampulla of Vater and accessory pancreatic duct enters to the duodenum proximal to the entrance of common bile duct. The endocrine pancreas is composed of islets of Langerhans which secrete hormones responsible for regulation of metabolism such as insulin and glucagon (12).

1.2.2 Pathophysiology of Hepatopancreatobiliary Disorders

Based on pathophysiology, we can consider three major categories of liver disorders: hepatocellular (due to injury, inflammation, and necrosis of hepatocytes), cholestatic (due to obstruction in the flow of bile), and mixed. In addition, liver disease could be acute or chronic (grading) as well as mild, moderate or severe (staging) (15-17). The clinical outcome is either due to hepatocyte dysfunction or portal hypertension (16).

Biliary tract disorders can be classified to congenital atresia or hypoplasia of extra-hepatic or large intra-hepatic bile ducts, choledochal cysts, choledocholithiasis, and biliary strictures which could be benign or malignant lesions. These primary lesions may be complicated by cholangitis, strictures, biliary obstruction, pancreatitis and secondary

biliary cirrhosis (17, 18). In addition to benign pathologies such as gallstones and cholecystitis, malignant lesions may occur in the gallbladder (16, 17, 18).

Inflammation of the pancreas (acute or chronic pancreatitis) and obstructive disorders such as stones and cystic fibrosis along with neoplastic lesions such as adenocarcinoma, and neuroendocrine tumors are the major pathologies of pancreas. Pancreatitis usually develops secondary to biliary tract obstruction and heavy alcohol abuse; however, it can happen following administration of some drugs, trauma, and viral infections or as part of general metabolic and connective tissue disorders (16, 17, 18).

1.2.3 Approach to the Patients with Hepatopancreatobiliary Disorders

Liver diseases are usually diagnosed based on history, physical examination and laboratory blood tests. Considering the role of the liver in conjugation and excretion of bilirubin as well as its involvement in the synthesis of plasma proteins such as albumin and coagulation factors, measuring the levels of bilirubin, and albumin along with prothrombin time (PT) are the best preliminary tests to evaluate the function of liver (17). Elevated liver enzymes or aminotransferases demonstrates hepatocyte injury. Following cell membrane damage and increased permeability, aspartate aminotransferase (AST) and alanine aminotransferase (ALT) are released from hepatocytes into the serum in higher concentrations. ALT is mainly found in hepatocytes; therefore it is more accurate in detection of liver injury. Radiologic evaluation and biopsy may be considered later (17).

Ultrasonography is the major diagnostic tool for detection of gallbladder disorders. Plain radiographs can detect the calcified gallstones and isotope scans have some limited use in the detection of the etiology of cholecystitis (17). Endoscopic retrograde

cholangiopancreatography (ERCP) and magnetic resonance cholangiopancreatography (MRCP) are the common diagnostic tools for the evaluation of the biliary tree (17, 18).

Pancreatic disorders are very difficult to diagnose in early stages due to nonspecific symptoms such as epigastric pain referring into the back and inaccessibility of the gland for physical examination. The only way is relying on laboratory blood tests specifically amylase and lipase which are usually diagnostic only in the acute cases. Ultrasonography cannot reveal most pancreatic pathologies. CT scan and MRCP are the radiographic evaluations of choice for pancreatic lesions (17, 18).

1.2.4 Cholestatic Hepatobiliary Disorders

Cholestasis results from insufficiency in the bile delivered to the duodenum. Any deficiency in the bile flow from canalicular membrane of hepatocytes to the common bile duct and sphincter of Oddi may cause cholestasis (19). Cholestasis is diagnosed by medical history (presence of fatigue, pruritus, and jaundice), physical examination and especially the cholestatic pattern in laboratory biochemical tests. The cholestatic pattern is presented by elevation in the activity of alkaline phosphatase (ALP) (more than four times), 5'-nucleotidase, and GGT. Considering that ALP and 5'-nucleotidase are located in the canalicular membrane of hepatocytes, their increase is more important in the diagnosis of cholestasis compared to GGT which is found in the endoplasmic reticulum of bile duct epithelial cells. Ultrasonography is the diagnostic test for further evaluation of the etiology of cholestasis. It can reveal dilation of the biliary tree or obstruction due to gallstones as well as cystic and solid masses of liver (17).

There are three major categories of cholestatic hepatobiliary disorders:

In the first group are the pathologies which affect the small intra-hepatic bile ducts at the level of interlobular and septal bile ducts. The most prevalent example of this group is primary biliary cirrhosis (PBC), a chronic cholestatic disorder of autoimmune nature which can result in extensive fibrosis, biliary cirrhosis, and possibly liver failure.

The second group includes the diffuse strictures of larger intra-hepatic and/or extra-hepatic bile ducts. The best-known disease in this group is primary sclerosing cholangitis (PSC). PSC is due to diffuse inflammation of the larger bile ducts with autoimmune etiology which can progress into fibrosis and biliary strictures.

The last group of pathologies is due to rare genetic defects of transporter genes at the level of canalicular membrane or cytosol of hepatocytes. These deficiencies may cause intra-hepatic cholestasis with intact biliary tree. The well-known diseases of this group are progressive familial intra-hepatic cholestasis (PFIC) due to deficiency in synthesis of one of the biliary lipids or bile salts, and recurrent benign intra-hepatic cholestasis (RBIC) due to abnormalities of chromosome 18 (19).

Benign and Malignant Biliary Strictures may Cause Cholestasis

Biliary strictures, either benign or malignant, should be considered in the evaluation of cholestatic patients. Considering the difficulty in distinguishing and big differences in the approach to these strictures, differentiating benign strictures from malignant ones has a great importance (20, 21). In 95% of cases, benign biliary strictures are caused by surgical anastomosis or injury during cholecystectomy and orthotopic liver transplantation (OLT) (18, 21). The last 5% usually occurs following blunt external trauma to the abdomen, pancreatitis, and erosion of the duct by a gallstone, or endoscopic sphincterotomy, and cholangitis such as primary sclerosing cholangitis (PSC), IgG4

sclerosing cholangitis, etc.(18,21). Serum biochemistry reveals mild hyperbilirubinemia and elevated ALP and GGT (18, 21). Malignant strictures are usually due to cholangiocarcinoma (CC). Differentiating benign strictures from malignant ones is usually quite challenging. The accuracy of serum and bile tumour markers in differentiating CC from benign strictures is controversial. Therefore it seems that they may only be used in combination with other techniques as complementary tools for the detection of malignant lesions (22, 23). Among tumor markers, carbohydrate antigen 19-9 (CA19-9), carbohydrate antigen 125 (CA125), and carcinoembryonic antigen (CEA) are widely used (22, 23). Imaging is one of the routine clinical tools in differentiating benign strictures from malignant lesions, detecting the extent of stricture and guiding biopsy. The evaluation begins with ultrasound in order to detect dilation and define the location of obstruction (21). MRCP has several advantages in providing a three dimensional reconstruction of the biliary tree above and below the stricture. This non-invasive technique is comparable in usefulness to invasive cholangiography including ERCP and percutaneous trans-hepatic cholangiopancreatography [PTC] for detecting the level of obstruction. It has much higher potential in presenting the anatomy of the tumour and evaluation of resectability (24). However, the differentiation ability of malignant from benign lesions for this technique is reported to be only 58% (25). ERCP is the gold standard technique for detection of biliary obstruction and evaluation of underlying etiology (21). However, it is difficult to distinguish a malignant stenosis from a benign dominant stricture using ERCP (26). ERCP along with endoscopic ultrasound-guided fine-needle aspiration are useful for taking a biopsy or aspirate in order to rule out the

malignancies by cytologic evaluations (21). Drik Domagk et al. reported 76% differentiation ability of malignant from benign lesions for ERCP (25).

1.2.5 Primary Sclerosing Cholangitis (PSC)

PSC is a chronic, progressive, cholestatic liver disease with continuing inflammation, destruction, and fibrosis leading to strictures of both intra-hepatic and extra-hepatic bile ducts (27). Population-based studies showed that the incidence rate of disease varies from a maximum of 1.3 cases per 100,000 persons/year in Norway (28) and 0.9 per 100,000 persons/year in the U.S. (29) to a minimum of 0.016-0.068 per 100,000 persons/year in Spain (30) and 10 new cases /10 years in Singapore (31). However, because of the long course of the disease, the prevalence is high enough to keep this life-limiting disease in mind. In the U.S., the prevalence is 21 per 100,000 men and 6 per 100,000 women (18).

The etiopathogenesis of PSC is unknown. However there are different propositions including genetic susceptibility, immune system dysfunction, toxic effects of bile acid metabolites, ischemic effects, and infectious agents. The major complication of PSC is CC. Other complications include cholangitis, choledocholithiasis, secondary biliary cirrhosis, and liver failure (21, 32).

PSC has four stages: (1) small duct cholangitis, (2) progressive cholestasis, (3) cirrhosis, (4) decompensation (33).

A typical patient is a middle-aged man, 20-50 years old, with history of ulcerative colitis (sometimes Crohn’s disease), and general symptoms such as fatigue and weight loss, along with hepatobiliary obstructive symptoms such as intermittent jaundice, and pruritus, and digestive manifestations like anorexia, and indigestion. The disease may be

accompanied by autoimmune hepatitis and/or pancreatitis. Blood biochemistry shows cholestatic pattern especially high ALP and GGT levels (18, 21, 33).

PSC should be differentiated from idiopathic adulthood ductopenia due to defect in the canalicular phospholipid transporter gene *ABCB4* and other cholangiopathies such as PBC, cystic fibrosis, eosinophilic cholangitis, AIDS cholangiopathy, etc. and biliary strictures due to surgery, trauma, ischemia, tumors and infections, such as cytomegalovirus (18,33).

Cholangiography reveals segmental fibrosis and sacular dilations of bile ducts between strictures (so called "beaded" appearance on MRCP). Liver biopsy confirms periductal mononuclear infiltrate with fibrosis, ductal proliferation, and ductopenia known as onion skinning pattern (18, 21). Sometimes PSC attacks the small biliary ducts. These patients have a normal cholangiogram in the presence of elevated cholestatic liver tests. The liver biopsy reveals typical PSC histology, onion skin pericholangiolar fibrosis (18, 19). Perinuclear ANCA (Anti myeloid-specific tubulin-beta isotype 5), antinuclear, anticardiolipin, and antithyroperoxidase antibodies, and rheumatoid factor may be positive (18, 33). Medical management of PSC is controversial. Ursodeoxycholic acid (UDCA) and immunosuppressant medications, especially steroids, are widely used. Dominant strictures are relieved with balloon dilation. Stents are placed whenever there is a constant need for opening up the strictures. Sometimes, in non-cirrhotic patients, bilioenteric bypass can be considered. However, most of the patients can just benefit from liver transplantation. The results of transplantation are outstanding with1-and 5-year survival rates of 90% and 85%, respectively (21, 27, 34). Unfortunately, 6% -30% of PSC patients finally experience CC (35) during an interval period of 0.8-15 years after

the diagnosis of PSC (36). This biliary tree adenocarcinoma is the principal cause of mortality in PSC patients (37). OLT is not effective in the presence of established CC (33). Therefore, screening patients with PSC for dysplastic changes in the biliary epithelia is helpful not only in selecting the best therapeutic procedures but also allocating donated livers to patients who can best benefit.

1.2.6 Cholangiocarcinoma (CC)

Cholangiocarcinoma is defined as the tumour of bile ducts. It originates from cholangiocytes (22, 38). PSC is the main predisposing factor with the life time risk of 1.5% per year of disease. Chronic inflammation caused by PSC may increase pro-inflammatory cytokines. These cytokines, especially interleukin 6 may trigger the expression of inducible nitric oxide synthase which in turn can produce nitric oxide (NO). NO or peroxynitrite can damage the DNA directly which may result in malignancy (38).

CC usually remains undiagnosed until the disease is advanced. Following progress, finally, a liver mass along with pain may reveal the malignancy. At this stage a biopsy from liver mass can confirm the diagnosis. Some perihilar tumours and extra-hepatic lesions usually present with obstructive symptoms such as jaundice, pale feces, dark urine, itching, etc.. Cholangitis may complicate the malignancy. It presents with right upper quadrant tenderness and pain, fever and chills (22, 38).

Liver tests reveal an obstructive pattern with elevated ALP, bilirubin, and GGT. Aminotransferases are only elevated in acute obstruction and cholangitis and do not indicate malignancy. Chronic obstruction may result in depletion of lipid-soluble vitamin sources and increase of PT. General predictors of malignancy include low albumin, hemoglobin, and lactate dehydrogenase (LDH) (22).

Serum tumour markers such as CA 19-9, CEA, and CA-125 have low accuracy and can only be used in combination with other diagnostic tools (22-23, 38).

Evaluation usually begins with MRCP which can investigate the anatomy and extent of tumour, bile duct involvement, liver metastasis, and hilar vascular lesions. ERCP is the gold standard technique which along with endoscopic ultrasound and fine-needle aspiration and brush biopsy can confirm the diagnosis. But the cytology of samples collected by endoscopic biopsy or brush can only confirm 40-70% of cases. In negative cases with high clinical suspicion, digitized image analysis (DIA) in order to look for cellular aneuploidy and fluorescent in situ hybridization (FISH) in order to detect chromosomal duplication may be advantageous (21-22, 25, 38).

The best therapeutic option is surgery with a 5-year survival rate of only 9-30% depending on the location of lesion. If surgery is not possible, palliative methods such as obstruction relief by placing stents, and pain management are the only available options (22).

1.2.7 MR Spectroscopy as a Medical Investigational Diagnostic Tool

MR Spectroscopy (MRS) is an emerging technique that makes the study of molecular composition and structure possible, on tissue or fluid samples, *in vitro* in a laboratory setting or, in humans/animals *in vivo*. (39). It can detect several early changes in low weight metabolites related to the disease process in a single experiment (39-41). Especially, MRS is useful for differentiating malignant tumours from benign diseases based on the metabolic changes in the tumour tissues (42) for example in cancers of the colon (43), prostate (44), breast (45), and brain (46).

MRS can detect low molecular weight mobile molecules with diagnostic value in a biologic sample. Positions (chemical shifts) of the peaks (resonances) in acquired spectra indicate the nature of the biochemical species in the sample and the area under the peaks are proportional to the concentration of the species (47). Choline, creatine, lactic acid, citrate, taurine, and lipids are some of the metabolites which can produce diagnostic peaks. In general, high levels of cell proliferation in tumour tissues initiate a series of metabolic changes: a large amount of glucose is converted to lactate by glycolysis to create energy for this high cellular turn over; high membrane turn over in cancer cells demands high phospholipid synthesis which increases choline levels. Unlimited cell turnover can increase the levels of taurine as well. On the other hand, creatine plays an important role in metabolic energy production and therefore it is considered important in cancer tissue MRS. In summary MRS can detect early premorphological biochemical changes that indicate the initiation of cancer before histopathological diagnosis (43-46, 48-50). *In vitro* MRS studies include the analysis of body fluids (such as plasma or bile), extracts of tissue or small biopsy-sized specimens of intact tissue. Non-invasive *in vivo* MRS is an ideal method. However, it is more complicated because of poorer resolution of metabolites due to the lower magnetic field strengths used (1.5–3.0 Tesla, compared to 11.7–14.1 Tesla for *in vitro* studies), magnetic susceptibilities and patient motion (39).

1.2.8 NMR Spectroscopy and the Hepatopancreatobiliary System

Several *in vitro* ^{31}P, ^{1}H and **^{13}C** MRS studies have been performed to evaluate the HPB system (39, 51). ^{1}H-MRS of liver is usually used for quantification of intra-hepatocellular lipid (IHCL) levels. In addition, *in vivo* ^{31}P MRS may evaluate the energy state and cell turnover. Six resolved peaks can be detected in a typical *in vivo* liver ^{31}P MRS spectrum.

First three peaks represent phosphomonoesters (PME), inorganic phosphate (Pi), and phosphodiesters (PDE) respectively and last three peaks represent the nucleoside triphosphates (NTP). *In vitro* studies can reveal more detailed information about PME and PDE peaks due to the higher magnetic fields. The PME peak may be resolved into cell membrane synthesis metabolites such as phosphorylcholine, and phosphoethanolamnine (PE), and energy pathway products such as adenosine monophosphate (AMP) and glucose-6-phosphate. PDE may be resolved into membrane degradation metabolites glycerophosphorylcholine (GPC) and glycerophosphorylethanolamine (GPE) and endoplasmic reticulum phospholipids.

Figure 1.2.8-1: A typical phosphorus spectrum of human liver spectrum (39). a, *in vivo*; b, *in vitro*.

Khan SA, Cox IJ, Hamilton G, Thomas HC, Taylor-Robinson SD. *In vivo* and *in vitro* nuclear magnetic resonance spectroscopy as a tool for investigating hepatobiliary disease: a review of H and P MRS applications. *Liver Int.* 2005; 25(2): p275, Fig2.

In the comparison made by Bell and colleagues between normal liver biopsies and tumour tissues using ^{1}H and ^{31}P-MR spectra, significant increases in PE, PC, taurine, citrate, alanine, lactate and glycine, and significant decreases in GPE, GPC, creatine and threonine in tumour biopsies have been notified (52). Recently, Soper et al. distinguished normal and cirrhotic liver tissues from hepatocellular carcinoma (HCC) with an accuracy

of 100% and 92%, respectively, with ^{1}HMR spectroscopy of liver biopsy samples using a computer-based statistical classification strategy (53).

In the *in vivo* ^{31}P-MRS study conducted by Cox et al., an increase in PME/PDE ratio was observed in all 17 patients with hepatic primary or secondary tumours (54). However increases in PME and decreases in PDE have been reported in different liver diseases including hepatitis, cirrhosis, PSC¸ and alcoholic liver disease (39). Therefore, it appears that these changes are mainly general metabolic ones, resulting from changes in cell turnover and metabolic state and not specific cancer markers.

Analysis of bile is the other main focus of *in vitro* MR Spectroscopy, due to the potential effect of diseases on bile composition (51).

Primary bile acids (chenodeoxycholic acid (CDCA) and cholic acid (CA)), and secondary bile acids (lithocholic acid (LCA) and deoxycholic acid (DOCA)) are secreted to bile via ABC biliary transporters following conjugation with glycine and taurine. PC is produced by hepatocytes and transported to bile via flippase multidrug resistant protein 3 (MDR3). Bile acids can make mixed micelles with PC and cholesterol in order to facilitate lipid digestion following emulsification. In this way, PC can protect the biliary epithelium from damage by bile acids (55).

Since the introduction of ERCP, bile collection and analysis have become a routine procedure especially when malignancy is suspected. ^{1}H MR Spectra of bile can provide valuable information about bile lipids including PC and cholesterol, and bile acids. Figure 1.2.8-2 shows a typical *in vitro* bile spectrum acquired with a 360 MHz instrument. As it is shown in the figure GCBAs at 3.74 ppm, TCBAs at 3.08 ppm, the amide proton region of both GCBAs and TCBAs in the 7.8-8.1 ppm region as well as chol-PLs at 3.22 ppm

and total bile acids (TBAs) plus cholesterol detected at 0.66 ppm are important resonances which can be easily detected in the bile spectrum with a mid-field spectrometer.

Figure 1.2.8-2: An *in vitro* bile spectrum acquired from a healthy volunteer using 360MHz instrument. Bile acids, and bile lipids including PC and cholesterol are detectable (55).

Ijare OB, Smith ICP, Mohajeri S, Bezabeh T. Magnetic resonance spectroscopy of bile in the diagnosis of hepatopancreaticobiliary diseases: past, presence and future. *In: Future directions of NMR.* Vol. 1, Khetrapal CL, Kumar A, Ramanathan KV (Eds). Springer (India): New Delhi, 2011, p 46, Fig 1.

Recently, in an *in vitro* study performed by Ijare et al. in our lab, the feasibility of simultaneous quantification of bile acids (GCBAs, TCBAs, and TBAs) along with the chol-PLs has been demonstrated (56).

Bile acids are the most important metabolites in hepatobiliary disease process. In a normal bile spectrum the ratio of GCBAs:TCBAs is expected to be 3:1(17). In a study performed by Bezabeh et al., it was noticed that in cholestatic patients this ratio is decreased due to both a decrease in GCBAs and an increase in TCBAs (57).

A similar pattern has been reported by Nagana Gowda et al. on hepatocellular carcinoma, cholangiocarcinoma and cirrhotic patients (58).

The amide proton region of a normal *in vitro* bile spectrum acquired by a 360 MHz instrument can be resolved into taurocholic acid (TCA), taurodeoxycholic acid (TDCA), and taurochenodeoxycholic acid (TCDCA) together, glycocholic acid (GCA), glycodeoxycholic acid (GDCA) and glycochenodeoxycholic acid (GCDCA) (51).

The absence of GCDCA may suggest a cholestatic pattern and warrant further evaluation. It may be due to retention of CDCA in the hepatocytes which has a toxic effect (59).

PC, another important component of bile, is decreased in cholestatic patients and absent in cholangiocarcinoma cases. Considering the protective effect of PC on biliary epithelium against the bile acid damage, reduction of PC levels may have a role in the pathophysiology of biliary disorders (51). Albiin et al. compared ^{1}H MRS spectra of bile samples acquired from CC patients with non-malignant biliary disorders including PSC and gallstones and noticed the differences between PC, bile acids, lipids and/or cholesterol regions in these two groups (60).

Lactate should not be detected in normal bile. Therefore, the presence of lactate peak in the bile spectrum suggests anaerobic respiration and a developing pathology. In the study of Nishijiama et al. ^{1}H -MRS has been used to measure levels of lactate in serum and bile in healthy volunteers and patients with non-malignant or malignant diseases of the liver and biliary tract. In bile spectra, lactate was observed in all of 16 patients with malignant diseases, but in none of two healthy volunteers and 12 patients with non-malignant diseases (50).

Considering that de-conjugation or hydrolysis of bile acids may happen during biliary disorders, 1D ^{13}C MRS of bile can detect the presence or absence of carbonyl carbon signal(s) near 187 ppm, in order to evaluate the percentage of unconjugated bile acids (51). ^{31}PMRS can easily differentiate PC from GPC and therefore reveal the reduction of PC in biliary disorders (61).

Because of the invasive nature of bile collection and biopsy, and dependency of them on ERCP or surgery, they cannot be used repeatedly. Therefore *in vivo* analysis of bile would be very valuable. Study performed by Prescot et al. (62) has shown the possibility of obtaining ^{1} HMRS spectra of human gallbladder bile *in vivo*. However, the published *in vivo* spectra are of low quality and cannot be used for quantification of individual bile components except phospholipids. The poor quality of the spectrum may be due to the low magnetic field strength (1.5 T), use of spin echoes with long delays, lipid contamination¸ and more importantly motion artifact mainly caused by breathing.

Künnecke et al. (63) attempted to obtain a high quality spectrum in cynomolgus monkeys using 4.7 T/40 cm instrument. Localized *in vivo* ^{1} HMRS produced high-resolution spectra of gallbladder bile. Therefore, for the first time, identification and quantification of phospholipids and different components of bile acids *in vivo* became possible.

MRS can be useful in the evaluation of pancreas as well. According to a recent study at 3 T, ^{1} HMRS of human pancreas *in vivo* detected four different peak areas: unsaturated fatty acids (-CH = CH-) at 5.4 ppm, chol-PLs at 3.2 ppm; unsaturated fatty acids (-CH2-CH = CH-) or a combination of N-acetylaspartate (NAA), N-acetylaspartylglutamate (NAAG), glutamine, glutamate, macromolecules and unsaturated fatty acids (-CH2-CH = CH-) at 2.0 ppm and lipids at 1.3 ppm. In pancreatic cancer patients, the ratio of lipids

and choline to unsuppressed water were significantly decreased and the ratio of fatty acids to lipids was significantly increased (64).

Considering the close relationship between the pancreas and the biliary system, there have been some attempts to evaluate the metabolic profile of bile in pancreatic disorders. In a recent study performed by Bezabeh et al. (65) high levels of D-glucuronic acid (GlcUA) is detected in the bile obtained from pancreatic cancer patients. Considering that this metabolite was negligible in pancreatitis, its presence may suggest malignancy.

Pancreatic juice is another biofluid which may have diagnostic value in detection of pancreatic pathologies especially cancer. However it is more challenging to obtain pancreatic juice (66).

1.3 HYPOTHESIS & OBJECTIVES

1.3.1 Hypothesis

Bile spectra obtained *in vivo* using localized 3 Tesla MR scanner can distinguish between healthy volunteers and cholestatic PSC patients.

1.3.2 Project Objectives

i. Locating the gallbladder using 3T MRI scanner.

ii. Obtaining MR spectra of the bile *in vivo* using 1D PRESS sequence.

iii. Modifying PRESS sequence to 2D COSY using a method described by Thomas et al. (67) and obtaining 2D MR spectra in order to detect overlapping signals.

iv. Comparing the MR spectra obtained from healthy controls with those of PSC patients.

v. Comparing the *in vivo* results with the results of *in vitro* bile experiments.

1.4 REFERENCES

1. McRobbie DW, Moore EA, Graves MJ, Prince MR. *MRI from picture to proton.* Ed 2, Cambridge University Press (UK): Cambridge, 2006.
2. Bushberg J T, Seibert JA, Leidholdt EM., Boone JM. *The essential physics of medical imaging*. Ed 2, Lippincott, Williams and Wilkins (USA): Philadelphia, PA, 2002.
3. Aiver N, Aiver MN .*All you really need to know about MRI physics*, University of Maryland (USA): Baltimore, 1996.
4. Hashemi RH, William G, Brandly JR, Lisanti CJ. *MRI: The Basics*, Ed 2, Lippincott, Williams and Wilkins (USA): Philadelphia, PA, 2004.
5. Qayyum A. MR Spectroscopy of the Liver: Principles and Clinical Applications. *Radiographics*, 2009: 29(6): 1653-1664.
6. Maher K. *Basic physics of nuclear* medicine. Hünniger D. (Ed), Wikibooks, 2004-2006; http://en.wikibooks.org/wiki/Basic_Physics_of_Nuclear_Medicine.
7. Boesch C. Molecular aspects of magnetic resonance imaging and spectroscopy. *Mol Aspects Med.* 1999; 20(4-5):185-318.
8. Hore PJ, Jones JA, Wimperis S. *NMR Toolkit*. London, Oxford University Press (UK), 2000.
9. Kwock L. Clinical proton Magnetic Resonance Spectroscopy. In: *Clinical Applications of MR Spectroscopy*. Mukherji SK (Ed), 1998, Wiley Liss. (USA): New York, 1998; p 1-33.
10. Bax A, Lerner L. Two-Dimensional Nuclear Magnetic Resonance Spectroscopy. *Science*. 1986: 23; 232(4753): 960-967.

11. Keeler J. Basic concepts for two-dimensional NMR. http://www-keeler.ch.cam.ac.uk/lectures/2d_a4.pdf
12. Morton DA, Foreman KB, Albertine KH. Foregut. In: *The Big Picture: Gross Anatomy*. Morton DA, Foreman KB, Albertine KH. (Eds), McGraw-Hill (USA): New York, 2011; http://www.accessmedicine.com/content.aspx?aID=8666565.
13. Barrett KE, Barman SM, Boitano S, Brooks HL. Transport & Metabolic Functions of the Liver. In: *Ganong's Review of Medical Physiology*. 24th ed, Barrett KE, Barman SM, Boitano S, Brooks HL (Eds), McGraw-Hill (USA): New York, 2012; http://www.accessmedicine.com/content.aspx?aID=56264282.
14. Barrett KE (Ed). *Gastrointestinal Physiology*. McGraw-Hill (USA): New York, 2006;http://www.accessmedicine.com.proxy2.lib.umanitoba.ca/resourceTOC.aspx?resourceID=77
15. Kuntz E., Kuntz H., Hepatology, Textbook and Atlas. Springer (USA): New York, 2008.
16. McPhee SJ, Hammer GD (Eds). *Pathophysiology of Disease: An Introduction to Clinical Medicine*, Ed6, McGraw-Hill (USA): New York, 2010; http://www.accessmedicine.com.proxy2.lib.umanitoba.ca/resourceTOC.aspx?resourceID=17
17. Longo DL, Fauci AS, Kasper DL, Hauser SL, Jameson JL, Loscalzo J (Eds). Harrison's Principles of Internal Medicine, (Harrison's online) Ed 18, McGraw-Hill (USA): New York, 2012. http://www.accessmedicine.com.proxy2.lib.umanitoba.ca/resourceTOC.aspx?resourceID=4

18. Friedman LS. Liver, Biliary Tract & Pancreas Disorders. In: *CURRENT Medical Diagnosis & Treatment 2014.* Papadakis MA, McPhee SJ, Rabow MW, Berger TG (Eds). McGraw-Hill (USA): New York, 2013. . http://www.accessmedicine.com/content.aspx?aID=7993.
19. Vleggaar FP, Van Ooteghem NA, Van Buuren HR, Van Berge Henegouwen GP. Cholestatic liver diseases: slow progress in understanding and treating slowly progressive disorders. *Scand J Gastroenterol Suppl.* 2000; (232): 86-92.
20. Langwieler TE, Kim JS, Mann O, Thonke F, Knoefel WT, Rogiers X, Izbicki JR. Management of an unclear bile duct stenosis. *Surg Endosc.* 2004; 18(4): 717-718.
21. Shanbhogue AK, Tirumani SH, Prasad SR, Fasih N, McInnes M. Benign biliary strictures: a current comprehensive clinical and imaging review. *AJR Am J Roentgenol.* 2011; 197(2): W295-306.
22. Khan SA, Davidson BR, Goldin R, Pereira SP, Rosenberg WM, Taylor-Robinson SD, Thillainayagam AV, Thomas HC, Thursz MR, Wasan H; British Society of Gastroenterology. Guidelines for the diagnosis and treatment of cholangiocarcinoma: consensus document. *Gut.* 2002; 51 Suppl 6:VI1-19.
23. Nehls O, Gregor M, Klump B. Serum and bile markers for cholangiocarcinoma. *Semin Liver Dis.* 2004; 24(2): 139-154.
24. Khan SA, Thomas HC, Davidson BR, Taylor-Robinson SD. Cholangiocarcinoma. *Lancet.* 2005; 366(9493):1303-1314.
25. Domagk D, Wessling J, Reimer P, Hertel L, Poremba C, Senninger N, Heinecke A, Domschke W, Menzel J. Endoscopic retrograde cholangiopancreatography, intraductal ultrasonography, and magnetic resonance cholangiopancreatography in

bile duct strictures: a prospective comparison of imaging diagnostics with histopathological correlation. *Am J Gastroenterol.* 2004; 99(9): 1684-1689.

26. Lindberg B, Arnelo U, Bergquist A, Thorne A, Hjerpe A, Granqvist S, Hansson LO, Tribukait B, Persson B, Broome U. Diagnosis of biliary strictures in conjunction with endoscopic retrograde cholangiopancreatography, with special reference to patients with primary sclerosing cholangitis. *Endoscopy*.2002; 34(11): 909-916.
27. Lee YM, Kaplan MM; Practice Guideline Committee of the ACG. American College of Gastroenterology. Management of primary sclerosing cholangitis. *Am. J. Gastroenterol.* 2002; 97(3): 528-534.
28. Boberg KM, Aadland E, Jahnsen J, Raknerud N, Stiris M, Bell H. Incidence and prevalence of primary biliary cirrhosis, primary sclerosing cholangitis, and autoimmune hepatitis in a Norwegian population. *Scand J Gastroenterol.* 1998; 33(1): 99-103.
29. Bambha K, Kim WR, Talwalkar J, Torgerson H, Benson JT, Therneau TM, Loftus EV Jr, Yawn BP, Dickson ER, Melton LJ 3rd. Incidence, clinical spectrum, and outcomes of primary sclerosing cholangitis in a United States community. *Gastroenterology.* 2003; 125(5): 1364-1369.
30. Escorsell A, Pares A, Rodes J, Solis-Herruzo JA, Miras M, de la Morena E. Epidemiology of primary sclerosing cholangitis in Spain. Spanish Association for the Study of the Liver. *J Hepatol.* 1994; 21(5): 787-791.
31. Ang TL, Fock KM, Ng TM, Teo EK, Chua TS, Tan JY. Clinical profile of primary sclerosing cholangitis in Singapore. *J Gastroenterol Hepatol.* 2002; 17(8): 908-913.

32. Rodriguez HJ, Bass NM. Primary sclerosing cholangitis. *Semin Gastrointest Dis.* 2003; 14(4): 189-198.

33. LaRusso NF, Shneider BL, Black D, Gores GJ, James SP, Doo E, Hoofnagle JH. Primary sclerosing cholangitis: summary of a workshop. *Hepatology.* 2006; 44(3): 746-764.

34. Cullen SN, Chapman RW. Review article: current management of primary sclerosing cholangitis. *Aliment Pharmacol Ther.* 2005; 21(8): 933-948.

35. Schrumpf E, Boberg KM. Epidemiology of primary sclerosing cholangitis. *Best Pract Res Clin Gastroenterol.* 2001; 15(4): 553-562.

36. Burak K, Angulo P, Pasha TM, Egan K, Petz J, Lindor KD. Incidence and risk factors for cholangiocarcinoma in primary sclerosing cholangitis. *Am J Gastroenterol.* 2004; 99(3): 523-526.

37. Bergquist A, Ekbom A, Olsson R, Kornfeldt D, Lööf L, Danielsson A, et al. Hepatic and extrahepatic malignancies in primary sclerosing cholangitis. *J Hepatol* 2002; 36: 321-327.

38. Gores GJ. Cholangiocarcinoma, Current concepts and insights. *Hepatology*. 2003; 37(5): 961-969.

39. Khan SA, Cox IJ, Hamilton G, Thomas HC, Taylor-Robinson SD. *In vivo* and *in vitro* nuclear magnetic resonance spectroscopy as a tool for investigating hepatobiliary disease: a review of H and P MRS applications. *Liver Int.* 2005; 25(2): 273-281.

40. Smith ICP, Baert R. Medical diagnosis by high resolution NMR of human specimens. *IUBMB Life.* 2003; 55(4-5): 273-277.

41. Mountford C, Smith ICP, Bourne R. Correlation of Histopathology with Magnetic Resonance Spectroscopy of Human Biopsies. In: *Modern Magnetic Resonance*. Vol. II, Webb GA (Ed). Springer (U.K.): London, 2006; p 1027-1036.

42. Leach MO. Introduction to *in vivo* MRS of cancer: new perspectives and open problems. *Anticancer Res.* 1996; 16(3B): 1503-1514.

43. Bezabeh T, Smith ICP, Krupnik E, Somorjai RL, Kitchen DG, Bernstein CN, Pettigrew NM, Bird RP, Lewin KJ, Briere KM. Diagnostic potential for cancer via ^{1}H magnetic resonance spectroscopy of colon tissue. *Anticancer Res.*1996; 16(3B): 1553-1558.

44. Hahn P, Smith ICP, Leboldus L, Littman C, Somorjai RL, Bezabeh T. The classification of benign and malignant human prostate tissue by multivariate analysis of ^{1}H magnetic resonance spectra. *Cancer Res.*1997; 57(16): 3398-3401.

45. Mountford CE, Somorjai RL, Malycha P, Gluch L, Lean C, Russel P, Barraclough B, Gillett D, Himmelreich U, Dolenko B, Nikulin AE, Smith ICP. Diagnosis and prognosis of breast cancer by magnetic resonance spectroscopy of fine-needle aspirates analyzed using a statistical classification strategy. *Br. J. Surg.* 2001; 88(9): 1234-1240.

46. Chen J, Huang SL, Li T, Chen XL. *In vivo* research in astrocytoma cell proliferation with ^{1}H-magnetic resonance spectroscopy: correlation with histopathology and immunohistochemistry. *Neuroradiology*. 2006; 48(5): 312-318.

47. Bezabeh T, Somorjai RL, Smith ICP, Nikulin AE, Dolenko B, Bernstein CN. The use of ^{1}H magnetic resonance spectroscopy in inflammatory bowel diseases:

distinguishing ulcerative colitis from Crohn's disease. *Am. J. Gastroenterol.* 2001; 96(2): 442-448.

48. Yerli H, Agildere AM, Ozen O, Geyik E, Atalay B, Elhan AH. Evaluation of cerebral glioma grade by using normal side creatine as an internal reference in multi-voxel ^{1}H-MR spectroscopy. *Diagn Interv Radiol.* 2007; 13(1): 3-9.
49. Menard C, Smith ICP, Somorjai RL, Leboldus L, Patel R, Littman C, Robertson SJ, Bezabeh T. Magnetic resonance spectroscopy of the malignant prostate gland after radiotherapy: a histopathologic study of diagnostic validity. *Int J Radiat Oncol Biol Phys.* 2001; 50(2): 317-323.
50. Nishijima T, Nishina M, Fujiwara K. Measurement of lactate levels in serum and bile using proton nuclear magnetic resonance in patients with hepatobiliary diseases: its utility in detection of malignancies. *Jpn J Clin Oncol.* 1997; 27(1): 13-17.
51. Bezabeh T, Ijare OB, Mohajeri S, Lipschitz J, Smith,ICP. Magnetic resonance spectroscopy of bile in the diagnosis of chronic cholestatic diseases. In: *Advances in Medicine and Biology.* Vol. 45, Berhardt, Leon V (Ed). Hauppauge, N.Y., Nova Science Publishers (USA), 2012; p 95 – 112.
52. Bell JD, Cox IJ, Sargentoni J, Peden CJ, Menon DK, Foster CS, Watanapa P, Iles RA, Urenjak J. A. ^{31}P and ^{1}H-NMR investigation *in vitro* of normal and abnormal human liver. *Biochim Biophys Acta.* 1993; 1225(1): 71-77.
53. Soper R, Himmelreich U, Painter D, Somorjai RL, Lean CL, Dolenko B, Mountford CE, Russell P. Pathology of hepatocellular carcinoma and its precursors using proton magnetic resonance spectroscopy and a statistical classification strategy. *Pathology*. 2002t; 34(5): 417-422.

54. Cox IJ, Menon DK, Sargentoni J, Bryant DJ, Collins AG, Coutts GA, Iles RA, Bell JD, Benjamin IS, Gilbey S, et al. Phosphorus-31 magnetic resonance spectroscopy of the human liver using chemical shift imaging techniques. *J Hepatol.* 1992; 14(2-3): 265-275.

55. Ijare OB, Smith ICP, Mohajeri S, Bezabeh T. Magnetic resonance spectroscopy of bile in the diagnosis of hepatopancreatobiliary diseases: past, presence and future. *In: Future directions of NMR.* Vol. 1, Khetrapal CL, Kumar A, Ramanathan KV (Eds). Springer (India): New Delhi, 2011, p 45-53.

56. Ijare OB, Bezabeh T, Albiin N, Bergquist A, Arnelo U, Lindberg B, Smith ICP. Simultaneous quantification of glycine- and taurine-conjugated bile acids, total bile acids, and choline-containing phospholipids in human bile using ^{1}H NMR spectroscopy. *J Pharm Biomed Anal.* 2010; 53(3): 667-673.

57. Bezabeh T, Ijare OB, Albiin N, Bergquist A, Arnelo U, Löhr M, Hov JR, Smith ICP. Alteration in the Conjugation Pattern of Bile acids in Human Bile during Cholestasis: A ^{1}H MRS Study. *Proc. Intl. Soc. Mag. Reson. Med*. 2010; 18: 4590.

58. Nagana Gowda GA, Shanaiah N, Cooper A, Maluccio M, Raftery D: Visualization of bile homeostasis using ^{1}H-NMR spectroscopy as a route for assessing liver cancer. *Lipids.* 2009; 44(1): 27-35.

59. Ijare OB, Bezabeh T, Albiin N, Arnelo U, Bergquist A, Lindberg B, Smith ICP. Absence of glycochenodeoxycholic acid (GCDCA) in human bile is an indication of cholestasis: a ^{1}H MRS study. *NMR Biomed.* 2009; 22(5): 471-479.

60. Albiin N, Smith ICP, Arnelo U, Lindberg B, Bergquist A, Dolenko B, Bryksina N, Bezabeh T. Detection of cholangiocarcinoma with magnetic resonance spectroscopy

of bile in patients with and without primary sclerosing cholangitis. *Acta Radiol.* 2008; 49(8): 855-862.

61. Ijare OB, Bezabeh T, Albiin N, Bergquist A, Arnelo U, Löhr M, Smith ICP. Potential of ^{31}P magnetic resonance spectroscopy of bile in the detection of cholestatic diseases. *Proc. Intl. Soc. Mag. Reson. Med*. 2011; 19: 5757.
62. Prescot AP**,** Collins DJ, Leach MO, Dzik-Jurasz AS. Human gallbladder bile: noninvasive investigation *in vivo* with single-voxel ^{1}H MR Spectroscopy. *Radiology* 2003; 229(2): 587-592.
63. Künnecke B, Bruns A, von Kienlin M. Non-invasive analysis of gallbladder bile composition in cynomolgus monkeys using *in vivo* ^{1}H magnetic resonance spectroscopy. *Biochim. Biophys. Acta.* 2007; 1771(4): 544-549.
64. Yao X, Zeng M, Wang H, Fei S, Rao S, Ji Y. Metabolite detection of pancreatic carcinoma by in vivo proton MR spectroscopy at 3T: initial results. *Radiol Med.* 2012; 117(5): 780-788.
65. Bezabeh T, Ijare OB, Albiin N, Arnelo U, Lindberg B, Smith ICP. Detection and quantification of D-glucuronic acid in human bile using ^{1}H NMR spectroscopy: relevance to the diagnosis of pancreatic cancer. *MAGMA.* 2009; 22(5): 267-275.
66. Wang J, Ma C, Liao Z, Tian B, Lu JP. Study on chronic pancreatitis and pancreatic cancer using MRS and pancreatic juice samples. *World J Gastroenterol.* 2011; 17(16): 2126-2130.
67. Thomas MA, Yue K, Binesh N, Davanzo P, Kumar A, Siegel B, Frye M, Curran J, Lufkin R, Martin P, Guze B. Localized two-dimensional shift-correlated MR spectroscopy of human brain. *Magn Reson Med.* 2001; 46(1): 58-67.

CHAPTER 2. MATERIALS & METHODS

2. 1 STUDY POPULATION

2.1.1 Inclusion Criteria

1. Known PSC cases.
2. Healthy volunteers.

2.1.2 Exclusion Criteria

1. Subjects who have metal objects inside their body who should be excluded from MR scanning such as people who have aneurysm and hemostatic clips, pacemakers, prosthetic heart valves, cerebral ventricular shunts, vascular access ports, intravascular coils, filters and stents, joint or limb replacements, orthopedic material and devices, intraocular implants, ear implants, contraceptive diaphragms or intrauterine contraceptive agents, bullets, shrapnel or other foreign metal bodies like metal slivers.
2. Subjects suffering from anxiety disorders such as claustrophobia.
3. Any subject at high risk for an exacerbation of a medical condition.
4. Women who are or may be pregnant. (We offered a pregnancy test before MRI to every woman).
5. Subjects who have more than 350 lb weight.
6. Healthy volunteers who have history of alcohol abuse, hepatopancreatobiliary disorders or taking liver toxic medication.
7. Healthy volunteers who have history of Inflammatory Bowel Diseases (IBD).

8. Patients whose physician recommended not participating in the study because of risk of MRI or doing the experiments out of hospital settings.

2.2 SUBJECT RECRUITMENT

Healthy volunteers and PSC patients were recruited according to a protocol approved by the Research Ethics Boards of the University of Manitoba and National Research Council of Canada (NRC). The presence of active hepatopancreatobiliary disorders was ruled out in healthy volunteers by medical history, physical examination, and laboratory blood tests including bilirubin (total and direct), aspartate aminotransferase (AST), alanine aminotransferase (ALT), gamma glutamyl transferase (GGT), lipase, alkaline phosphatase (ALP) and international normalized ratio (INR) under the supervision of a hepatologist.

After explaining the protocol and addressing all the questions/concerns, the patient's consent was obtained. Subjects were given enough time to review the information before they have to sign the consent.

2.2.1 Recruitment Challenges

Patient recruitment was a very challenging procedure. Considering the low incidence of PSC, the total number of patients in Manitoba could barely be over 100. Moreover, because of co-incidence of PSC with other inflammatory conditions such as autoimmune hepatitis, by excluding patients suffering from such overlapping conditions, the number of possible subjects further decreased. In addition, a number of subjects who were interested in the study were excluded due to the possibility of having metal objects in their body. Therefore, finally we just recruited 11 PSC patients.

2.3 *IN VIVO* MRS EXPERIMENTS

The *in vivo* MRS experiments were performed using a 3 Tesla Siemens Trio instrument at the NRC-IBD and a custom-built surface coil. After the localization of the gallbladder by conventional abdominal MRI using half-fourier single-shot turbo-spin echo (HASTE) sequences (VB15 & VB17, Siemens, Erlangen, Germany), MR spectra were obtained using the single voxel localization (SVS) method, (PRESS, VB15 & VB17, Siemens, Erlangen, Germany) and 2D L-COSY (1,2) sequence. The voxel size was adjusted to 12 × 12× 12 mm^3. Water suppression was performed using chemical shift selective suppression pulses (CHESS) (3). The study proceeded in two phases. The initial phase was more of a technical development and feasibility study. The experimental parameters were optimized for both signal-to-noise-ratio (SNR) and resolution using 10 healthy volunteers. In phase 2, 1D and 2D MR spectra from healthy volunteers were compared with those acquired from PSC patients.

2.4 DATA PROCESSING

The raw data was first processed by a MATLAB program generated at UCLA, and modified at NRC. Using this program, we decoded the raw file, extracted data, scaled, reviewed the data scan by scan and discarded the distorted ones. The scans were then averaged after aligning all of them. Eddy current correction applied (4), and the data from different channels of the coil were combined using an optimal combination utilizing the noise correlation (5) in order to make a single good quality spectrum. After this preliminary processing, the data was transferred to the FELIX-2007 software (FELIX NMR Inc., San Diego, California, USA) for analysis. Using FELIX, an exponential apodization function with 0.5 Hz line broadening was applied. Following Fourier transformation, first and second order phase and baseline corrections were performed.

Then different peaks in the water-suppressed bile ^{1}H spectrum were fitted to Lorentzian line shapes by deconvolution based on a simulated annealing algorithm (FELIX NMR Inc., San Diego, California, USA). Similarly, the water peak of the bile spectrum obtained without water suppression was fitted and used as an internal reference. Then the ratios of peak areas of the metabolites of interest to the unsuppressed water peak area were calculated. Based on the molecular weight of each metabolite and water, the concentration of each metabolite of interest was calculated. The concentrations were corrected for T_1 and T_2 relaxation times (6) and water content of gallbladder bile (7).

2.5 STATISTICAL ANALYSIS

In order to compare the spectral data of patients with controls, the means of corrected molar concentration of each metabolite were compared between the PSC patients and healthy controls. In all cases Student's t-test was performed except for glycine conjugated bile acids (GCBAs). In that case the variance of corrected molar concentration of the metabolite in PSC patients was completely different from the control group. Therefore non parametric tests looked more suitable. We used Mann-Whitney U Test for comparing the means in that case.

The next step of statistical analysis was evaluation of confounding effects of variables such as age, and gender. Unfortunately, our sample size was small and there were not enough subjects in some age groups. As a result, it was not possible to test the confounding effect of age. Regarding gender, we compared the means of corrected molar concentrations of each metabolite between males and females using Student's t-test and there were no significant differences.

The next step was evaluation of the correlation between laboratory blood biochemistry and molar concentrations of metabolites detected in 1D spectra. Considering that majority of our patients did not have hyperbilirubinemia, or considerably increased liver enzymes, but showed cholestatic pattern (elevated ALP and/or GGT), we decided to perform a correlation analysis between ALP and GGT and each bile metabolite.

2.6 TECHNICAL CHALLENGES

2.6.1 Use of Surface Coil in order to Increase the Signal-to-Noise-Ratio

One of the major challenges we faced was improving the SNR. Considering the small size of gallbladder and its motion due to breathing, we had to use a 12x12x12 mm^3 voxel. Due to the small volume of this voxel (1.72 mm^3), the SNR obtained by Siemens flexible body coil was not enough especially for 2D spectrum. Fortunately, the gallbladder is superficial and located very close to the skin. As it was measured by Warren et. al using computed tomography on 100 patients: "The mean anterior distance from the skin to the gallbladder was 5.0 cm (range, 2.0-10 cm±1.9 cm). The mean lateral distance was 5.8 cm (range, 2.0-10.0 cm; ±2.0 cm). The mean shortest distance from the skin to the gallbladder fundus wall was 4.2 cm (±1.5 cm)" (8).

Therefore, it seemed suitable to use a surface coil in order to increase the SNR. We have used a phase array receive surface coil designed at NRC-IBD. The coil passed all safety checks of NRC-IBD and approved to be used in this research on human subjects by the research ethics boards of both NRC and University of Manitoba.

2.6.2 Challenges due to Gallbladder Motion and Respiratory-gated Sequence

The liver is attached to the diaphragm by ligaments (9), therefore the motion of the diaphragm during breathing is transferred to the liver and gallbladder accordingly. In

order to deal with this issue, we used bellow respiratory-gated sequences which scan just at specific level of inspiration or expiration. The Siemens instrument has a sensor which can be fixed over the abdomen by a belt. The sensor can measure the abdominal motion during breathing. Based on this measurement the Siemens program can trigger the pulse sequence at a certain level of inspiration or expiration. We triggered during the last 10-30 % of expiration, therefore, at least, 70% of motion has been eliminated. As reported by Mochzuki et al. (10), the maximum vertical and antero-posterior motion of liver and gallbladder during breathing is 2.5 cm, and 1 cm, respectively. The lateral motion is negligible. By eliminating the 70% of motion via triggering during the last 30% of expiration, about 0.8 cm motion in the vertical dimension and 0.3 cm in the antero-posterior dimension were left. Therefore, when we were positioning the voxel, we had to give 0.8 cm distance between the voxel and walls of gallbladder in the vertical dimension and 0.3 cm in the antero-posterior dimension. Considering the 7-10 cm length of gallbladder (11), this approach was feasible.

2.6.3 Lipid Contamination

One of the major challenges of *in vivo* spectroscopy is contamination due to signals arising from surrounding tissues. One of the well-known solutions is using spatial saturation bands in order to suppress the contaminating signals (12). In our experiments, the major problem was body fat around gallbladder and lipid signals from liver. We positioned 6-8 spatial saturation bands around the gallbladder with 70-100 mm thickness. However, we could not eliminate the lipid contamination completely. Unfortunately, it was difficult to measure the percentage of contamination. Among the signals with diagnostic value that we quantified, the lipid contamination mainly overlapped with the

signal at 0.66 ppm, which was assigned to the -CH_3 group of total bile acids (TBAs) + cholesterol (13). However the contamination may overlap with other peaks such as the signal at 5.26 ppm which represents the olefinic [-CH=CH-] protons of choline containing phospholipids (chol-PLs) (13). In some cases, it may appear as a new signal such as the signal at 1.58 ppm (shown in Figure 2.6.3-1).

Figure 2.6.3-1: 1D spectrum of bile with apparent lipid contamination.

1, -CH_3 group of total bile acids (TBAs) + cholesterol at 0.66 ppm; 2, lipid contamination at 1.58 ppm; 3, residual water; 4, olefinic [-CH=CH-] protons of choline containing phospholipids (chol-PLs) at 5.26 ppm. In this case, lipid contamination appeared as a new peak at 1.58 ppm without affecting peaks 1 and 4.

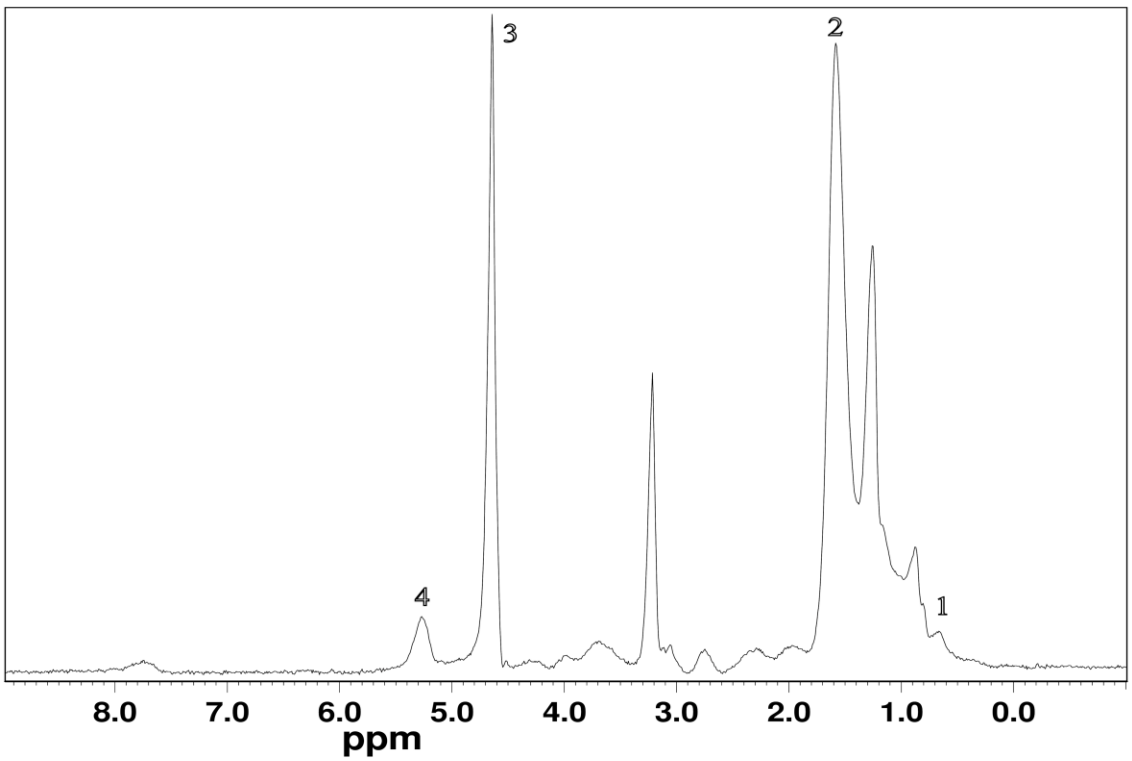

2.6 REFERENCES:

1. Thomas MA, Yue K, Binesh N, Davanzo P, Kumar A, Siegel B, Frye M, Curran J, Lufkin R, Martin P, Guze B. Localized two-dimensional shift-correlated MR spectroscopy of human brain. *Magn Reson Med.* 2001; 46(1): 58-67.
2. Thomas MA, Hattori N, Umeda M, Sawada T, Naruse S. Evaluation of two-dimensional L-COSY and JPRESS using a 3 T MRI scanner: from phantoms to human brain *in vivo*. *NMR Biomed.* 2003; 16(5): 245-251.
3. Barker PB, Lin DDM. In vivo proton MR spectroscopy of the human brain. Progress in Nuclear Magnetic Resonance Spectroscopy. 2006; 49: 99–128.
4. Klose U. *In vivo* proton spectroscopy in presence of eddy currents. *Magn Reson Med.* 1990; 14(1): 26-30.
5. Roemer PB, Edelstein WA, Hayes CE, Souza SP, Mueller OM. The NMR phased array. *Magn Reson Med.* 1990; 16(2): 192-225.
6. Fayad LM, Salibi N, Wang X, Machado AJ, Jacobs MA, Bluemke DA, Barker PB. Quantification of muscle choline concentrations by proton MR spectroscopy at 3 T: technical feasibility. *AJR Am J Roentgenol.* 2010; 194(1): W73-79.
7. van Erpecum KJ. Biliary lipids, water and cholesterol gallstones. *Biol Cell.* 2005; 97(11): 815-822.
8. Warren LP, Kadir S, Dunnick NR. Percutaneous cholecystostomy: anatomic considerations. *Radiology*. 1988; 168(3): 615-616.
9. Standring S, Borley NR, Collins P, Crossman AR, Gatzoulis MA, Healy JC, Johnson D, Mahadevan V, Newell RLM, Wigley BC. Liver. In: *Gray's Anatomy*.

Hyde M, Ozols I, Mellor M, Smith G, Whitehouse A, Goolsby J, Jackson L (Eds). Elsevier Limited (USA), 2008; p 1163-1175.

10. Mochzuki T, Kunta M, Toyama Y, Maruhashi A, Murayama S. Real-time respiration phase monitoring system using ultrasonic bi-plane imaging data for proton beam therapy. *IEEE Ultrasonics Symposium.* 2004; 1441-1444.
11. Standring S, Borley NR, Collins P, Crossman AR, Gatzoulis MA, Healy JC, Johnson D, Mahadevan V, Newell RLM, Wigley BC. Gallbladder and biliary tree. In: *Gray's Anatomy.* Hyde M, Ozols I, Mellor M, Smith G, Whitehouse A, Goolsby J, Jackson L (Eds). Elsevier Limited (USA), 2008; p 1177-1181
12. Hetherington HP, Avdievich NI, Kuznetsov AM, Pan JW. RF shimming for spectroscopic localization in the human brain at 7 T. *Magn Reson Med.* 2010; 63(1): 9-19.
13. Ijare OB, Bezabeh T, Albiin N, Bergquist A, Arnelo U, Lindberg B, Smith ICP. Simultaneous quantification of glycine- and taurine-conjugated bile acids, total bile acids, and choline-containing phospholipids in human bile using ^{1}H NMR spectroscopy. *J Pharm Biomed Anal.* 2010; 53(3): 667-673.

CHAPTER 3.

MAGNETIC RESONANCE SPECTROSCOPY OF HUMAN GALLBLADDER BILE AT 3 T: CAN *IN VIVO* ^{1}H MRS OF BILE HAVE DIAGNOSTIC VALUE IN THE NEAR FUTURE?

Sanaz Mohajeri[1], Omkar B. Ijare[2], Tedros Bezabeh[1,2], Scott B. King[3], M. Albert Thomas[4], Gerald Minuk[1], Jeremy Lipschitz[1], Iain Kirkpatrick[1], Mike Smith[3], and Ian C.P. Smith[1,2]

[1]University of Manitoba, Winnipeg, Manitoba, Canada, [2]University of Winnipeg, Winnipeg, Manitoba, Canada, [3]National Research Council of Canada, Winnipeg, Manitoba, Canada, [4]University of California, Los Angeles, California, United States

This article has been submitted to NMR in Biomedicine

Contributions:

Sanaz Mohajeri: optimizing the experimental parameters, Modifying PRESS sequence to L-COSY based on the method designed by Dr. Albert Thomas, subject recruitment, participating in modifying MATLB code designed at UCLA, collecting the data, analyzing the data, writing the paper.

Omkar B. Ijare: consultant at data collection, analysis, and writing paper.

Tedros Bezabeh: supervising data collection, analysis, and writing paper.

Scott B. King: designer of coil.

M. Albert Thomas: consultant in 2D experiments, IDEA programming. MATLAB code originally designed in his lab.

Gerald Minuk, Jeremy Lipschitz, and Iain Kirkpatrick: clinical collaborators.

Mike Smith: modifying MATLAB code for combining the data acquired from different coil elements.

Ian C.P. Smith: defining the original question, supervising data collection, analysis, and writing paper.

3.1 ABSTRACT

In vitro ^{1}H MRS of human bile has shown potential in the diagnosis of various hepatopancreatobiliary (HPB) diseases. Previously, *in vivo* ^{1}H MRS of human bile in gallbladder using a 1.5 T scanner demonstrated the possibility of quantification of choline-containing phospholipids (chol-PLs). However, other lipid components such as bile acids play an important role in the pathophysiology of the HPB system. We have employed a higher magnetic field strength (3 T), and a custom-built receive array coil, to improve the quality of *in vivo* ^{1}H MRS of human bile in gallbladder. We obtained significant improvement in the quality of 1D spectra (17 healthy volunteers) using a bellow respiratory-gated PRESS sequence with well distinguished signals for total bile acids (TBAs) plus cholesterol resonating at 0.66 ppm, taurine-conjugated bile acids (TCBAs) at 3.08 ppm, chol-PLs at 3.22 ppm, glycine-conjugated bile acids (GCBAs) at 3.74 ppm, amide proton [NH] region arising from GCBAs and TCBAs in the region 7.76 – 8.05 ppm. The peak areas of these signals were measured by deconvolution, and subsequently the molar concentrations of metabolites were estimated with good accuracy, except for that of TBAs plus cholesterol. The concentration of TBAs plus cholesterol was overestimated in some cases, which could be due to lipid contamination. In addition, we report the first 2D L-COSY spectra of human bile *in vivo* (obtained in 15 healthy volunteers). This shows a potential to detect biochemicals such as lactate which are

generally overlapping with those of lipids in the corresponding 1D ^{1}H MR spectrum. 2D L-COSY spectra will also be helpful in differentiating various biliary chol-PLs in pathological conditions of the HPB system.

Key words**:** human bile*; in vivo* ^{1}H MRS; total bile acids; glycine-conjugated bile acids; taurine-conjugated bile acids ; choline-containing phospholipids; PRESS; L-COSY**.**

Abbreviations**:** ALP, alkaline phosphatase; ALT, alanine aminotransferase; AST, aspartate aminotransferase; chol-PLs, choline-containing phospholipids; DSS, 3-(trimethylsilyl)-1-propanesulfonic acid sodium salt; ERCP, endoscopic retrograde cholangiopancreatography; GCBAs, glycine-conjugated bile acids; GDCA, glycodeoxycholic acid sodium salt; GGT, gamma-glutamyl transferase; GI, gastrointestinal; HASTE, half-fourier acquisition single-shot turbo spin-echo; HPB, hepatopancreatobiliary; INR, international normalized ratio; PC, phosphatidylcholine; PhC, phosphocholine chloride calcium salt tetrahydrate; SVS, single voxel spectroscopy; TBAs, total bile acids; TCA, taurocholic acid sodium salt; TCBAs, taurine-conjugated bile acids; TR_{eff}, effective TR.

3.2 INTRODUCTION

Bile is a yellowish green fluid secreted by liver, stored and concentrated in the gallbladder and released to the duodenum in response to cholecystokinin following ingestion of food (1). It is mainly composed of water, pigments such as bilirubin, lipids including chol-PLs, cholesterol, and bile salts such as GCBAs and TCBAs (2-4). Bile salts play a major role in emulsification, digestion and absorption of lipids. Moreover, the common bile duct receives pancreatic secretions through pancreatic duct before emptying to the duodenum (2). Therefore, the metabolic profile of bile delivered to the intestine is

mainly under the control of cellular secretions of liver, gallbladder, pancreas and bile ducts. As a result, any pathological changes in the gastrointestinal (GI) system, especially the HPB part can affect the metabolic profile of the bile (1 – 4). Among these metabolites, cholesterol, chol-PLs and bile acids have captured more attention due to their higher concentration and greater role in the disease processes (4 – 8).

Various *in vitro* studies have demonstrated the potential of MRS in the diagnosis of HPB pathologies, especially in differentiating benign changes from malignant ones through analysis of chol-PLs, bile acids, and cholesterol in the bile (4, 6, 7, 9). The recent success from our laboratory in the simultaneous quantification of bile acids (GCBAs, TCBAs, and TBAs) along with the chol-PLs, is an important development in the application of *in vitro* ^{1}H MRS of bile (10). This progress has generated hope for following the metabolic footprints of different HPB disorders (10). Moreover, analyzing the ratio of concentrations of metabolites can also provide additional diagnostic information. For example, in our previous study (11), comparing cholestatic hyperbilirubinemic hepatobiliary patients with normobilirubinemic cases, the ratio of biliary glycine to taurine conjugated bile acids was found to decrease significantly. However, the changes in the concentration of the individual glycine and taurine conjugated bile acids were not statistically significant. However, analysis of bile spectra has its own difficulties. The similarities in the structures of constituent bile acids in bile may result in significant overlap of peaks of interest, especially in *in vivo* MRS studies. To overcome such difficulty, different NMR methods have been developed (12, 13). Spectral editing MRS sequences may overcome this problem (14), but they can only measure one metabolite at a time. However, 2D MRS techniques such as COSY may virtually separate multiple

overlapping peaks in a single measurement, providing unambiguous assignment. Therefore, they may become the techniques of choice in such cases (15, 16).

For years, providing metabolic information using MRS non-invasively was difficult, primarily due to the complexities of *in vivo* MRS. The challenges include overlapping of metabolite peaks due to the use of lower magnetic field strengths (typically 1.5 T, compared to 9.4 – 14.1 T for *in vitro* studies), magnetic susceptibility effects and motion artifacts (17). Advances in MR technology, both at the level of hardware and software, have decreased such bottlenecks to a large extent. The increase in magnetic field strength of clinical scanners (≥3 T), and the development of gated sequences (to minimize the effect of motion artifacts), has been quite helpful. As a result, there has been a great interest in the detection and quantification of bile metabolites with diagnostic potential using *in vivo* ^{1}H MRS (18, 19). Prescot et al. performed the first *in vivo* ^{1}H MRS study on human gallbladder bile, using a 1.5 T MRI scanner and a surface coil in receive mode (18). However, the published *in vivo* spectra were of low quality, and the authors were unable to quantify individual bile components other than chol-PLs. This could be due to the lower magnetic field strength (1.5 T), use of a spin echo sequence with long delays (TE = 60 ms), and/or lipid contamination (18). Künnecke et al. were successful in obtaining a better quality spectrum of bile *in vivo* in cynomolgus monkeys using a 4.7 T animal scanner and a custom-built surface coil in transmit/receive mode with the aid of a respiratory-gated sequence (19). They identified and quantified different bile components, bile acids and their taurine and glycine conjugates, including the previously reported phospholipids (19).

Our preliminary study on pigs using a 3 T clinical scanner and a custom-built receive array coil revealed a significant improvement in the spectral quality of *in vivo* ^{1}H spectra of gallbladder bile (20, 21). The resultant spectra were promising enough to recommend exploring the possibility of acquiring such spectra in humans. In the current study, we report 1D ^{1} H MRS of human gallbladder bile at 3 T including the detection and quantification of major lipid components. In addition, we report the first acquisition of 2D L-COSY data for human gallbladder bile *in vivo.*

3.3 METHODS

3.3.1 Subject Characteristics

Healthy volunteers were recruited at the National Research Council (NRC) and Health Sciences Centre, University of Manitoba, Winnipeg according to the protocol approved by the Research Ethics Boards of the University of Manitoba and the NRC. Informed consent was obtained from each subject and the study protocol conforms to the ethical guidelines of the 1975 Declaration of Helsinki. The subjects had no history of acute or chronic liver disease, inflammatory bowel disease or heavy alcohol use (>3 drinks/day). None of the subjects was on medication which could cause liver toxicity. The possibility of active HPB disorders was ruled out in all subjects using a combination of medical history, physical examination, and laboratory blood tests including bilirubin (total and direct), aspartate aminotransferase (AST), alanine aminotransferase (ALT), gamma-glutamyl transferase (GGT), lipase, alkaline phosphatase (ALP) and international normalized ratio (INR).

After optimizing the scanning parameters on a number of healthy volunteers, MRS data were acquired from 22 subjects. We collected 1D data from 17/22 subjects and 2D data

from 15/22 subjects. We were able to acquire both 1D and 2D data in 7/22 subjects. Out of the 17 1D spectra, 3 were excluded due to lipid contamination, ineffective water suppression, or motion artifacts due to failed respiratory gating. The 14 subjects included in the final 1D analysis comprised 11 females and 3 males (mean ages 40 and 33 respectively, range 21 – 55). In the case of 2D, data from 4/15 subjects were excluded due to low SNR and the same issues described above. The 11 subjects included in the final 2D analysis were 7 females and 4 males (mean ages 41 and 35 respectively, range 26 – 55). Details of the subjects' characteristics and biochemical data are given in Table 3.4-3.

3.3.2 MRS Experiments

MRS experiments were performed on a Siemens 3 T Magnetom Trio clinical scanner (RF transmitter frequency = 123.22 MHz). The body coil transmitted the RF pulses. A custom-built surface receive array coil, which passed the safety checks of the NRC and was approved by both Research Ethics Boards of the NRC and the University of Manitoba, was used as an RF receiver. Single voxel spectroscopy (SVS) was performed using the PRESS sequence with bellow respiratory-gating (VB15 & VB17, Siemens, Erlangen, Germany). 1D experiments were performed on solutions of phosphocholine chloride calcium salt tetrahydrate (PhC), taurocholic acid sodium salt (TCA), and glycodeoxycholic acid sodium salt (GDCA) representing three major biliary biochemicals – chol-PLs, TCBAs and GCBAs, respectively. These experiments were used to verify the accuracy of quantification of chol-PLs, TCBAs and GCBAs in the bile at 3 Tesla. The 1D ^{1}H spectra were then acquired from human gallbladder bile *in vivo*. Finally, we edited the PRESS sequence to L-COSY as described by Thomas et al (15,

16). In this method, the last 180° refocusing pulse of the PRESS sequence was replaced by a hyperbolic secant 90^0, the same as the first 90^0 excitation RF pulse and a 0.8 msec time increment (Δt_1) was applied between the first refocusing and the second 90^0 (coherence transfer) RF pulses in each measurement (15, 16). In both 1D and 2D experiments, we optimized the voxel size to 12×12×12 mm^3 to minimize the effect of lipid contamination from the liver or the body fat outside the gallbladder. Spatial saturation bands were positioned around the gallbladder in order to further minimize such effects. Application of bellow respiratory-gated sequences reduced the extent of motion artifact due to breathing. A manual localized shimming was performed before the acquisition of spectroscopic data (Full Width Half-Maximum (FWHM) of < 15 Hz for water peak). Water suppression was applied with a band width in the range 35 – 50 Hz.

One-dimensional (1D) ^{1}H MRS Experiments

In vitro Phantom Measurements

Aqueous solutions of PhC, TCA, and GDCA representing the major bile components (chol-PLs, TCBAs, and GCBAs) were prepared based on a method described in the LCModel User's Manual (22). Each phantom contained a solution of a metabolite with known concentration (21.24 mM PhC, 20.18 mM TCA, or 37.42 mM GDCA), 210 mM sodium formate, and 2.0 mM 3-(trimethylsilyl)-1-propanesulfonic acid sodium salt (DSS). The pH of all the phantom solutions was adjusted to 7.2 using 1.0 M hydrochloric acid/sodium hydroxide. The above solutions of each metabolite were held in a sealed container which was immersed in a water container (by gluing it to the bottom) surrounded by an oil container resembling the fat around the gallbladder.

Three orthogonal MR images were acquired using half-fourier acquisition single-shot turbo spin-echo (HASTE) sequences (VB15 & VB17, Siemens, Erlangen, Germany) (matrix = 192×256, slice thickness = 6mm, FOV = 270×360 mm^2, TE/TR =101/1000 msec) in order to localize the solution container. Six spatial saturation bands were placed around the water container in order to minimize the effect of the surrounding oil. After adjusting the frequency and the receiver gain, manual shimming and water suppression were performed. 1D ^1H spectra were acquired from the above three solutions using the PRESS sequence. The following acquisition parameters were used: voxel size = 12×12×12 mm^3, TE = 30 msec, TR = 10000 msec, band width = 2000 Hz, vector size: 2048 points, and NS = 256. A second spectrum with 8 and/or 16 scans was acquired from the same voxel using the same parameters but without water suppression in each experiment.

In vivo measurements

The subjects fasted for at least 4 hours before the study. Three orthogonal MR images were used to localize the gallbladder. The images were obtained during breath-hold at the end of a regular expiration using HASTE sequences with identical acquisition parameters as mentioned above. A 12×12×12 mm^3 voxel was positioned in the gallbladder using these images. Six spatial saturation bands were positioned around the gallbladder in order to reduce lipid contamination. After adjusting the frequency and setting the receiver gain to high, manual shimming and water suppression were performed. 1D spectra were obtained using the bellow respiratory-gated PRESS sequence during last 10 – 30% of quiet expiration. The acquisition parameters were the same as those of *in vitro* experiments except for TR which was 2000 msec. We used the minimum possible TE of

the Siemens PRESS sequence (30 msec) in order to reduce signal loss due to T_2 relaxation. Although the TR was 2000 msec, one FID was recorded in each breath. Therefore, the effective TR (TR_{eff}) was equal to the average breathing cycle length in each subject. Considering that the scanning time obtained for each sequence from the scanner includes the adjustment time, we could not use the water suppressed 1D or 2D spectra for calculating breathing cycle length. Because the unsuppressed water 1D spectrum was acquired immediately after the 1D spectrum with the same parameters (no need for adjustments), we used this data for calculating TR_{eff}. We divided the scanning time by the number of scans to calculate the average breathing cycle length which is equal to TR_{eff}. As a result, the TR_{eff} in different subjects was variable in the range of 3750 – 7438 msec, and the mean of TR_{eff} in all subjects was 5366 msec. Therefore, our spectra in most cases were almost fully relaxed. NS was 256 except in one case which was 128. The average time for gallbladder localization, adjustment of parameters, and data acquisition was 42 minutes. Considering the average TR_{eff} was 5366 msec, the average time for 256 scans was 22.89 minutes. The rest of the time was needed for acquiring localizer images, manual adjustments (specially shimming and water suppression) and acquiring 1D spectrum with unsuppressed water.

Two-dimensional (2D) in vivo ^{1}H MRS Experiments

Although it is possible to identify and quantify different metabolites using 1D ^{1}H MRS, the presence of overlapping signals from structurally similar metabolites makes the identification of some of the resonances very challenging. Therefore, we made use of 2D L-COSY experiments to detect some of these signals unambiguously (15, 16).

A 12×12×12 mm^3 voxel was positioned in the gallbladder using the three orthogonal localizer images. Spatial saturation bands were positioned around the gallbladder to reduce lipid contamination. After adjusting the frequency, and setting the receiver gain to high, manual shimming and water suppression were performed. 2D L-COSY data were acquired during the last 10-30% of quiet expiration using the bellow respiratory-gated sequence. The following spectral parameters were used throughout: TE = 30 msec, TR = 2000 msec, band width = 2000 Hz, vector size = 2048 points, NS =12, time increment ($\Delta t1$) = 0.8 msec and number of measurements = 50 or 64 except in one case which had only 40 measurements. The original minimum TR was set to 2000 msec. Considering that in each breath one FID was recorded, the TR_{eff} was variable. The approximate time for adjusting parameters and the collection of 2D data was 49 minutes. In the majority of cases, since 2D data were acquired right after 1D, there was no need for repeating the localizers and we used the adjusted parameters from the 1D as a guideline and performed only fine adjustments (which took a very short time). As a result, if we ignore the adjustment time, the average TR_{eff} for 2D will be 4548 msec which is shorter than 1D.

3.3.3 Data Processing

1D ^{1}H MRS Experiments

The raw data were first processed by an in-house MATLAB program generated at UCLA, and modified at NRC. This program facilitated the inspection of individual scans. The scans which were distorted by lipid contamination, failed water suppression or with very low SNR (no detectable signal) were discarded. Out of the 256 scans acquired, 216 undistorted scans were averaged in all subjects except for two cases. In the first case, only 128 scans were acquired due to time limitation. Out of 128 scans, 119 were analyzed

after eliminating the distorted scans. In the other case, out of 256 scans only 52 were analyzed. The individual spectra in all scans were aligned (using the methylene [-CH_2-] proton signal of the lipid peak at 1.26 ppm or the trimethylammonium [-N^+-$(CH_3)_3$] signal of chol-PLs at 3.22 ppm) to minimize frequency drifts due to breathing motion artifacts, and then averaged. Eddy current correction was applied using the unsuppressed water signal (23) and the data from individual coil elements were combined using an optimized method based on noise correlation (24). After this preliminary processing, the data were transferred to FELIX-2007 software (FELIX NMR Inc., San Diego, California, USA). The data were then apodized using an exponential function with a line broadening of 0.5 Hz, and Fourier transformed. First and second order phase and baseline corrections were applied on the real part of the spectrum. Finally, the spectrum was referenced to the lipid -CH_2- peak at 1.26 ppm or the -N^+-$(CH_3)_3$ signal of chol-PLs at 3.22 ppm.

The data acquired from phantom solutions were processed similarly. The first 216 scans were averaged and the spectrum was referenced to the DSS signal at 0 ppm.

Quantification of Biliary Biochemicals

Chemical shift assignments in the bile ^{1}H spectrum were made according to the previous *in vitro* (10, 12) and *in vivo* studies on human (18) and monkey bile (19). Twenty-one different peaks in the water-suppressed bile ^{1}H spectrum were fitted to Lorentzian line shapes by deconvolution based on a simulated annealing algorithm (FELIX NMR Inc., San Diego, California, USA). Similarly, the water peak of the bile spectrum obtained without water suppression was fitted and used as an internal reference. After fitting, the peak areas of methyl [-CH_3] signal representing TBAs plus cholesterol at 0.66 ppm, the -CH_2- signal of TCBAs at 3.08 ppm, the –$N^+(CH_3)_3$ signal of chol-PLs at 3.22 ppm, the

-CH_2- signal of GCBAs at 3.74 ppm, and the amide signals [-NH] of GCBAs and TCBAs in the region 7.76 – 8.05 ppm were measured. Molar concentrations of all the above biliary lipids were calculated by using the following equation, similar to that reported by Fayad et al. (25):

$$[Lipid](mM) = \frac{PeakArea\,(Lipid)}{PeakArea\,(H2O)} \cdot \frac{No.of\ \mathrm{Protons}(H2O)}{No.of\ \mathrm{Protons}(Lipid)} \cdot \frac{10^6}{Mol.Wt.(H2O)} \cdot \frac{fT1(H2O)}{fT1(Lipid)} \cdot \frac{fT2(H2O)}{fT2(Lipid)} \cdot CF(H2O)$$

……Eq. (1)

Where, CF(H_2O) = 0.9, is a conversion factor for the water content of human gallbladder bile which is considered to be 90% by weight (26), $fT1 = 1 - \exp(-TR/T1)$ and $fT2 = \exp(-TE/T2)$ are correction factors due to the T_1 and T_2 relaxation times of water and individual lipid molecules and were calculated as reported elsewhere (25, 27). In order to confirm the accuracy of the calculations, the peak areas of the signals acquired from phantom solutions were also quantified similarly.

2D L-COSY Experiments

After the preliminary processing with MATLAB program as described for the 1D experiments, the 2D raw data were transferred to FELIX-2007 software (FELIX NMR Inc., San Diego, California, USA), and processed in the magnitude mode. The first 256 points in the $\mathbf{t_2}$ dimension and the first 50 measurements in the $\mathbf{t_1}$ dimension were processed. The $\mathbf{t_1}$ dimension was linear-predicted to 64 measurements. The raw data were zero filled to 2048 and 128 points along $\mathbf{t_2}$ and $\mathbf{t_1}$ dimensions respectively. In order to reduce noise, a skewed sine-bell apodization function with 0° shift (skew parameter of 0.5-0.6) was applied in both dimensions. After complex Fourier transformation in both

dimensions, the spectra were referenced to the diagonal peak of chol-PLs ($\mathbf{F_2} = \mathbf{F_1} = 3.22$ ppm) or to the diagonal peak of the amide signal ($\mathbf{F_2} = \mathbf{F_1} = 7.8$ ppm).

3.4 RESULTS

Figure 3.4-1 represents the ^1H spectra of PhC, TCA, and GDCA solutions representing three major biliary biochemicals – chol-PLs, TCBAs and GCBAs. The assignment of peaks and their selection for the quantification was based on the results from previous *in vitro* (10, 12) and i*n vivo* studies (18, 19). Figure 1(A) shows the ^1H MR spectrum of aqueous solution of PhC. We used PhC instead of phosphatidylcholine (PC) due to the similarity of its head group with that of PC and also due to its free solubility in water. The peak at 3.20 ppm was assigned to the $-N^+(CH_3)_3$ group of PhC. Figure 1(B) was obtained from the phantom solution of TCA representing TCBAs. The triplet at 3.06 ppm is due to its H-26 $-CH_2-$ signal whereas peaks at 0.68 and 7.99 ppm were assigned to the H-18 $-CH_3$ and amide [-NH] groups of TCBAs respectively. Figure 1(C) represents the spectrum recorded from a GDCA solution. The signals resonating at 0.68, 3.72, and 7.83 ppm were assigned to the H-18 $-CH_3$ group, the H-25 $-CH_2-$ group, and the amide [-NH] group of GCBAs respectively. All these spectra were recorded using a TR of 10000 msec and TE of 30 msec, ensuring complete relaxation and with negligible T_2 loss.

Figure 3.4-1: ^{1}H spectra of (A) Phosphocholine chloride calcium salt tetrahydrate (PhC), (B) Taurocholic acid sodium salt (TCA), and (C) Glycodeoxycholic acid sodium salt (GDCA) solutions representing three major biliary biochemicals – chol-PLs, TCBAs and GCBAs respectively. The signals were assigned based on the previous *in vitro* (10, 12) and *in vivo* studies (18, 19). *Assignments:* 1, 3-(trimethylsilyl)-1-propanesulfonic acid sodium salt (DSS); 2, $-N^{+}-(CH_3)_3$ group of PhC; 3, residual water; 4, H-18 protons of $-CH_3$ group of TCA; 5, H-26 protons of $-CH_2-$ group of TCA; 6, amide [-NH] group of TCA; 7, H-18 protons of $-CH_3$ group of GDCA; 8, H-25 protons of $-CH_2-$ group of GDCA; 9, amide [-NH] group of GDCA.

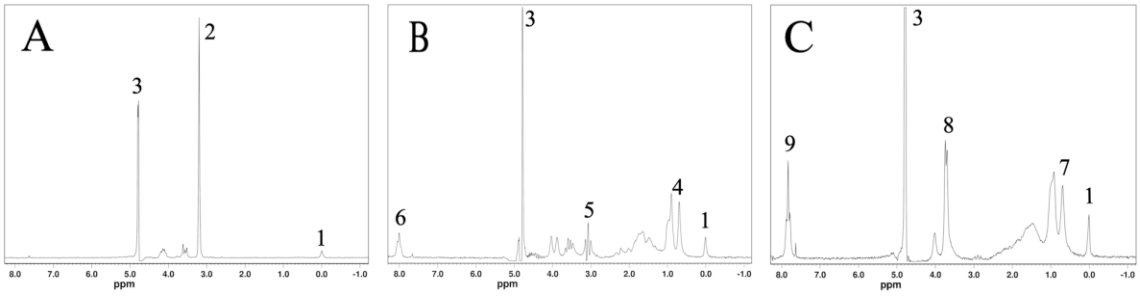

T_1 and T_2 relaxation times of various bile metabolites were measured using porcine bile. Table 3.4-1 lists the T_1 and T_2 values of major bile metabolites quantified in this study including water which was used as an internal reference.

Table 3.4-1: T_1, T_2 relaxation times of major bile metabolites calculated using porcine bile

Metabolite	TBAs 0.65 ppm	TCBAs 3.01 ppm	chol-PLs *3.22 +3.15ppm	GCBAs 3.74 ppm	GCBAs+TCBAs 7.95ppm	Water 4.78 ppm
T_1 value (msec)	233	383	298	360	352	780
T_2 value (msec)	25	93	155	84	36	172

GCBAs, glycine-conjugated bile acids; TCBAs, taurine-conjugated bile acids; chol- PLs, choline containing phospholipids.

T_1 and T_2 relaxation times were calculated using FELIX 2007 software.

*, Porcine bile used for T_1 and T_2 measurements showed an additional peak at 3.15 ppm in the chol-PLs region.

Table 3.4-2 lists actual and calculated concentrations of biochemicals from phantom solutions determined using current quantification methodology. The concentrations of metabolites before and after applying T_1 and T_2 corrections were compared with the actual concentration of each phantom solution to prove the reliability of the quantification. The concentrations of metabolites determined after applying both T_1 and T_2 corrections were very close to the actual concentrations except for GCBAs which was quantified using the amide [-NH] signal resonating at 7.83 ppm. From Table 3.4-2, it is clear that no corrections were required for the quantification of GCBAs determined using its amide signal. Since the amide peak in human/porcine bile is a combination of both TCBAs and GCBAs, the T_1 and T_2 corrections are mainly required for the amide signal of TCBAs. Since the H-26 -CH_2- signal of TCA at 3.06 ppm [peak **5** in Figure 3.4-1(B)] had an apparent phasing problem, the quantification of this signal in the phantom experiments was not feasible.

Table 3.4-2: Concentrations of metabolites (mM) before and after T_1, and T_2 corrections compared to the actual concentrations of phantom solutions

Metabolite (peak used)	PhC (3.20 ppm)	TCA (0.68 ppm)	TCA (7.99 ppm)	GDCA (0.68 ppm)	GDCA (3.72 ppm)	GDCA (7.83 ppm)
Concentration (mM)	22.69	7.08	11.26	13.74	32.41	37.04
Corrected concentration (mM)	23.13	19.74	21.77	38.31	38.90	71.59
Actual solution concentration (mM)	21.24	20.18	20.18	37.42	37.42	37.42

PhC, phosphocholine chloride calcium salt tetrahydrate; GDCA, glycodeoxycholic acid sodium salt; TCA, taurocholic acid sodium salt.

Figure 3.4-2 illustrates a typical ^{1}H MR spectrum recorded from the gallbladder bile of a healthy volunteer *in vivo* at 3 T using a custom-built receive-only coil. Panels (A), (B), and (C) represent three orthogonal images acquired at the end of expiration during a regular breath-hold in order to position a 12x12x12 mm^3 voxel in the gallbladder. Panel (D) shows the corresponding ^{1}H MR spectrum obtained from this voxel. The majority of signals belong to major biliary lipids – chol-PLs, cholesterol and various bile acids. The peaks were assigned based on the *in vitro* studies performed by Ijare et al. (10) and Gowda et al. (12) and the *in vivo* studies on human (18) and monkey bile (19). The signal at 0.66 ppm, marked as peak **1**, was assigned to the -CH_3 group of TBAs (H-18 protons). This peak has contributions from cholesterol as well (10, 19). Peak **2** at 0.88 ppm was assigned to protons of the ring bound -CH_3 group of bile acids (H-19 protons). Peak **3** in the region 0.99 – 1.02 ppm was assigned to the H-21 -CH_3 protons of bile acids (12, 19). The signal at 1.26 was assigned to the -CH_2- protons of the aliphatic tail of phospholipids (peak **4**). A group of overlapping peaks in the region 1.45 – 2.73 ppm (region **5**) represents the remainder of the aliphatic protons in bile acids, chol-PLs, and cholesterol (10, 19). The $–N^{+}(CH_3)_3$ group of chol-PLs was observed at 3.22 ppm, peak **7** (10, 18, 19). The peak at 3.08 ppm (peak **6**) was assigned to the H-26 -CH_2- group of TCBAs, whereas the signal at 3.74 ppm was assigned to the H-25 -CH_2- group of GCBAs (peak **8**) (10,19). The olefinic [-CH=CH-] protons of chol-PLs resonate at 5.26 ppm, were marked as peak **10** (19). Lastly, the broad overlapping region (peak **11**) resonating in the region 7.76 – 8.05 ppm was assigned to the amide [-NH] groups of both GCBAs and TCBAs (10, 19). Panel (E) compares the actual spectrum of human bile *in vivo* (bottom) with its

synthesized spectrum obtained by FELIX-2007 software, based on Lorentzian fitting (middle) and the residual spectrum (top).

Figure 3.4-2: ^{1}H MR spectrum of human gallbladder bile acquired from a healthy volunteer *in vivo* at 3 T Siemens scanner using a custom-built receive only coil. Panels (A), (B), and (C) show the transverse, coronal and sagittal images acquired at the end of expiration during a regular breath-hold and used for the positioning of a 12x12x12 mm^3 voxel in the gallbladder. (D) The corresponding ^{1}H MR spectrum of gallbladder bile obtained from the above voxel. The peaks were assigned based on the previous *in vitro* (10, 12) and *in vivo* (18, 19) studies. *Assignments:* 1, H-18 protons of -CH_3 group of TBAs. This peak also has contribution from cholesterol H-18 protons of -CH_3 peak; 2, protons from the ring bound -CH_3 group of bile acids (H-19); 3, H-21 -CH_3 protons of bile acids; 4, -CH_2- protons of aliphatic tail of chol-PLs; 5, the remainder of the aliphatic protons in bile acids, chol-PLs, and cholesterol; 6, H-26 protons of -CH_2- group of TCBAs; 7, $–N^{+}(CH_3)_3$ group of chol-PLs; 8, H-25 protons of -CH_2- group of GCBAs; 9, residual water; 10, olefinic [-CH=CH-] protons of chol-PLs; 11, amide [-NH] group of both GCBAs and TCBAs. Panel (E) compares the actual spectrum of human bile *in vivo* (at the bottom) with its synthesized spectrum (in the middle); and the residual spectrum is shown at the top.

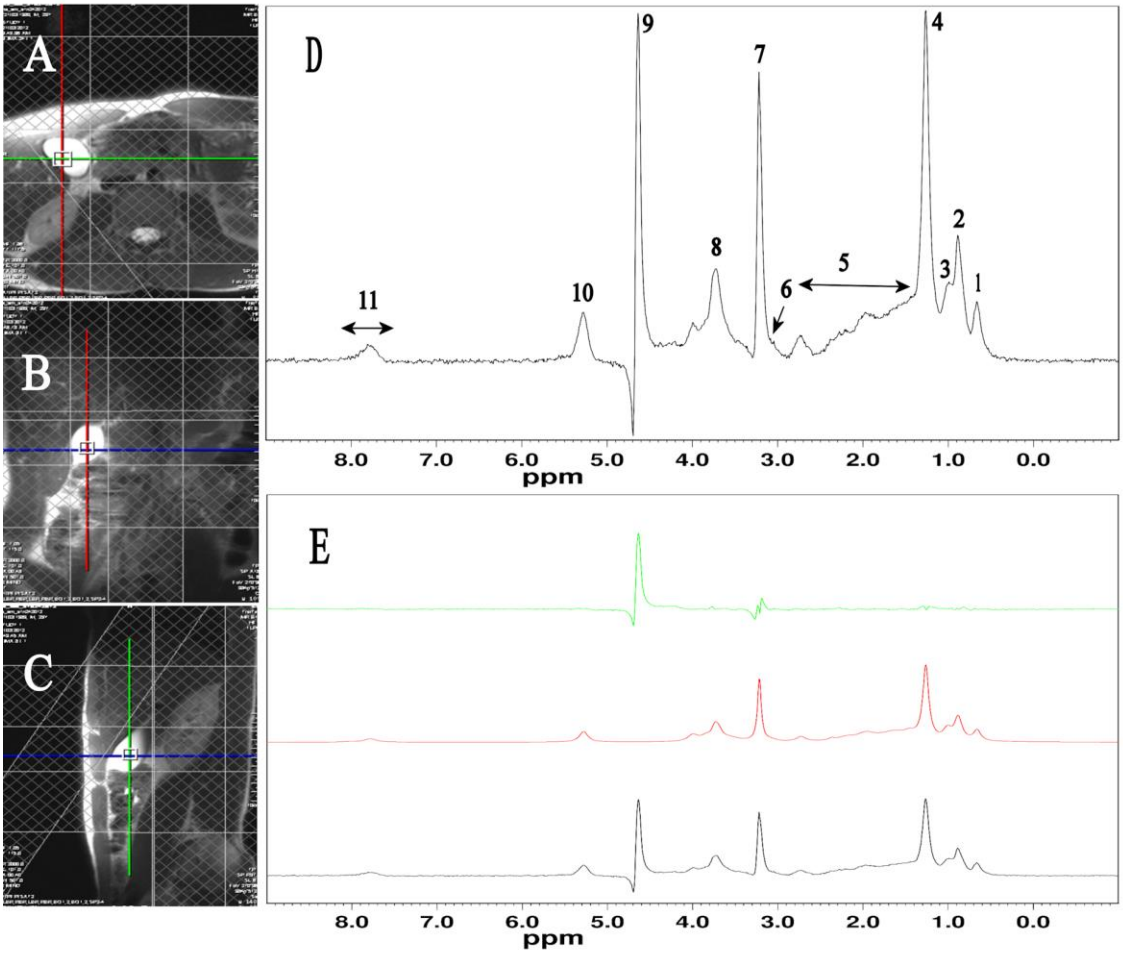
A
B
C
D
9
7
4
8
2
5
3
6
1
11
10
8.0
7.0
6.0
5.0
4.0
3.0
2.0
1.0
0.0
ppm
E
8.0
7.0
6.0
5.0
4.0
3.0
2.0
1.0
0.0
ppm

Out of the 17 spectra obtained from healthy volunteers, 14 were included in the quantification (see Table 3.4-3 for details).

Table 3.4-3: Age, sex and blood biochemistry of healthy volunteers participated in the study

Subject	Age	Sex	Bilirubin Total (μM)	Bilirubin Direct (μM)	AST (U/L)	ALT (U/L)	GGT (U/L)	Lipase (U/L)	ALP (U/L)	INR
1	41	F	9	3	22	14	-	69	77	-
2	43	M	5	2	21	19	-	40	69	1.2
3	21	F	7	-	19	20	-	31	74	0.9
4*	26	F	6	<2	17	15	13	30	41	1
5*	36	F	20	4	22	13	22	35	51	-
6*	54	F	8	2	23	14	18	30	84	1
7*	27	M	-	5	31	24	14	20	80	1
8	55	F	3	<2	22	20	-	44	86	1.1
9	31	F	4	<2	19	17	-	84	50	1
10	44	F	10	<2	20	12	11	41	43	1
11*	26	F	13	3	19	14	14	35	50	1
12	49	F	4	<2	20	15	14	50	59	0.9
13*	54	F	6	<2	20	17	10	-	73	0.9
14*	29	M	15	3	35	17	13	46	71	1
15#	36	M	9	2	19	21	-	45	102	1
16#	49	M	3	<2	22	43	37	39	72	1
17#	55	F	4	<2	24	15	20	45	75	1
18#	38	F	8	<2	26	33	35	23	55	0.9

-, not reported by the clinical laboratory; *, participated in both 1D and 2D experiments; #, participated only in 2D experiments. AST, aspartate aminotransferase; ALT, Alanine aminotransferase; GGT, gamma-glutamyl transferase; ALP, alkaline phosphatase; INR, international normalized ratio; μM, micromolar; U/L, unit/liter; M, male; F, female.

The normal values of blood biochemistry: Bilirubin Total, 2-20 μM; Bilirubin Direct, <7 μM; AST, 10-32 U/L; ALT, M, <30, F, <25 U/L; GGT, M, 5-38, F, 5-29 U/L; Lipase, < 60U/L; ALP, 30-120 U/L; INR, 0.9-1.1.

Peaks of bile metabolites with a known role in HPB disorders (7-11,17,28), and which were resolved in the *in vivo* ^{1}H MR spectrum were selected for the quantification (i.e. peaks **1**, **6**, **7**, **8**, and **11** in panel D). Table 4 lists the concentrations (mM) of metabolites quantified after applying T_1, T_2 and CF(H_2O) corrections as discussed in the methods section. Mean and standard deviation for TBAs plus cholesterol, TCBAs, GCBAs, and chol-PLs were calculated. From Table 3.4-4, it is obvious that the mean concentrations of all the quantified metabolites were well within the range of biliary biochemicals reported earlier (10, 18, 29).

Table 3.4-4: Concentration of metabolites (mM) in healthy volunteers and their mean and SD

Subject	(TBAs+ Cholesterol) 0.66 ppm	TCBAs 3.08 ppm	chol-PLs 3.22 ppm	GCBAs 3.74 ppm	TBAs (amide group) 7.76-8.05 ppm
1	120.43	56.71	69.90	51.44	102.18
2	NR	NR	69.58	98.88	106.87
3	97.73	15.36	44.64	NR	96.29
4	115.55	50.92	70.97	36.98	108.29
5	186.25	29.32	66.47	78.75	99.50
6	115.21	17.36	31.41	23.79	40.16
7	82.76	NR	25.21	43.68	22.39
8	133.16	16.38	37.75	73.59	83.90
9	72.09	5.83	21.95	12.75	21.32
10	47.58	NR	24.43	28.18	20.61
11	230.24	29.62	79.55	101.51	ND
12	91.28	19.76	36.78	26.03	ND
13	235.15	30.41	58.34	76.13	93.97
14	77.71	11.34	29.08	58.68	72.77
Mean	123.47	25.73	47.58	54.65	72.35
SD	59.09	15.96	20.65	29.21	35.80

TBAs, total bile acids; GCBAs, glycine-conjugated bile acids; TCBAs, taurine-conjugated bile acids; chol-PLs, choline-containing phospholipids; NR, not resolved; ND, not detected.

Figure 3.4-3 shows the 2D L-COSY spectrum of human gallbladder bile obtained *in vivo* from a healthy volunteer. This is the first report of an *in vivo* 2D L-COSY spectrum of human gallbladder bile. The i*n vivo* 2D L-COSY spectrum was compared with its *in vitro* counterpart (8, 13), and the following assignments were made: Diagonal peak ($\mathbf{F_2}$ = $\mathbf{F_1}$ = 7.81 ppm) along with a cross peak ($\mathbf{F_2}$ = 7.81, $\mathbf{F_1}$ = 3.62 ppm) represent the amide group of TCBAs and GCBAs (contours **1** and **1a**). It should be noted that both TCBAs and GCBAs were overlapping compared to the *in vitro* spectra (8). This is due to the use of a relatively lower magnetic field strength (3 T vs. 8.5 T) in this study. Diagonal peak ($\mathbf{F_2}$ = $\mathbf{F_1}$ = 5.24 ppm) represents the olefinic [-CH=CH-] protons of chol-PLs (marked as **2)** along with the cross peaks ($\mathbf{F_2}$ = 5.24, $\mathbf{F_1}$ = 2.75 ppm) and ($\mathbf{F_2}$ = 5.24, $\mathbf{F_1}$ = 1.96 ppm) represent J-coupling of the olefinic protons with neighbouring methylene protons (contours **2a**, and **2b**). The glyceryl 2-CH signals of PC appeared as a cross peak ($\mathbf{F_2}$ = 5.24, $\mathbf{F_1}$ = 4.18 ppm) with low intensity (marked as **3**). This cross peak would serve as a marker in detecting the presence/absence of PC in bile and will be valuable in differentiating PC from other chol-PLs (8). The diagonal peak at ($\mathbf{F_2}$ = $\mathbf{F_1}$ =3.20 ppm) was assigned to the [$-N^+(CH_3)_3$] group of chol-PLs (marked as **4**), and the symmetric cross peaks at ($\mathbf{F_2}$ = 4.3, $\mathbf{F_1}$ = 3.6 ppm), and ($\mathbf{F_2}$ = 3.6, $\mathbf{F_1}$ = 4.3 ppm) represent J-coupling between [-N-CH_2-] and [-CH_2-O-] of chol-PLs (marked as **5a** and **5b**). The diagonal peak at ($\mathbf{F_2}$ = $\mathbf{F_1}$ = 3.00 ppm) (marked as **6**), was assigned to the H-26 -CH_2- protons of TCBAs along with the cross peak at ($\mathbf{F_2}$ = 3.5, $\mathbf{F_1}$ = 3.00 ppm) representing coupling between the H-25 and H-26 -CH_2- protons of TCBAs (marked as **6a**). The diagonal peak ($\mathbf{F_2}$ = $\mathbf{F_1}$ = 0.60 ppm) represents TBAs plus cholesterol (marked as **7**). It should be noted that the chemical shift values recorded in the 2D spectrum were slightly different from

those of 1D spectrum due to the limited number of data points available in the 2D spectrum in both dimensions.

Figure 3.4-3: 2D L-COSY spectrum of human gallbladder bile *in vivo* obtained from a healthy volunteer. The following diagonal peaks and cross peaks were assigned based on the *in vitro* studies (8, 13): 1and 1a, diagonal and cross peaks representing the amide group of TCBAs and GCBAs; 2, 2a and 2b, diagonal peak representing the olefinic [-CH=CH-] protons of chol-PLs and two cross peaks representing J-coupling of the olefinic protons with neighbouring methylene protons; 3, cross peak representing J-coupling of the glyceryl 2-CH with 3-CH_2 of PC; 4, diagonal peak representing the [-N^+-$(CH_3)_3$] group of chol-PLs; 5a and 5b, symmetric cross peaks showing J-coupling between [-N-CH_2-] and [-CH_2-O-] of chol-PLs; 6 and 6a, diagonal peak representing the H-26 -CH_2- protons of TCBAs and cross peak representing J-coupling between the H-25 and H-26 -CH_2- protons of TCBAs; 7, diagonal peak assigned to TBAs plus cholesterol.

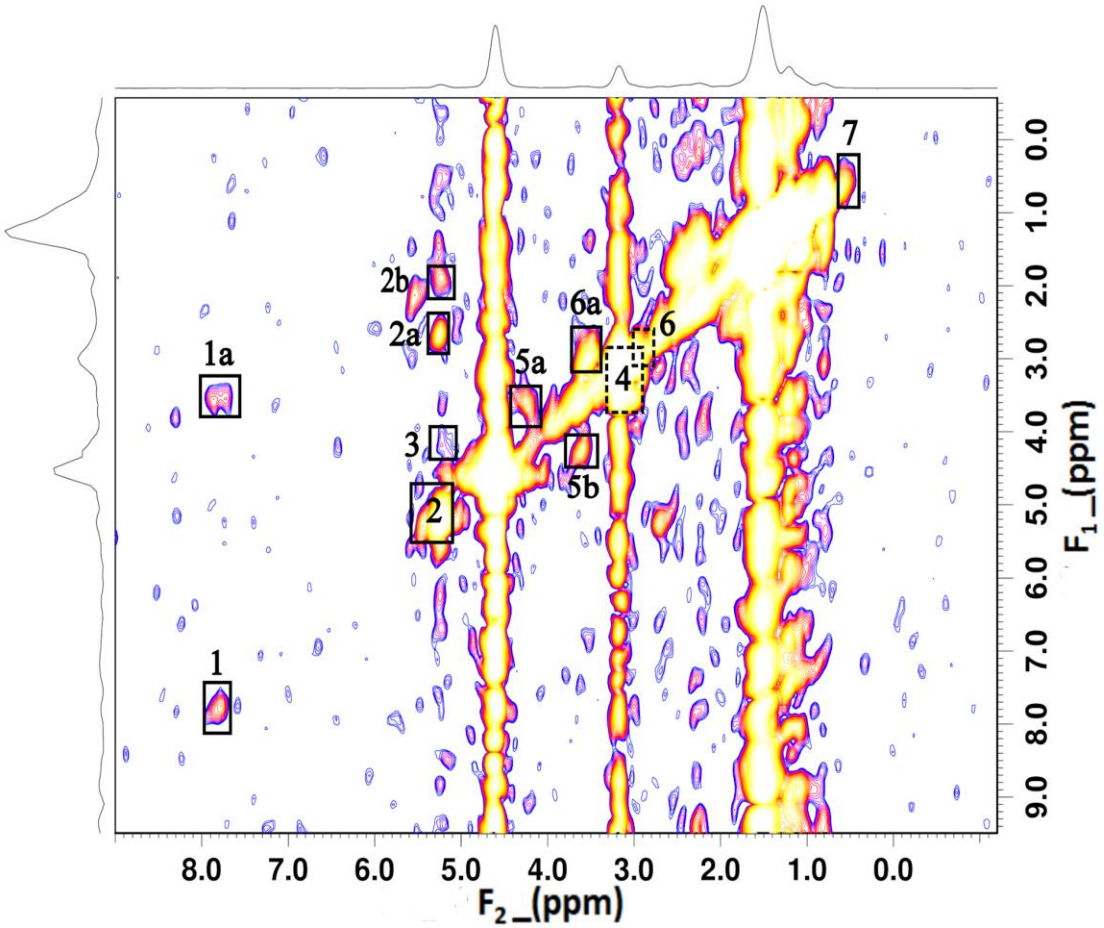
1a
2b
2a
3
2
1
5a
6a
6
4
5b
7
8.0
7.0
6.0
5.0
4.0
3.0
2.0
1.0
0.0
F2_(ppm)
0.0
1.0
2.0
3.0
4.0
5.0
6.0
7.0
8.0
9.0
F1_(ppm)

3.5 DISCUSSION

MR Spectroscopy can reveal subtle changes in biochemistry (due to its high resolution) following the metabolic alterations in the early stages of disease in a single experiment. This makes MRS an attractive tool in medical diagnosis (29, 30). In particular, it is a potential non-invasive tool for differentiating malignant changes from benign disorders (31).

In the past, a number of *in vitro* bile MRS studies introduced the value of this technique in the early diagnosis of HPB disorders (3-8, 17, 28, 32). Bile for such studies was collected during invasive procedures such as endoscopic retrograde cholangiopancreatography (ERCP) or surgery. *In vivo* MRS would have enormous potential in the analysis of bile non-invasively. The first attempt by Prescot et al. (18) was successful in quantifying only one component of bile, chol-PLs. The spectral quality was low and other components of bile such as GCBAs and TCBAs which have major role in the pathophysiology of HPB diseases were not quantified. This could be due to the low magnetic field strength, the use of spin echoes with long delays, magnetic susceptibilities, motion of gallbladder especially due to breathing, and/or lipid contamination. In the second attempt, Künnecke et al. obtained a good quality *in vivo* ^{1}H MR spectrum of gallbladder bile from cynomolgus monkeys using a 4.7 T animal scanner with the aid of a transmit/receive surface coil (19). However, the 4.7 T scanner and transmit/receive surface coils are not routine for clinical use. The current study showed the feasibility of acquiring a good quality ^{1}H MR spectrum under current clinical settings (3 T scanner and receive surface array coils).

To overcome some of the limitations of the previous study in humans (18), we employed a field strength of 3 T, and decreased TE from 60 to 30 msec which can significantly reduce the T_2 loss. Moreover, we used a bellow respiratory-gated sequence to reduce the motion artifacts due to breathing. With these improvements, we were able to quantify other major lipid components of bile – TBAs plus cholesterol, TCBAs and GCBAs including the previously reported chol-PLs (18). The peak resonating at 0.66 ppm has contributions from the H-18 methyl protons of TBAs and cholesterol. However, earlier *in vitro* studies have revealed that the percentage of cholesterol contributing to this signal is very low. As a result, the peak mostly represents the sum of TCBAs and GCBAs (10). This fact could partially be explained by lower mobility of cholesterol molecules due to their participation in phospholipid membranes. This results in loss of cholesterol signals due to shorter T_2 relaxation time (33). However, in the current study, the concentration of TBAs + cholesterol quantified from the 0.66 ppm peak was 123.47 ± 59.09 mM (mean ± SD) which is higher compared to the previous *in vitro* study (TBAs + cholesterol, 72.76 ± 55.06 mM, mean ± SD) as reported by Gowda et al. (29). However, most of the individual values (except in 3 cases, Table 3.4-4) fall in the range (0.38 – 178.61 mM) as reported by Gowda et al. (29). In the majority of *in vitro* studies, the samples were collected from participants who were suffering from some sort of HPB disorders, the major reason for ERCP to be performed. As a result, the concentrations determined in *in vitro* studies may reasonably be expected to differ from our *in vivo* results gathered non-invasively from healthy volunteers, without any medical interference and use of radiopaque agents.

Given that the TBAs pool in the bile is almost completely conjugated to glycine and/or taurine, and under the conditions of low biliary cholesterol, the levels of lipids determined from the 0.66 ppm peak should be comparable to the sum of TCBAs and GCBAs (10). However, in the current study, the concentration of lipids calculated from the 0.66 ppm peak is on average 53% higher than the sum of GCBAs and TCBAs (as opposed to the 10% expected due to contamination from cholesterol (19, 34). Surprisingly, the study by Künnecke et al. (19) on the gallbladder bile of monkeys revealed even higher concentrations of lipids in this region (267±47 mM (mean ± SD). One explanation could be the effect of lipid contamination by body fat surrounding the gallbladder in *in vivo* studies. Although we used spatial saturation bands around the gallbladder to suppress contribution from outside fat, it is difficult to remove such effects completely. Despite the use of respiratory-gated sequences, a residual breathing motion artifact may also contribute to the apparent lipid contamination.

Since a majority of bile acids in bile are conjugated to glycine and/or taurine, Ijare et al. explored the use of the amide protons of conjugated bile acids (resonating in the region 7.80 – 8.10 ppm) to quantify the sum of GCBAs and TCBAs for *in vitro* applications (13). However, the amide protons are in dynamic exchange with biliary water at physiologic pH (7.0 – 7.7) (35), and do not represent the true signal intensity. As a result, one of the prerequisites for using such a methodology was to adjust the pH of bile to a value slightly lower than the physiologic pH (6 ± 0.5). In *in vivo* studies such manipulation of pH is not possible; however, the pH of bile is generally decreased during its concentration in the gallbladder (36). This could be an advantage for *in vivo* studies. Our subjects had fasted overnight or for at least four hours in order to have a gallbladder

that was completely filled with bile. Therefore, the pH of bile should not affect the signal intensity of amide protons in the bile concentrated after overnight fasting. Based on Table 3.4-4, in most cases the concentrations of GCBAs and TCBAs calculated from the amide region are slightly less than the sum of concentrations calculated from 3.74 and 3.08 peaks. In two cases the signal from the amide region was not detected. This could be due to the very high pH of the bile. However, in three cases the concentrations of GCBAs and TCBAs calculated from amide region were slightly more than the sum of concentrations of GCBAs and TCBAs calculated from 3.74 and 3.08 peaks. Considering the breadth of the amide region, there could be a random error in measuring the area under these peaks.

A more accurate method of quantifying TCBAs and GCBAs is to use their -CH_2- peaks resonating at 3.08 and 3.74 ppm, respectively (10). This approach is independent of a pH effect. Moreover, these peaks are not affected by lipid contamination. Since the ratio of GCBAs/ TCBAs plays an important role in HPB disorders (10), determining this ratio may be valuable in the diagnosis of HPB diseases. In this study, the mean of the GCBAs/ TCBAs ratio was 2.48 (2.48 ± 1.51, mean ± SD) which is very close to the expected value, 3 (37). However, there were cases in which this ratio was even <1. Given the small sample size, it is difficult to make a rigorous conclusion in this study.

The chol-PLs were quantified from the signal resonating at 3.22 ppm following a strategy similar to that of Prescot et al. (18). The levels of chol-PLs determined in this study (47.58 ± 20.65 mM, mean ± SD) were comparable to those reported earlier (35.8 ± 9.8 mM, mean ± SD) (18).

As it is presented in Table 3.4- 4 there was a considerable variability in the concentration of biliary metabolites which may raise concerns regarding diagnostic value of these

metabolites. Such variability was noticed in the previous *in vitro* (29) and *in vivo* (18) studies as well. As it was explained by Khan et al. (17), the concentration of bile metabolites varies between subjects and within a subject over time. This is primarily due to variations in diet, nutritional status, drugs and environmental exposure. In an *in vitro* study by Albiin et al. (7), although there were also similar variabilities, the differences between normalized intensities of PC and TCBAs in non-cancer and cancer patients were statistically significant. Therefore, although there is a considerable variability in the concentrations of bile metabolites, the quantification of these metabolites is still useful and can be used for the differentiation of different hepatopancreatobiliary disorders.

Considering that age, sex, variation in diet, and exposure to drugs and environmental chemicals are responsible for part of variation in the concentrations of biliary metabolites (17, 19), eliminating such confounding factors may help decrease the variability. In the study by Künnecke et al. (19), the researchers selected male monkeys with similar ages and put them on a similar diet. The SD of total bile acids decreased to only 20% of the mean. Based on this study the biliary metabolites may represent the individual metabolism, as a result, if we follow the bile composition in a patient, we may be able to follow up the progress of the disease and this can be quite useful in the clinic.

In our phantom experiments (Table 3.4-2), the estimated concentrations of PhC, TCA, and GDCA determined from their representative peaks were very close to the actual concentrations of the solutions, following T_1 and T_2 corrections. The only exception was the amide region of GDCA which was overestimated. However, without any corrections the calculated concentration was very close to the actual concentration. Since the amide peak in porcine bile had overlapping signals from both GCBAs and TCBAs, the

determined T_1 and T_2 relaxation times may originate exclusively from TCBAs. Therefore, we didn't apply any corrections to the amide signal of GDCA during its quantification.

1D spectra cannot provide complete information regarding the metabolite composition of the bile. Furthermore, signals arising from some of the bile metabolites important in HPB pathologies, such as lactate and the glyceryl region of PC, overlap with lipid signals (8). Moreover, some important regions such as the amide region have a very low intensity in the 1D spectrum and are not detectable in some subjects. In order to detect such signals separately, 2D L-COSY spectra (15, 16) were obtained for the first time from human gallbladder bile *in vivo*. Cross peak from the PC-glyceryl signals ($\mathbf{F_2}$ = 5.24, $\mathbf{F_1}$ = 4.18 ppm) has been detected in the L-COSY spectrum which overlapped the lipid signal in the corresponding 1D spectrum. Detection of these signals may be helpful in the diagnosis of HPB pathologies (8).

3.6 CONCLUSION

This study showed the possibility of obtaining good quality 1D ^{1}H MR spectra of gallbladder bile *in vivo* using a 3 T clinical scanner. It facilitated the simultaneous quantification of TBAs plus cholesterol, TCBAs, and GCBAs including the previously reported chol-PLs, which have a major role in the pathophysiology of HPB diseases. This approach may be helpful in the early diagnosis of HPB disorders non-invasively. 2D techniques such as L-COSY will be valuable in the differentiation of PC from its hydrolysis products such as lysophosphatidylcholine and phosphorylcholine which are detrimental to the HPB system. Moreover, 2D techniques can augment the diagnostic

accuracy of 1D methods. However, 2D techniques are time-consuming and warrant further development in order to improve the spectral quality and reduce scanning time.

3.7 REFERENCES

1. Sherwood L. The digestive system. In: *Human Physiology: From Cells to Systems.* Alexander S, Glubka A, Crosby L, Oliveira L (Eds), Brooks/Cole Cengage Learning (USA): Belmont, CA, 2013; p 581-634.
2. Silverthorn D.U. The digestive system. In: *Human Physiology: An Integrated Approach*. Volker KK, Scanlan-Rohrer A, Reid AA, Williams A, Cogan D, Tabor N, Padial A (Eds). Pearson Education Inc. (USA): Boston, 2012; p 696-735.
3. Gowda GA. NMR spectroscopy for discovery and quantitation of biomarkers of disease in human bile. *Bioanalysis.* 2011; 3(16): 1877-1890.
4. Gowda GA. Human bile as a rich source of biomarkers for hepatopancreatobiliary cancers. *Biomark Med.* 2010; 4(2): 299-314.
5. Hofmann AF. The continuing importance of bile acids in liver and intestinal disease. *Arch Intern Med.* 1999; 159(22): 2647-2658.
6. Bezabeh T, Ijare OB, Albiin N, Arnelo U, Lindberg B, Smith ICP. Detection and quantification of D-glucuronic acid in human bile using ^{1}H NMR spectroscopy: relevance to the diagnosis of pancreatic cancer. *MAGMA.* 2009; 22(5): 267-275.
7. Albiin N, Smith ICP, Arnelo U, Lindberg B, Bergquist A, Dolenko B, Bryksina N, Bezabeh T. Detection of cholangiocarcinoma with magnetic resonance spectroscopy of bile in patients with and without primary sclerosing cholangitis. *Acta Radiol.* 2008; 49(8): 855-862.

8. Ijare OB, Bezabeh T, Albiin N, Arnelo U, Bergquist A, Lindberg B, Smith ICP. Absence of glycochenodeoxycholic acid (GCDCA) in human bile is an indication of cholestasis: a ^{1}H MRS study. *NMR Biomed.* 2009; 22(5): 471-479.
9. Nagana Gowda GA, Shanaiah N, Cooper A, Maluccio M, Raftery D: Visualization of bile homeostasis using ^{1}H-NMR spectroscopy as a route for assessing liver cancer. *Lipids.* 2009; 44(1): 27-35.
10. Ijare OB, Bezabeh T, Albiin N, Bergquist A, Arnelo U, Lindberg B, Smith ICP. Simultaneous quantification of glycine- and taurine-conjugated bile acids, total bile acids, and choline-containing phospholipids in human bile using ^{1}H NMR spectroscopy. *J Pharm Biomed Anal.* 2010; 53(3): 667-673.
11. Bezabeh T, Ijare OB, Albiin N, Bergquist A, Arnelo U, Löhr M, Hov JR, Smith ICP. Alteration in the Conjugation Pattern of Bile acids in Human Bile during Cholestasis: A ^{1}H MRS Study. *Proc. Intl. Soc. Mag. Reson. Med*. 2010; 18: 4590.
12. Gowda GA, Ijare OB, Somashekar BS, Sharma A, Kapoor VK, Khetrapal CL. Single step analysis of individual conjugated bile acids in human bile using ^{1} H NMR spectroscopy. *Lipids*. 2006; 41(6): 591-603.
13. Ijare OB, Somashekar BS, Gowda GA, Sharma A, Kapoor VK, Khetrapal CL. Quantification of glycine and taurine conjugated bile acids in human bile using ^{1} H NMR spectroscopy. *Magn. Reson. Med.* 2005; 53(6): 1441-1446.
14. Rothman DL, Behar KL, Hetherington HP, Shulman RG. Homonuclear ^{1}H double-resonance difference spectroscopy of the rat brain *in vivo*. *Proc Natl Acad Sci U S A.* 1984; 81(20): 6330-6334.

15. Thomas MA, Yue K, Binesh N, Davanzo P, Kumar A, Siegel B, Frye M, Curran J, Lufkin R, Martin P, Guze B. Localized two-dimensional shift-correlated MR spectroscopy of human brain. *Magn Reson Med.* 2001; 46(1): 58-67.
16. Thomas MA, Hattori N, Umeda M, Sawada T, Naruse S. Evaluation of two-dimensional L-COSY and JPRESS using a 3 T MRI scanner: from phantoms to human brain *in vivo*. *NMR Biomed.* 2003; 16(5): 245-251.
17. Khan SA, Cox IJ, Hamilton G, Thomas HC, Taylor-Robinson SD. *In vivo* and *in vitro* nuclear magnetic resonance spectroscopy as a tool for investigating hepatobiliary disease: a review of H and P MRS applications. *Liver Int.* 2005; 25(2): 273-281.
18. Prescot AP**,** Collins DJ, Leach MO, Dzik-Jurasz AS. Human gallbladder bile: noninvasive investigation *in vivo* with single-voxel ^{1}H MR spectroscopy. *Radiology* 2003; 229(2): 587-592.
19. Künnecke B, Bruns A, von Kienlin M. Non-invasive analysis of gallbladder bile composition in cynomolgus monkeys using *in vivo* ^{1}H magnetic resonance spectroscopy. *Biochim. Biophys. Acta.* 2007; 1771(4): 544-549.
20. Mohajeri S, Bezabeh T, King SB, Ijare OB, Minuk GY, Lipschitz J, and Smith ICP. *In vivo* ^{1}H MRS of gallbladder bile using an optimized 8-Channel phased array at 3T: towards improved diagnosis of hepatopancreatobiliary diseases. *Proc. Intl. Soc. Mag. Reson.* Med. 2010; 18: 4595.
21. Ijare OB, Smith ICP, Mohajeri S, Bezabeh T. Magnetic resonance spectroscopy of bile in the diagnosis of hepatopancreaticobiliary diseases: past, presence and future.

In: *Future directions of NMR.* Vol. I, Khetrapal CL, Kumar A, Ramanathan KV (Eds). Springer (India): New Delhi, 2011; p 45-53.

22. Provencher S. Making the basis set. In: *LCModel & LCMgui User's Manual*. LCMODEL Inc. (Canada): Oakville, Ontario, 2013; p 79-102. http://lcmodel.ca/pub/LCModel/manual/manual.pdf.
23. Klose U. *In vivo* proton spectroscopy in presence of eddy currents. *Magn Reson Med.* 1990; 14(1): 26-30.
24. Roemer PB, Edelstein WA, Hayes CE, Souza SP, Mueller OM. The NMR phased array. *Magn Reson Med.* 1990; 16(2): 192-225.
25. Fayad LM, Salibi N, Wang X, Machado AJ, Jacobs MA, Bluemke DA, Barker PB. Quantification of muscle choline concentrations by proton MR spectroscopy at 3 T: technical feasibility. *AJR Am J Roentgenol.* 2010; 194(1): W73-79.
26. Van Erpecum KJ. Biliary lipids, water and cholesterol gallstones. *Biol Cell.* 2005; 97(11): 815-822.
27. Bolan PJ, Meisamy S, Baker EH, Lin J, Emory T, Nelson M, Everson LI, Yee D, Garwood M. *In vivo* quantification of choline compounds in the breast with ^{1}H MR spectroscopy. *Magn Reson Med.* 2003; 50(6): 1134-1143.
28. Cox IJ, Sharif A, Cobbold JF, Thomas HC, Taylor-Robinson SD. Current and future applications of *in vitro* magnetic resonance spectroscopy in hepatobiliary disease. *World J. Gastroenterol.* 2006; 12(30): 4773-4783.
29. Gowda GA, Somashekar BS, Ijare OB, Sharma A, Kapoor VK, Khetrapal CL. One-step analysis of major bile components in human bile using ^{1}H NMR spectroscopy. *Lipids.* 2006; 41(6): 577-589.

30. Smith ICP, Baert R. Medical diagnosis by high resolution NMR of human specimens. *IUBMB Life.* 2003; 55(4-5): 273-277.

31. Mountford C, Smith ICP, Bourne R. Correlation of Histopathology with Magnetic Resonance Spectroscopy of Human Biopsies. In: *Modern Magnetic Resonance*. Vol. II, Webb GA (Ed). Springer (U.K.): London, 2006; p 1027-1036.

32. Nishijima T, Nishina M, Fujiwara K. Measurement of lactate levels in serum and bile using proton nuclear magnetic resonance in patients with hepatobiliary diseases: its utility in detection of malignancies. *Jpn J Clin Oncol.* 1997; 27(1): 13-17.

33. Ellul JP, Murphy GM, Parkes HG, Slapa RZ, Dowling R.H. Nuclear magnetic resonance spectroscopy to determine the micellar cholesterol in human bile. *FEBS Lett.* 1992; 300 (1): 30–32.

34. Stephan ZF, Armstrong MJ, Hayes KC. Bile lipid alterations in taurine depleted monkeys. *Am. J. Clin. Nutr.* 1981; 34(2): 204–210.

35. Murray RK, Granner DK, Mayes PA, Rodwell VM. Harper's Biochemistry. Prentice-Hall (USA): Connecticut, 1988; p 580.

36. Marteau C, Sastre B, Iconomidis N, Portugal H, Pauli AM, Gérolami A. pH regulation in human gallbladder bile: study in patients with and without gallstones. *Hepatology.* 1990; 11(6): 997-1002.

37. Bove KE, Heubi JE, Balistreri WF, Setchell KD. Bile acid synthetic defects and liver disease: a comprehensive review. *Pediatr Dev Pathol.* 2004; 7(4): 315-334.

CHAPTER 4
IN VIVO ^{1}H MRS OF HUMAN GALLBLADDER BILE: A POTENTIAL NON-INVASIVE METHOD FOR THE DIAGNOSIS OF PRIMARY SCLEROSING CHOLANGITIS

Sanaz Mohajeri[1,], Tedros Bezabeh[1,2], Omkar B. Ijare[2], Scott B. King[3], M. Albert Thomas[4], Gerald Minuk[1], Jeremy Lipschitz[1], Iain Kirkpatrick[1], Allan B. Micflikier[1], Randy Summers, and Ian C.P. Smith[1,2]

[1]University of Manitoba, Winnipeg, Manitoba, Canada, [2]University of Winnipeg, Winnipeg, Manitoba, Canada, [3]National Research Council of Canada, Winnipeg, Manitoba, Canada, [4]University of California, Los Angeles, California, United States.

Contributions:

Sanaz Mohajeri: optimizing the experimental parameters, Modifying PRESS sequence to L-COSY based on the method designed by Dr. Albert Thomas, subject recruitment, participating in modifying MATLB code designed at UCLA, collecting the data, analyzing the data, writing the paper.

Omkar B. Ijare: consultant at data collection, analysis, and writing paper.

Tedros Bezabeh: supervising data collection, analysis, and writing paper.

Scott B. King: designer of coil.

M. Albert Thomas: consultant in 2D experiments, and IDEA programming. MATLAB code originally designed in his lab.

Gerald Minuk, Jeremy Lipschitz, Iain Kirkpatrick, and Allan B. Micflikier: clinical collaborators.

Randy Summers: helping in statistical analysis

Ian C.P. Smith: designing project, supervising data collection, analysis, and writing paper.

4.1 ABSTRACT

Primary sclerosing cholangitis (PSC) is a chronic inflammatory cholestatic disorder with diffuse strictures in the intra- and/or extra-hepatic bile ducts. Endoscopic retrograde cholangiopancreatography (ERCP) is the current gold standard for the diagnosis of PSC. Magnetic resonance cholangiopancreatography (MRCP) as a non-invasive alternative to the ERCP is not accurate enough to substitute for ERCP. There is a need for other non-invasive techniques which can augment the diagnostic accuracy of MRCP. In the current study, we have investigated the role of *in vivo* ^{1}H MRS of bile in differentiating the PSC patients from healthy controls. A total of 24 subjects (10 PSC patients; 14 Healthy controls) were included in the 1D study. The concentrations of major biliary lipids – total bile acids (TBAs) plus cholesterol, glycine-conjugated bile acids (GCBAs), taurine-conjugated bile acids (TCBAs), choline-containing phospholipids (chol-PLs) were compared between two groups. This study revealed that there was a significant decrease in the levels of all the above metabolites in the PSC patients compared to the healthy subjects (controls: TBAs + cholesterol = 123.47 ± 59.09 mM, TCBAs = 25.73 ± 15.96 mM, GCBAs = 54.65 ± 29.21 mM, TCBAs + GCBAs (amide group) = 72.35 ± 35.80 Mm, and chol-PLs = 47.58 ± 20.65 mM; PSC patients: TBAs + cholesterol = 60.57 ± 40.71 mM, TCBAs = 10.69 ± 8.30 mM, GCBAs = 20.32 ± 15.00 mM, TCBAs + GCBAs (amide group) = 35.30 ± 26.65, and chol-PLs = 19.74 ± 20.55 mM). In 2D study, the spectra from 6 PSC patients and 8 healthy controls were compared qualitatively.

Especially the importance of cross peak from phosphatidylcholine-glyceryl was considered. This is the first report of *in vivo* ^{1}H MRS of gallbladder bile, comparing the levels of biliary lipids in PSC patients with those of healthy subjects, using a 3 T MRI/MRS scanner.

Key words: primary sclerosing cholangitis**;** *in vivo* ^{1}H MRS; human bile; L-COSY; choline-containing phospholipids; glycine-conjugated bile acids; taurine-conjugated bile acids**.**

Abbreviations: ALP, alkaline phosphatase; ALT, alanine aminotransferase; AST, aspartate aminotransferase; CC, cholangiocarcinoma; chol-PLs, choline-containing phospholipids; DIA, digitized image analysis; ERCP, endoscopic retrograde cholangiopancreatography; FISH, fluorescent in-situ hybridization; GCBAs, glycine-conjugated bile acids; GCDCA ,glycochenodeoxycholic acid; GGT, gamma-glutamyl transferase; GI, gastrointestinal; GlcUA, D-glucuronic acid; HASTE, half-fourier acquisition single-shot turbo spin-echo; HPB, hepatopancreatobiliary; IBD, inflammatory bowel disease; INR, international normalized ratio; MRCP, magnetic resonance cholangiopancreatography; PC, phosphatidylcholine; PSC, primary sclerosing cholangitis; SVS, single voxel spectroscopy; TBAs, total bile acids; TCBAs, taurine-conjugated bile acids; TR_{eff}, effective TR.

4.2 INTRODUCTION

Cholestasis is a well-known hepatobiliary pathology characterized by the stasis in the flow of bile from the liver to the duodenum (1). In cholestasis, the excretion of bile salts into bile is inhibited, leading to the accumulation of bile acids in the hepatocytes. Intracellular accumulation of bile salts within the hepatocytes plays a pivotal role in

cholestatic liver injury (2). Primary sclerosing cholangitis (PSC) is an inflammatory cholestatic liver disease characterized by progressive obliteration of intra- and extra-hepatic bile ducts (3). The incidence of PSC in the USA is 0.9/ 100,000 (4). However, considering the long clinical course of the disease, the reported prevalence is as high as 21/100,000 men and 6/100,000 women (5). A typical patient is a middle-aged man with a history of inflammatory bowel disease (IBD) complaining from general symptoms such as fatigue and weight loss plus cholestatic symptoms including pruritus and intermittent jaundice (6). In addition, the clinical course of the disease may be complicated by choledocholithiasis, cholangitis, secondary biliary cirrhosis and especially cholangiocarcinoma, a very aggressive bile duct tumour (5, 7). Blood biochemistry mainly reveals a cholestatic pattern with elevated alkaline phosphatase (ALP) and gamma-glutamyl transpeptidase (GGT), and sometimes shows increased levels of liver enzymes (7). The only cure for PSC is orthotopic liver transplantation (OLT) which is contraindicated in the presence of CC (3, 6). Endoscopic retrograde cholangiopancreatography (ERCP) is the gold standard for the diagnosis of PSC (8). Due to the invasive nature of the technique, there has been an effort to replace ERCP with non-invasive techniques such as magnetic resonance cholangiopancreatography (MRCP) (9). However, MRCP is not accurate enough to substitute for ERCP. Given the fact that PSC is a known risk factor for the development of CC (7), early diagnosis of PSC (before the development of CC) is essential in the treatment of the disease.

MRS is a reasonably sensitive technique that can detect several small metabolites in a single experiment both *in vitro* and *in vivo* and follow their variations over time or under pathological conditions (10-12). *In vitro* and *in vivo* MRS techniques have been utilized

to detect metabolic changes in liver tissue in pathological conditions including malignancy (13-15).

Bile is a site-specific biological specimen which has potential to reflect the cellular and/or metabolic changes in the hepatopancreatobiliary (HPB) system with a disease process. Despite the complex nature of bile, including variations due to diet, medication, and environmental factors (10), *in vitro* MRS of bile has been successful in differentiating various HPB disorders. Among the major bile metabolites, alterations in the levels of chol-PLs, cholesterol, TCBAs and GCBAs have been observed in HPB disorders (16-24). In our laboratory, ^{1}H MRS-based analysis of bile obtained from patients with hyper-bilirubinemia showed alteration in the ratio of GCBAs to TCBAs. (16). In addition, some of the PSC patients showed the absence of glycochenodeoxycholic acid (GCDCA) in their bile (17). Nagana Gowda et al. have made similar observations in patients with hepatocellular carcinoma, CC and cirrhosis (18). Moreover, the study by Albiin et al. on the ^{1}H MRS analysis of bile samples from patients with CC compared to benign conditions (including PSC) revealed decreases in the levels of PC, bile acids, and cholesterol (19). Other researchers have also reported the altered bile acid and phospholipid metabolism in HPB disorders including CC (20, 21). Nishijima et al. noticed the presence of lactate in the bile of patients suffering from hepatobiliary malignancies (25); significant elevation in D-glucuronic acid levels was observed in pancreatic cancer patients by Bezabeh et al. (22).

Given the invasive nature of ERCP procedure used for the collection of bile for *in vitro* studies, *in vivo* alternatives have been considered. Prescot et al. (26) pioneered the idea of obtaining an *in vivo* ^{1}H MR spectrum of human bile using a 1.5 T MRI/MRS scanner and

a surface receiver coil. However, the spectral quality was low and they were not able to quantify the major bile metabolites except for the chol-PLs. This may have been due to the use of low magnetic field strength (1.5 T), the use of a spin echo sequence with long delays (TE = 60 msec), and/or lipid contamination. Later, Künnecke et al. (27) were successful in obtaining a good quality spectrum of bile *in vivo* in cynomolgus monkeys by increasing the magnetic field strength from 1.5 T to 4.7 T. That study used a custom-built surface coil in transmit/receive mode, and applied a respiratory-gated sequence to minimize the motion artifact due to breathing. Recently, we obtained a high quality *in vivo* ^{1}H spectrum from gallbladder bile in healthy volunteers using a 3 T Siemens scanner and a custom-built receive array coil (28). We were able to detect and quantify major biliary lipids: TBAs plus cholesterol (0.66 ppm), TCBAs (3.08 ppm), chol-PLs (3.22 ppm), GCBAs (3.74 ppm), and sum of TCBAs and GCBAs determined from amide proton region (7.76 – 8.05 ppm). In the current study, we extended our methodology to the study of PSC patients in order to determine whether the *in vivo* ^{1}H MRS of bile might have any value in the diagnosis of PSC.

4.3 METHODS

4.3.1 Subject Characteristics

The study was designed based on the ethical guidelines of the 1975 Declaration of Helsinki. PSC patients were recruited at the Health Sciences Centre, University of Manitoba, Winnipeg, according to the protocol approved by the Research Ethics Boards of the University of Manitoba and the National Research Council of Canada (NRC). Informed consent was obtained from each subject prior to the study. A total of 11 PSC patients were recruited for the study. 1D spectra were acquired from these patients. One

spectrum was excluded due to poor water suppression. The included patients were 5 females and 5 males (mean ages 47 and 41 respectively, range: 24 – 54). The diagnosis of PSC was made by a hepatologist based on the clinical, radiological and laboratory findings and in suspicious cases was confirmed by ERCP. Seven patients had inflammatory bowel disease (IBD). And one patient had already developed cirrhosis.

1D spectra from14 healthy volunteers who were recruited for our recent study (28) (11 females and 3 males, mean ages 40 and 33 respectively, range: 21 – 55), were included as control datasets. The healthy volunteers had no history of chronic liver disease or IBD. They were not heavy alcohol drinkers (>3 drinks/day) and they were not on any medication which could cause liver injury. Active HPB disorders were ruled out in control subjects following medical history, physical examination, and blood biochemistry.

Eight PSC patients participated in our 2D experiments as well. Two datasets were excluded due to low signal-to-noise-ratio (SNR), lipid contamination, breadth of residual water, and artifact due to gallbladder motion during breathing. The included patients were composed of 3 females and 3 males (mean ages 43 and 36 respectively, range: 24 – 48). After applying the same exclusion criteria, eleven 2D L-COSY spectra from our recent study on healthy volunteers (28) were included as a control group. The included healthy volunteers were composed of 7 females and 4 males (mean ages 41 and 35 respectively, range: 26 –55). The demographic and biochemical characteristics of the included healthy volunteers and PSC patients are presented in Table 4.4-1.

4.3.2 MRS Experiments

MRS experiments were performed on a Siemens 3 T Magnetom Trio clinical scanner. The RF pulses were transmitted through the body coil and received by a custom-built surface receive array coil. The receiver coil was used after passing all safety checks of NRC and obtaining approval from both Research Ethics Boards of NRC and the University of Manitoba. We performed single voxel spectroscopy (SVS) on the gallbladder bile using the Siemens PRESS sequence with bellow respiratory-gating (VB15 & VB17, Siemens, Erlangen, Germany). We also acquired 2D L-COSY spectra using the sequence edited from Siemens PRESS as described by Thomas et al (29, 30). In 1D and 2D experiments, a voxel size of 12×12×12 mm^3 was used. In order to decrease lipid contamination from liver and body fat around gallbladder, 6-8 spatial saturation bands were placed around the gallbladder. Manual localized shimming (Full Width Half-Maximum (FWHM) of < 15 Hz for water peak) and water suppression were performed before the acquisition of spectroscopic data.

One-dimensional (1D) ^1H MRS Experiments

In vivo measurements

The subjects were fasted for at least 4 hours before the study. Three orthogonal MR images were acquired using half-fourier acquisition single-shot turbo spin-echo (HASTE) sequences to localize the gallbladder and position the voxel. Subjects were scanned during breath-hold at the end of a regular expiration using the following acquisition parameters: matrix = 192×256, slice thickness = 6 mm, FOV = 270×360 mm^2, TE/TR =101/1000 msec. A 12×12×12 mm^3 voxel was placed in the gallbladder. 6-8 spatial saturation bands were placed around the gallbladder. Manual adjustments were performed for frequency, and receiver gain followed by shimming and water suppression.

1D PRESS single voxel spectra were acquired using a bellow respiratory-gated sequence during the last 10 – 30% of quiet expiration. The following acquisition parameters were applied throughout the experiments: TE = 30 msec, TR = 2000 msec, band width = 2000 Hz, vector size = 2048 points and NS = 256. Considering that one FID was acquired in each breath, the effective TR (TR_{eff}) was dependent on the rate of breathing which was different for each subject. We calculated the mean TR based on breathing rate in each subject. Considering that the scanning time obtained for each sequence from the scanner includes the adjustment time, we could not use the water suppressed 1D or 2D spectra for calculating breathing cycle length. Because the unsuppressed water 1D spectrum was acquired immediately after the 1D spectrum with the same parameters (no need for adjustments), we used this data for calculating TR_{eff}. We divided the scanning time by the number of scans to calculate the average breathing cycle length which is equal to TR_{eff}. The mean TR for all PSC patients was 5469 msec (range: 4250 - 6625 msec) compared to 5366 ms (range: 3750 – 7438 ms) for controls from our recent study (28). 8 or 16 scans were acquired from the same voxel using the same parameters without water suppression. The average time for gallbladder localization, manual adjustment of parameters, and data collection was 46 min. in PSC patients while this was 42 min. in controls. Considering the average TR_{eff} for controls and patients were 5366 and 5469 msec respectively, the average time for 256 scans was 22.89 minutes for controls and 23.33 min for patients. The rest of the time was needed for acquiring localizer images, manual adjustments (specially shimming and water suppression) and acquiring 1D spectrum with unsuppressed water.

Two-dimensional (2D) in vivo ^{1}H MRS Experiments

2D L-COSY experiments were performed in order to identify some of the overlapping signals in the corresponding 1D spectra. As in the 1D experiments, a 12×12×12 mm^3 voxel was positioned in the gallbladder and spatial saturation bands were placed around the gallbladder. After adjusting the frequency, and setting the receiver gain to high, manual shimming and water suppression were performed. 2D L-COSY data were acquired during the last 10-30% of quiet expiration using the bellow respiratory-gated sequence. The following spectral parameters were used in all measurements: TE = 30 msec; TR = 2000 msec; band width = 2000 Hz; vector size = 2048 points; NS =12; time increment ($\Delta t1$) = 0.8 msec; and number of measurements = 50 or 64 except in one case which was 40. The original minimum TR was set to 2000 msec. The Average time for adjustment of parameters, and acquisition of L-COSY data was 46 min. compared to 49 min. in healthy volunteers.

4.3.3. Data Processing

One-dimensional (1D) ^1H MRS Experiments

The raw data were first processed by MATLAB code generated at UCLA, and modified at the NRC. This code helped to check individual scans and eliminate distorted ones due to lipid contamination, failed water suppression and low SNR. Undistorted scans (216) were analyzed in all cases except for 1 PSC patient (75 scans) and 2 normals (119, and 52 scans). Frequency drifts due to gallbladder movement during breathing were reduced by aligning of the individual scans based on the methylene proton signal [$-CH_2-$] of lipid peak at 1.26 ppm or the trimethylamine signal [$-N^+-(CH_3)_3$] of PC at 3.22 ppm. After averaging the aligned scans, eddy current correction was performed using the unsuppressed water signal (31), and the data from separate coil elements were combined

using an optimized combination method involving the noise correlation (32). The data were then imported to the FELIX-2007 software (FELIX NMR Inc., San Diego, California, USA). After exponential apodization with 0.5 Hz line broadening and Fourier transformation, first and second order phase and baseline corrections were performed on the real part of the spectrum. The spectra were referenced to the methylene proton signal [-CH_2-] of the lipid peak at 1.26 ppm or the trimethylamine signal [-N^+-$(CH_3)_3$] of chol-PLs at 3.22 ppm.

Quantification of Biliary Biochemicals

The peaks from 1D bile ^{1}HMR spectra with water suppression were assigned according to the previous *in vitro* (33, 34) and *in vivo* studies on human and monkey bile (26-28). They were fitted to Lorentzian line shapes by deconvolution based on a simulated annealing algorithm [FELIX NMR Inc., San Diego, California, USA]. The water peak of the bile spectrum acquired without water suppression was used as an internal reference after fitting. The peak areas of the methyl [-CH_3] signal representing TBAs plus cholesterol at 0.66 ppm, the methylene [-CH_2-] signal of TCBAs at 3.08 ppm, the trimethylammonium [–$N^+(CH_3)_3$] signal of chol-PLs at 3.22 ppm, the methylene [-CH_2-] signal of GCBAs at 3.74 ppm, and the amide signal [-NH] of GCBAs and TCBAs in the 7.76-8.05 ppm region as well as unsuppressed water, were integrated. The molar concentrations of biliary lipid metabolites were quantified using the following equation, as described by Fayad et al. (35):

$$[Lipid](mM) = \frac{PeakArea(Lipid)}{PeakArea(H2O)} \cdot \frac{No.of\ \mathrm{Protons}(H2O)}{No.of\ \mathrm{Protons}(Lipid)} \cdot \frac{10^6}{Mol.Wt.(H2O)} \cdot \frac{fT1(H2O)}{fT1(Lipid)} \cdot \frac{fT2(H2O)}{fT2(Lipid)} \cdot CF(H2O)$$

…Eq.(1)

Where $CF(H_2O)$ = 0.9, is a conversion factor for the percent of water content of human gallbladder bile (36), *f(T1)* and *f(T2)* are correction factors due to T_1 and T_2 relaxation times of water and individual lipid molecules (35).

Two-dimensional (2D) in vivo ^{1}H MRS Experiments

After the preliminary processing with MATLAB code similar to that in the 1D experiments, the 2D raw data were imported to FELIX software (FELIX NMR Inc., San Diego, California, USA) and analyzed in magnitude mode. In the $\mathbf{t_2}$ and $\mathbf{t_1}$ dimensions, the first 256 and 50 points were selected for processing, respectively. The $\mathbf{t_1}$ dimension was linear predicted up to 64 points using the 50 points collected. The raw data were zero filled to 2048 and 128 points in $\mathbf{t_2}$ and $\mathbf{t_1}$ dimensions respectively. The noise was reduced by applying a skewed sine-bell apodization function with 0° shift and a skew parameter of 0.5-0.6. After complex Fourier transformation, the spectra were referenced to the diagonal peak of chol-PLs ($\mathbf{F_2}$ = $\mathbf{F_1}$ = 3.22 ppm) or to the diagonal peak of the amide signal ($\mathbf{F_2}$ = $\mathbf{F_1}$ = 7.8 ppm).

4.3.4 Statistical Analysis

The Student's t-test was used for comparing the mean values of corrected concentrations of major biliary lipids quantified in both study groups except for GCBAs. In the case of GCBAs, there was a significant difference in the variance of data in the two groups; as a result, this comparison did not satisfy the t-test criteria. Therefore, the means of corrected concentration of GCBAs were compared between controls and patients using the non-parametric Mann-Whitney U Test. In order to test whether there was a gender difference in the corrected concentrations of these metabolites, we compared the means of corrected concentration of each metabolite between males and females using the Student's t-test.

We also performed a correlation analysis between the cholestatic pattern of bile represented by elevated ALP or GGT and the molar concentrations of major bile metabolites.

4.4 RESULTS

The demographical and biochemical characteristics of all subjects in the study are presented in Table 4.4-1.

Table 4.4-1: Comparisons between characteristics of healthy controls and PSC patients

Average or ratio	Healthy controls in 1D experiments	PSC patients in 1D experiments	Healthy controls in 2D experiments	PSC patients in 2D experiments
Age	38.29 ± 11.84	44.30 ± 9.50	39.09 ± 11.86	39.67 ± 9.50
Sex M/F	3/11	5/5	4/7	3/3
Bilirubin Total (μM)	8.46±4.96*	13.70±10.35	9.20±5.31*	16.50±12.47
Bilirubin Direct (>7μM)	0/14*	2/10	0/11	2/6
AST (U/L)	22.14±4.93	76.30±52.59	23.45±5.43	78.50±59.53
ALT(U/L)	16.50±3.32	85.90±67.03	20.55±9.49	77±68.84
GGT (U/L)	14.33±3.64*****	262.20±261.07	19.60±9.37*	198.33±147.28
Lipase (U/L)	42.69±17.24*	N/A	34.80±9.16*	N/A
ALP (U/L)	64.86±15.74	384.40±274.78	68.55±17.78	432.67±327.20
INR	1±0.09 **	1.01±0.12	0.98±0.04	1.03±0.15
AFP >7	N/A	0/9	N/A	0/6
CEA >5	N/A	1/9	N/A	1/6
CA19-9 >34	N/A	1/9	N/A	1/6
UC	0/14	6/10	0/11	4/6
Crohn's disease	0/14	1/10	0/11	1/6
Cirrhosis	0/14	1/10	0/11	1/6

-: not reported by the lab; *, 1 missing value. **, 2 missing values; ***** , 5 missing values; NA, not applicable; AST, aspartate aminotransferase; ALT, Alanine transaminase; GGT, gamma-glutamyl transferase; ALP, alkaline phosphatase; INR, international normalized ratio; μM, micromolar; U/L, unit/liter; M, male; F, female; UC,

ulcerative colitis; AFP, α-fetoprotein; CEA, carcinoembryonic antigen; CA19-9, carbohydrate antigen 19-9.

The normal values of blood biochemistry are as follows:

Bilirubin Total, 2-20 μM; Bilirubin Direct, <7 μM; AST, 10-32 U/L; ALT, M, <30, F, <25 U/L; GGT, M, 5-38, F, 5-29 U/L; Lipase, < 60U/L; ALP, 30-120 U/L; INR, 0.9-1.1; AFP, 0-7; CEA, 0-5; CA19-9, 0-34.

Figure 4.4-1 compares a typical ^{1}H MR spectrum of gallbladder bile acquired from a healthy volunteer *in vivo* using a 3 T Siemens scanner with a similar spectrum acquired from gallbladder bile of a PSC patient. Panels (A) and (B) represent axial, coronal, and sagittal images obtained at the end of expiration during a regular breath-hold in the healthy volunteer and the PSC patient, respectively. These images were used for positioning a 12x12x12 mm^3 voxel on the gallbladder. Panels (C) and (D) show the corresponding ^{1}H MR spectra recorded from the same healthy volunteer and the PSC patient, respectively. The peaks were assigned based on reported *in vitro* studies (33, 34) and *in vivo* studies on human and monkey bile (26-28).

Figure 4.4-1: Comparison of ^{1}H MR spectrum of human bile *in vivo* from a healthy volunteer and a PSC patient obtained at 3 T Siemens scanner using a custom-built receive array coil.

Panels (A), and (B) represent the positioning a 12x12x12 mm^3 voxel on the three orthogonal images of gallbladder in a healthy volunteer and a PSC patient, respectively. Panels (C), and (D) show Corresponding ^{1}H MR spectra of gallbladder bile in the healthy volunteer and the PSC patient. The peaks were assigned based on the previous *in vitro* (33, 34) and *in vivo* (26-28) studies.1, methyl [-CH_3] group of TBAs (H-18 protons); this peak has contribution from cholesterol. 2, protons of ring bound -CH_3 group of bile acids (H-19 protons); 3, H-21 -CH_3 protons of bile acids; 4, -CH_2- protons of aliphatic tail of phospholipids; 5, remainder of the aliphatic protons in bile acids, phospholipids, and cholesterol; 6, H-26 -CH_2- group of TCBAs; 7,trimethylammonium [$–N^+(CH_3)_3$] group of chol-PLs; 8, H-25 -CH_2- group of GCBAs; 9, residual water; 10, olefinic [-CH=CH-] protons of phospholipids; 11, amide [-NH] group of both GCBAs and TCBAs.

*, indicates the peak areas that showed a statistically significant difference between healthy volunteers and PSC patients.

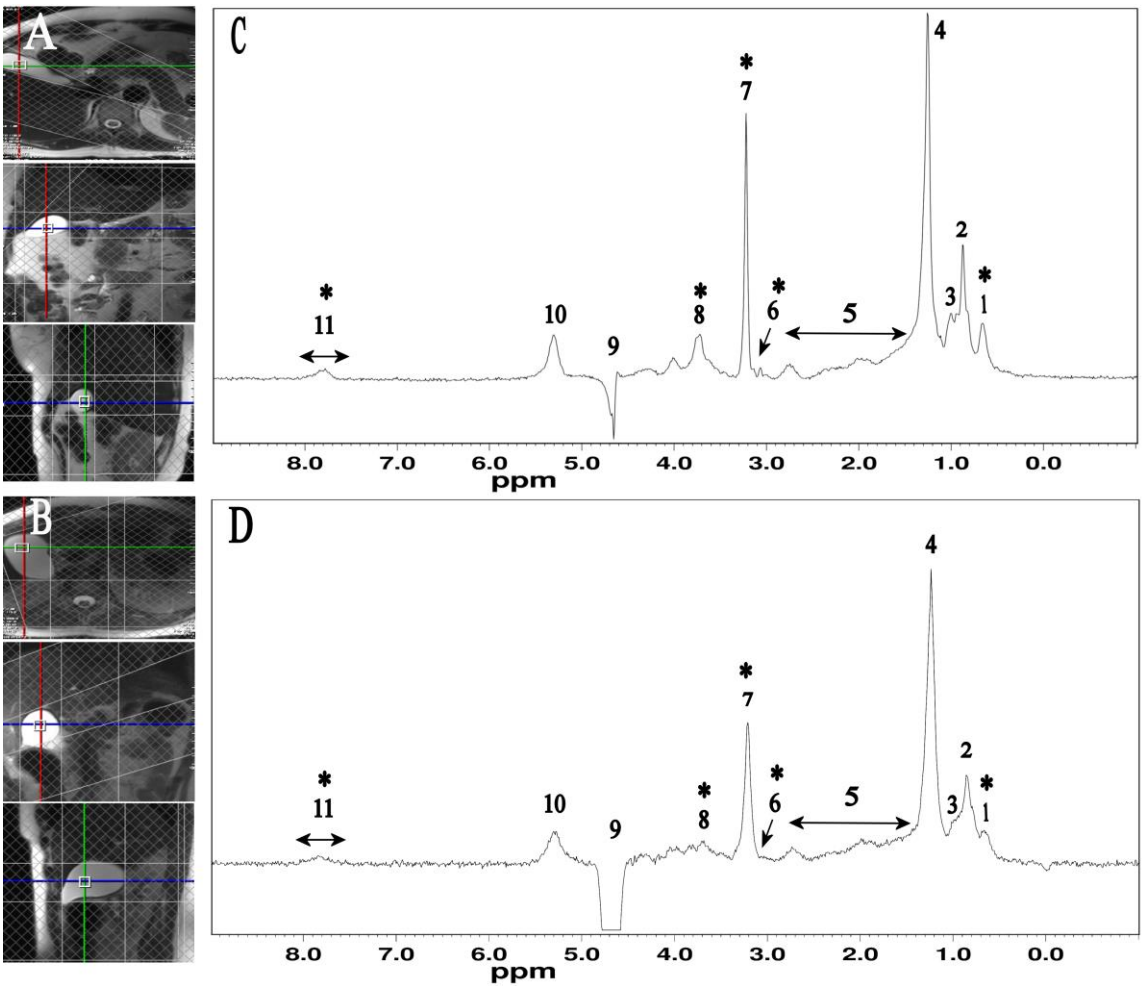
A
B
C
D
11
10
9
8
7
6
5
4
3
2
1
8.0
7.0
6.0
5.0
4.0
3.0
2.0
1.0
0.0
ppm

Molar concentrations of the major bile metabolites – TBAs plus cholesterol, chol-PLs, GCBAs, TCBAs and TBAs (amide region) were calculated using Eq (1) in PSC patients and compared with healthy volunteers from our recent study (28) (Table 4.4-2).

Table4.4-2: Concentration of metabolites (mM) in healthy controls and PSC patients and the Mean and SD

Healthy control	(TBAs+ Cholesterol) 0.66 ppm Peak #1	TCBAs 3.08 ppm Peak #6	chol-PLs 3.22 ppm Peak #7	GCBAs 3.74 ppm Peak #8	TBAs (amide group) 7.76-8.05 ppm Peak #11	GCBAs/TCBAs Peak #8/ Peak #6
1	120.43	56.71	69.90	51.44	102.18	0.91
2	NR	NR	69.58	98.88	106.87	NR
3	97.73	15.36	44.64	NR	96.29	NR
4	115.55	50.92	70.97	36.98	108.29	0.73
5	186.25	29.32	66.47	78.75	99.50	2.69
6	115.21	17.36	31.41	23.79	40.16	1.37
7	82.76	NR	25.21	43.68	22.39	NR
8	133.16	16.38	37.75	73.59	83.90	4.49
9	72.09	5.83	21.95	12.75	21.32	2.19
10	47.58	NR	24.43	28.18	20.61	NR
11	230.24	29.62	79.55	101.51	ND	3.43
12	91.28	19.76	36.78	26.03	ND	1.32
13	235.15	30.41	58.34	76.13	93.97	2.50
14	77.71	11.34	29.08	58.68	72.77	5.17
Mean	123.47	25.73	47.58	54.65	72.35	2.48
SD	59.09	15.96	20.65	29.21	35.80	1.51
PSC patients						
1	123.71	18.44	21.70	27.39	51.91	1.48
2	57.48	9.22	13.02	12.75	22.62	1.38
3	87.04	16.79	33.12	38.29	86.54	2.28
4	42.65	ND	11.91	11.75	11.69	ND
5	109.34	26.97	73.16	43.90	69.97	1.63
6	20.15	5.43	6.31	9.56	16.55	1.76
7	25.15	3.70	5.70	9.32	11.86	2.52
8	23.72	2.77	9.95	7.75	23.44	2.80
9	98.61	4.07	15.76	38.09	44.26	9.37
10	17.80	8.84	6.77	4.39	14.13	0.50
Mean	60.57	10.69	19.74	20.32	35.30	2.64
SD	40.71	8.30	20.55	15.00	26.65	2.62

TBAs, total bile acids; GCBAs, glycine-conjugated bile acids; TCBAs, taurine-conjugated bile acids; chol- PLs, choline containing phospholipids; NR, not resolved; ND, not detected.

The means of corrected molar concentrations of the above metabolites except GCBAs in both groups were compared using Student's t-test. Because of significant difference in the variances of healthy controls and PSC patients, the means of corrected molar concentrations of GCBAs were compared using non parametric Mann-Whitney U Test. The results of these comparisons are presented in Table 4.4-3. The corrected molar concentrations of TBAs + cholesterol calculated from methyl [-CH_3] signal (H-18 protons) resonating at 0.66 ppm (peak **1**), (27, 28, 33) were significantly lower (P = 0.009) in PSC patients (mean ± SD, 60.57 ± 40.71) compared to the healthy controls (mean ± SD, 123.47 ± 59.09). The corrected levels of chol-PLs quantified using the trimethylammonium [$–N^+(CH_3)_3$] signal at 3.22 ppm (peak 7) in PSC patients (mean ± SD, 19.74 ± 20.55) were lower significantly (P = 0.004) compared to those of the healthy controls (mean ± SD, 47.58 ± 20.65). The corrected molar concentrations of TCBAs determined by the H-26 -CH_2- group at 3.08 ppm (peak **6**) were significantly lower (P= 0.020) in the PSC patients (mean ± SD, 10.69± 8.30) compared to the healthy controls (mean ± SD, 25.73± 15.96); Similarly, the corrected molar concentrations of GCBAs, quantified by using the H-25 -CH_2- group at 3.74 ppm (peak **8**) in PSC patients (mean ± SD, 20.32 ± 15), were also significantly lower (P=0.005) compared to the healthy controls (mean ± SD, 54.65± 29.21) However, there was no statistically significant difference in the ratio GCBAs/TCBAs (P = 0.873) between controls (mean ± SD, 2.48 ± 1.51) and PSC patients (mean ± SD, 2.64 ± 2.62). Finally, the sum of corrected molar

concentrations of GCBAs and TCBAs represented by the broad overlapping region of the amide [-NH] group (peak **11**) resonating in the region 7.76 – 8.05 ppm were compared between patients (mean ± SD, 35.30± 26.65) and the control group (mean ± SD, 72.35± 35.80) using Student's t-test, and were statistically lower (P = 0.014) in the PSC group.

Table 4.4-3: Results of t-tests comparing molar concentrations of different bile metabolites determined *in vivo* corrected for T_1 and T_2 relaxation times and 90% water content between healthy controls and PSC patients

Peak area	Mean - control	Mean - Patient	t-value	df	P
(TBAs+ Cholesterol) at 0.66 ppm	123.47	60.57	-2.87519	21	0.009
TCBAs at 3.08 ppm	25.73	10.69	-2.54992	18	0.020
chol-PLs at 3.22 ppm	47.58	19.74	-3.26234	22	0.004
*GCBAs at 3.74 ppm	54.65	20.32	-	-	-
TBAs (amide group) 7.76-8.05 ppm	72.35	35.30	-2.70397	20	0.014
GCBAs/TCBAs	2.48	2.64	0.162472	17	0.873

*, In GCBAs the means were compared using Mann-Whitney U test (P=0.005), because the variances were different between PSC datasets and control spectra.

TBAs, total bile acids; GCBAs, glycine-conjugated bile acids; TCBAs, taurine-conjugated bile acids; chol- PLs, choline-containing phospholipids.

To test whether the results were confounded by gender differences, the means of molar concentrations of major bile metabolites were compared between males and females using the Student's t-test. There was no statistically significant difference between males and females (Table 4.4-4).

Table 4.4-4: Results of t-tests between genders for corrected molar concentrations of major biliary metabolites

Peak area	Mean - M	Mean - F	t-value	Df	P
(TBAs+ Cholesterol) at 0.66 ppm	70.57	107.30	-1.37868	21	0.183
TCBAs at 3.08 ppm	13.08	21.48	-1.16562	18	0.259
chol-PLs at 3.22 ppm	30.53	38.70	-0.76189	22	0.454
GCBAs at 3.74 ppm	37.37	40.97	-0.27447	21	0.786
TBAs (amide group) 7.76-8.05 ppm	46.56	60.62	-0.86367	20	0.398

TBAs, total bile acids; GCBAs, glycine-conjugated bile acids; TCBAs, taurine-conjugated bile acids; chol- PLs, choline containing phospholipids; M, male; F, female.

Finally, in order to determine any relationship between the blood biochemical parameters of cholestasis (elevated ALP or GGT) and the changes in the MRS-based metabolic pattern of bile, correlation analysis were performed between the levels of ALP and GGT and each bile metabolite in all subjects (Table 4.4-5). Both ALP and GGT showed a negative correlation ($P<0.05$) with TBAs + cholesterol (0.66 ppm), GCBAs (3.74 ppm), and chol-PLs (3.22 ppm). Similarly, there was a negative correlation between the amide region (7.76 – 8.05 ppm) and ALP ($P<0.05$).

Table 4.4-5: Correlation analysis between cholestatic blood Biochemistry and major bile metabolites performed in all subjects

Bile metabolite	GGT (M : 5-38, F : 5-29 U/L)	ALP (30-120 U/L)
(TBAs+ Cholesterol) at 0.66 ppm	-0.54 *	-0.51*
TCBAs at 3.08 ppm	-0.31	-0.36
chol-PLs at 3.22 ppm	-0.49 *	-0.56*
GCBAs at 3.74 ppm	-0.56 *	-0.51*
TBAs (amide group) 7.76-8.05 ppm	-0.37	-0.43*

Marked correlations are significant at $p < 0.05$ N=19 for GGT, N=24 for ALP

GGT, gamma-glutamyl transferase; ALP, alkaline phosphatase; M, male; F, female.

Figure 4.4-2 shows typical 2D L-COSY spectra of human gallbladder bile obtained from a healthy volunteer (top) and a PSC patient (bottom). It is obvious from visual inspection that the signal intensities of various peaks assigned in the PSC patient are very low compared to those of healthy control. The following diagonal and cross peaks were assigned based on *in vitro* studies (17, 34, 37) and our recent *in vivo* study (28). The diagonal peak ($\mathbf{F_2}$ = $\mathbf{F_1}$ = 7.81 ppm) along with a cross peak ($\mathbf{F_2}$ = 7.81, $\mathbf{F_1}$ = 3.62 ppm) represent J-coupling between the amide group [-NH] of TCBAs (H-25) and GCBAs (H-25) (contours **1** and **1a**). The contours **1** and/or **1a** were detected in 7/11 controls whereas only 1 of the 6 PSC patients showed these contours. Similarly, a diagonal peak ($\mathbf{F_2}$ = $\mathbf{F_1}$ = 5.24 ppm) represents the olefinic [-CH=CH-] protons of chol-PLs (marked as **2**) along with the cross peaks ($\mathbf{F_2}$ = 5.24, $\mathbf{F_1}$ = 2.75 ppm) and ($\mathbf{F_2}$ = 5.24, $\mathbf{F_1}$ = 1.96 ppm) represent J-coupling of the olefinic protons with neighbouring methylene protons (contours **2a**, and **2b**) had lower intensities in PSC patients. The glyceryl 2-CH signals of PC (cross peak, $\mathbf{F_2}$ = 5.24, $\mathbf{F_1}$ = 4.18 ppm) (marked as **3**) which is an important marker for distinguishing PC from other chol-PLs, was expected to decrease in PSC patients due to cholestasis (17). Given the lower SNR in 2D spectra, this contour was detected only in 3/11 healthy controls and 1/6 PSC patients. The diagonal peak at ($\mathbf{F_2}$ = $\mathbf{F_1}$ = 3.20 ppm) represents the [$-N^{+}(CH_3)_3$] group of chol-PLs (marked as **4**), and had lower intensity in PSC patients. The symmetric cross peaks at ($\mathbf{F_2}$ = 4.3, $\mathbf{F_1}$ = 3.6 ppm), and ($\mathbf{F_2}$ = 3.6, $\mathbf{F_1}$ = 4.3 ppm) arising from J-coupling between the [-N-CH_2-] and [-CH_2-O-] of chol-PLs (marked as **5a** and **5b**) were detected in 6/11 controls and in 2/6 PSC patients. The diagonal peak at ($\mathbf{F_2}$ = $\mathbf{F_1}$ = 3.07 ppm) due to the H-26 signal of TCBAs had lower intensity in PSC patients compared to that of healthy controls (marked as **6**), and the cross peak at ($\mathbf{F_2}$ = 3.5, $\mathbf{F_1}$ =

3.07 ppm) arising from coupling between the H-25 and H-26 -CH_2- protons of TCBAs (marked as **6a**), was detected in 8/11 controls and in 2/6 PSC patients and the diagonal peak ($\mathbf{F_2}$ = $\mathbf{F_1}$ = 0.60 ppm) representing TBAs plus cholesterol (marked as **7**) had lower intensity in PSC patients compared to that from healthy controls.

Figure 4.4-2: : Comparison of 2D L-COSY spectrum of human bile *in vivo* between a representative healthy control (top) and a representative PSC patient (bottom) obtained with 3 T Siemens MRI/MRS using a custom-built receive array coil. Diagonal peaks and cross peaks were assigned based on the previous *in vitro* studies (17, 34, 37) and our recent *in vivo* study (28).

1and 1a, diagonal and cross peak representing amide group of TCBAs and GCBAs; 2, and 2a and 2b, diagonal peak assigned to the olefinic [-CH=CH-] protons of chol-PLs and two cross peaks representing J-coupling of the olefinic protons with neighbouring methylene protons; 3,Cross peak representing J-coupling of the glyceryl 2-CH with 3- -CH_2- of PC; 4, diagonal peak assigned to the [-N^+-$(CH_3)_3$] group of chol- PLs; 5a and 5b, symmetric cross peaks showing J-coupling between the [-N-CH_2-] and [-CH_2-O-] of chol- PLs; 6 and 6a, diagonal and cross peak representing coupling between the H-25 and H-26 -CH_2 protons of TCBAs; 7, diagonal peak assigned to TBAs plus cholesterol.

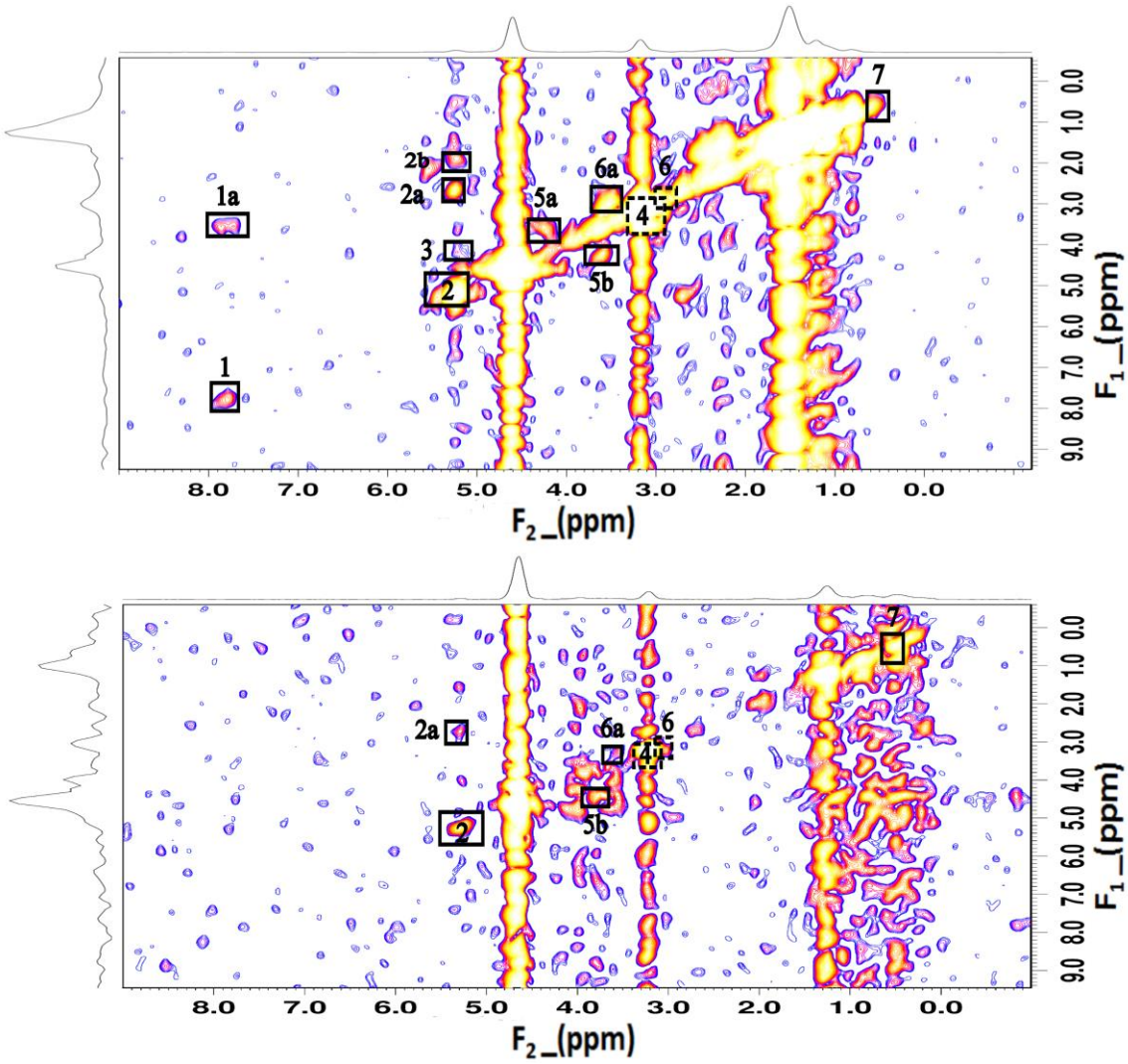
1a
2b
2a
3
2
1
5a
6a
6
4
5b
7
8.0 7.0 6.0 5.0 4.0 3.0 2.0 1.0 0.0
F2_(ppm)
9.0 8.0 7.0 6.0 5.0 4.0 3.0 2.0 1.0 0.0
F1_(ppm)
2a
6a
6
4
5b
2
7

4.5 DISCUSSION

The use of MR Spectroscopy, as an investigational technique for the early detection of metabolic changes, has shown potential in the early diagnosis of HPB disorders (10, 13-25, 38). MRS (both *in vitro* and *in vivo*) has been utilized in unravelling metabolic changes in different liver and pancreatic diseases including malignancies, hepatitis, cirrhosis, PSC, and alcoholic liver disease (10, 13-15, 38). *In vivo* MRS of abdominal organs is particularly challenging due to problems associated with breathing motion. Bile would serve as a valuable biological specimen for the *in vivo* MRS of HPB diseases. Since bile is fluid, it is possible to obtain well-resolved spectra compared to the solid organs such as liver and/or pancreas.

There are a number of *in vitro* studies that used MRS for the detection and quantification of major bile metabolites having diagnostic value (16-25). We extended our recent *in vitro* results (33) to *in vivo* MRS application, and devised a method for the simultaneous quantification of major biliary lipids in gallbladder bile using a 3 T scanner and a custom-built receive array coil (28). In the current study, we used this methodology to analyze bile inside the gallbladder of PSC patients and healthy controls to identify metabolic signatures specific to PSC patients.

The most important observation in this study was the significant decrease in the levels of major biliary lipid components in PSC patients compared to the controls (Table 4.4-3). This decrease indicates interruption in the normal function of the liver. Reduction in the levels of PC has been observed in the *in vitro* study by Albiin et al. (19) in CC and PSC (with underlying CC) patients. Although they observed a significant difference between benign (gallstones and PSC) and malignant (CC) cases, their study did not differentiate

between controls (gallstones, pancreatitis induced by gallstones and or bile duct dilatation) and PSC patients. In the current study, we observed a statistically significant difference in the levels of chol-PLs between controls and PSC patients. Bile samples for *in vitro* studies are generally obtained from patients referred to an ERCP procedure for the relief of some HPB condition. Such patients may have some degree of inflammation in their HPB system, and therefore, bile from these patients may show metabolic similarities to those of PSC patients. In the current study, our control group was comprised of healthy controls without any history of HPB disorders (based on the medical history, physical examination, and blood biochemistry). Nagana Gowda et al. have observed a decrease in the ratio of GCBAs/TCBAs (generally, 3:1 in healthy subjects, (39)) in patients suffering from hepatocellular carcinoma, cholangiocarcinoma and cirrhosis (18). In a recent *in vitro* study (16), we observed an alteration in the ratio of GCBAs/TCBAs in hyperbilirubinemic (>26 μM) cholestatic patients compared to those of normobilirubinemic patients (<=26 μM). This ratio changed from (mean ± SD) 2.88 ± 1.47 in normobilirubinemic to (mean ± SD) 1.47 ± 0.83 in hyperbilirubinemic patients. Hyperbilirubinemic patients showed a considerable decrease in the levels of GCBAs compared to normobilirubinemic patients (mean ± SD, 12.48 ± 6.28 compared to 21.71 ± 12.06), and a slight increase in the levels of TCBAs (mean ± SD, 10.05 ± 6.25 compared to 9.16 ± 7.01).

In the current study, a statistically significant decrease was observed in both GCBAs (determined from the H-25 -CH_2 group resonating at 3.74 ppm) and TCBAs (determined from the H-26 -CH_2 group resonating at 3.08 ppm) in PSC patients compared to the controls. Unlike our *in vitro* study (16), there was no significant difference (P = 0.873) in

the ratio of GCBAs/TCBAs between controls (mean ± SD, 2.48 ± 1.51) and PSC patients (mean ± SD, 2.64 ± 2.62). Although 9/10 PSC patients showed a cholestatic pattern (elevated ALP and/or GGT), just one of them had mild hyperbilirubinemia (37 μM according to the classification in our *in vitro* study (16). Therefore, the PSC patient-cohort in this study had normobilirubinemic cholestatic pattern.

There was a significant difference between controls and PSC patients with respect to a number of biliary metabolites, and we ruled out any confounding effect due to a gender difference. However, since bile composition is under the influence of different environmental factors such as diet, toxins, and medications (10), there was a great variability in the concentration of biliary metabolites in healthy volunteers and patients. Moreover, because of a small sample size, it was difficult to eliminate the possible confounding effect of age. Consequently, the comparisons reported here are under the possible confounding effects of such variables. The wide variations interfere with decision making in the borderline cases that might fit well in either group. Moreover, considering that changes in the same peak areas have been reported by a number of *in vitro* studies for different HPB disorders (16-25), further evaluation using a larger sample size and different HPB disorders is required in order to differentiate various cholestatic and non- cholestatic HPB disorders using MRS technique with more confidence.

The statistically significant negative correlations between biochemical markers of cholestasis (elevated ALP and GGT) and metabolites that changed between PSC patients and control subjects (TBAs + cholesterol, GCBAs or chol-PLs) confirm the value of these metabolites in detection of cholestasis. Considering the contamination of the 0.66 ppm peak (representing TBAs + cholesterol) by body fat (28), the chol-PLs at 3.22 ppm

and GCBAs at 3.74 ppm are more reliable. Moreover, the statistically significant negative correlation between GCBAs + TCBAs (determined from the amide proton region, 7.76 – 8.05 ppm) and ALP suggests importance of amide region in the detection of cholestasis.

1D spectra cannot provide information on overlapping signals. A better resolution is required to detect some of these metabolites which have a major role in the disease processes. Especially, in 1D spectra under current clinical magnetic field strengths (1.5or 3 T) PC appears at 3.22 ppm along with metabolites produced from its hydrolysis and other chol-PLs. In 2D spectra we can detect the glyceryl 2-CH of PC separately. This metabolite may decrease following hydrolysis of PC under pathological conditions (17). Hence, 2D spectroscopy becomes necessary to resolve the overlapping signals. The other advantage of 2D data is the simplicity of reading it in the clinic where decisions can be made based on the presence or absence of certain cross peaks. For example, in the current study, the diagonal peak which represents the amide protons of conjugated bile acids ($\mathbf{F_2}$ = $\mathbf{F_1}$ = 7.81 ppm) could not be differentiated from noise in a majority of PSC patients (detected in only 1/6 PSC patients). Moreover, cross peaks from PC-glyceryl signals ($\mathbf{F_2}$ = 5.24, $\mathbf{F_1}$ = 4.18 ppm) have been detected in the L-COSY spectra of 3 controls and none of the PSC patients. Absence of this signal may indicate a pathologic process because it shows the reduction of PC following hydrolysis by phospholipases regurgitated into the common bile duct or gallbladder due to pancreatobiliary reflux or reaction with the oxygen species during cholestasis (40). However, due to low intensity of PC-glyceryl signals, the detection is still difficult even in controls. Therefore, the future diagnosis of hepatobiliary pathologies based on this metabolite still requires further improvement of the quality of 2D spectra.

4.6 CONCLUSION

This study showed the possibility of differentiating PSC patients from healthy controls based on 1D and 2D spectra obtained from bile *in vivo* using a 3 T scanner. However, future studies should compare the PSC spectra with those acquired from subjects suffering from different HPB pathologies. Some of the changes might be general metabolic changes happening in a wide range of pathologies, while others might be specific to certain pathology. Moreover, the spectra from PSC patients should be compared with those from CC patients. This is specifically important to make decision about allocation of the donated livers to the patients who can best benefit from liver transplantation. In addition, studies with larger sample sizes are required to eliminate the effect of confounding elements especially age. Considering the simplicity in reading 2D spectra based on the presence or the absence of certain diagonal or cross peaks, and with further improvement in the spectral quality and decrease in the duration of scanning time, 2D in particular, has potential to serve as a valuable investigational technique in the clinic.

Acknowledgements

We would like to thank Mr. Mike Smith for modifying MATLAB code for combining the data acquired from different coil elements.

4.7 REFERENCES

1. Vleggaar FP, Van Ooteghem NA, Van Buuren HR, Van Berge Henegouwen GP. Cholestatic liver diseases: slow progress in understanding and treating slowly progressive disorders. *Scand J Gastroenterol Suppl.* 2000; (232): 86-92.
2. Spivey JR, Bronk SF, Gores GJ. Glycochenodeoxycholate-induced lethal hepatocellular injury in rat hepatocytes, role of ATP depletion and cytosolic free calcium. *J. Clin. Invest.* 1993; 92(1): 17-24.
3. Lee YM, Kaplan MM; Practice Guideline Committee of the ACG. American College of Gastroenterology. Management of primary sclerosing cholangitis. *Am. J. Gastroenterol.* 2002; 97(3): 528-534.
4. Bambha K, Kim WR, Talwalkar J, Torgerson H, Benson JT, Therneau TM, Loftus EV Jr, Yawn BP, Dickson ER, Melton LJ 3rd. Incidence, clinical spectrum, and outcomes of primary sclerosing cholangitis in a United States community. *Gastroenterology.* 2003; 125(5): 1364-1369.
5. Friedman LS. Liver, Biliary Tract & Pancreas Disorders. In: *CURRENT Medical Diagnosis & Treatment 2014.* Papadakis MA, McPhee SJ, Rabow MW, Berger TG (Eds), McGraw-Hill (USA): New York, 2013. http://www.accessmedicine.com/content.aspx?aID=7993.
6. Shanbhogue AK, Tirumani SH, Prasad SR, Fasih N, McInnes M. Benign biliary strictures: a current comprehensive clinical and imaging review. *AJR Am J Roentgenol.* 2011; 197(2): W295-306.
7. Rodriguez HJ, Bass NM. Primary sclerosing cholangitis. *Semin Gastrointest Dis.* 2003; 14(4): 189-198.

8. LaRusso NF, Shneider BL, Black D, Gores GJ, James SP, Doo E, Hoofnagle JH. Primary sclerosing cholangitis: summary of a workshop. *Hepatology.* 2006; 44(3): 746-764.
9. Fulcher AS, Turner MA, Franklin KJ, Shiffman ML, Sterling RK, Luketic VA, Sanyal AJ. Primary sclerosing cholangitis: evaluation with MR cholangiography—a case-control study. *Radiology.* 2000; 215: 71–80
10. Khan SA, Cox IJ, Hamilton G, Thomas HC, Taylor-Robinson SD. *In vivo* and *in vitro* nuclear magnetic resonance spectroscopy as a tool for investigating hepatobiliary disease: a review of H and P MRS applications. *Liver Int.* 2005; 25(2): 273-281.
11. Smith ICP, Baert R. Medical diagnosis by high resolution NMR of human specimens. IUBMB Life. 2003; 55(4-5): 273-277.
12. Mountford C, Smith ICP, Bourne R. Correlation of Histopathology with Magnetic Resonance Spectroscopy of Human Biopsies. In: *Modern Magnetic Resonance*. Vol. II, Webb GA (Ed), Springer (U.K.): London, 2006; p 1027-1036.
13. Bell JD, Cox IJ, Sargentoni J, Peden CJ, Menon DK, Foster CS, Watanapa P, Iles RA, Urenjak J. A ^{31}P and ^{1}H-NMR investigation *in vitro* of normal and abnormal human liver. *Biochim Biophys Acta.* 1993; 1225(1): 71-77.
14. Soper R, Himmelreich U, Painter D, Somorjai RL, Lean CL, Dolenko B, Mountford CE, Russell P. Pathology of hepatocellular carcinoma and its precursors using proton magnetic resonance spectroscopy and a statistical classification strategy. *Pathology.* 2002; 34(5): 417-422.

15. Cox IJ, Menon DK, Sargentoni J, Bryant DJ, Collins AG, Coutts GA, Iles RA, Bell JD, Benjamin IS, Gilbey S, et al. Phosphorus-31 magnetic resonance spectroscopy of the human liver using chemical shift imaging techniques. *J Hepatol.* 1992; 14(2-3): 265-275.
16. Bezabeh T, Ijare OB, Albiin N, Bergquist A, Arnelo U, Löhr M, Hov JR, Smith ICP. Alteration in the Conjugation Pattern of Bile acids in Human Bile during Cholestasis: A ^{1}H MRS Study. *Proc. Intl. Soc. Mag. Reson. Med*. 2010; 18: 4590.
17. Ijare OB, Bezabeh T, Albiin N, Arnelo U, Bergquist A, Lindberg B, Smith ICP. Absence of glycochenodeoxycholic acid (GCDCA) in human bile is an indication of cholestasis: a ^{1}H MRS study. *NMR Biomed.* 2009; 22(5): 471-479.
18. Nagana Gowda GA, Shanaiah N, Cooper A, Maluccio M, Raftery D. Visualization of bile homeostasis using ^{1}H-NMR spectroscopy as a route for assessing liver cancer. *Lipids*. 2009; 44(1): 27-35.
19. Albiin N, Smith ICP, Arnelo U, Lindberg B, Bergquist A, Dolenko B, Bryksina N, Bezabeh T. Detection of cholangiocarcinoma with magnetic resonance spectroscopy of bile in patients with and without primary sclerosing cholangitis. *Acta Radiol.* 2008; 49(8): 855-862.
20. Hashim Abdalla MS, Taylor-Robinson SD, Sharif AW, Williams HR, Crossey MM, Badra GA, Thillainayagam AV, Bansi DS, Thomas HC, Waked IA, Khan SA. Differences in phosphatidylcholine and bile acids in bile from Egyptian and UK patients with and without cholangiocarcinoma. *HPB (Oxford).* 2011; 13(6): 385-390.
21. Sharif AW, Williams HRT, Lampejo T, Khan SA , Bansi DS, Westaby D, Thillainayagam AV, Thomas HC, Cox IJ, Taylor-Robinson SD. Metabolic profiling

of bile in cholangiocarcinoma using *in vitro* magnetic resonance spectroscopy. *HPB (Oxford)* .2010; 12(6): 396-402.

22. Bezabeh T, Ijare OB, Albiin N, Arnelo U, Lindberg B, Smith ICP. Detection and quantification of D-glucuronic acid in human bile using ^{1}H NMR spectroscopy: relevance to the diagnosis of pancreatic cancer. *MAGMA.* 2009; 22(5): 267-275.
23. Gowda GA. NMR spectroscopy for discovery and quantitation of biomarkers of disease in human bile. *Bioanalysis.* 2011; 3(16): 1877-1890.
24. Gowda GA. Human bile as a rich source of biomarkers for hepatopancreatobiliary cancers. *Biomark Med.* 2010; 4(2): 299-314.
25. Nishijima T, Nishina M, Fujiwara K. Measurement of lactate levels in serum and bile using proton nuclear magnetic resonance in patients with hepatobiliary diseases: its utility in detection of malignancies. *Jpn J Clin Oncol.* 1997; 27(1): 13-17.
26. Prescot AP**,** Collins DJ, Leach MO, Dzik-Jurasz AS. Human gallbladder bile: noninvasive investigation *in vivo* with single-voxel ^{1}H MR spectroscopy. *Radiology* 2003; 229(2): 587-592.
27. Künnecke B, Bruns A, von Kienlin M. Non-invasive analysis of gallbladder bile composition in cynomolgus monkeys using *in vivo* ^{1}H magnetic resonance spectroscopy. *Biochim. Biophys. Acta.* 2007; 1771(4): 544-549.
28. Mohajeri S, Bezabeh T, King SB, Ijare OB, Thomas MA, Minuk G, Lipschitz J, Kirkpatrick I, and Smith ICP. In vivo ^{1}H MRS of human Gallbladder Bile using an Optimized 16-Channel Phased Array at 3T. *Proc. Intl. Soc. Mag. Reson. Med*. 2011; 19: 870.

29. Thomas MA, Yue K, Binesh N, Davanzo P, Kumar A, Siegel B, Frye M, Curran J, Lufkin R, Martin P, Guze B. Localized two-dimensional shift-correlated MR spectroscopy of human brain. *Magn Reson Med.* 2001; 46(1): 58-67.

30. Thomas MA, Hattori N, Umeda M, Sawada T, Naruse S. Evaluation of two-dimensional L-COSY and JPRESS using a 3 T MRI scanner: from phantoms to human brain *in vivo*. *NMR Biomed.* 2003; 16(5): 245-251.

31. Klose U. *In vivo* proton spectroscopy in presence of eddy currents. *Magn Reson Med.* 1990; 14(1): 26-30.

32. Roemer PB, Edelstein WA, Hayes CE, Souza SP, Mueller OM. The NMR phased array. *Magn Reson Med.* 1990; 16(2): 192-225.

33. Ijare OB, Bezabeh T, Albiin N, Bergquist A, Arnelo U, Lindberg B, Smith ICP. Simultaneous quantification of glycine- and taurine-conjugated bile acids, total bile acids, and choline-containing phospholipids in human bile using ^{1}H NMR spectroscopy. *J Pharm Biomed Anal.* 2010; 53(3): 667-673.

34. Gowda GA, Ijare OB, Somashekar BS, Sharma A, Kapoor VK, Khetrapal CL. Single step analysis of individual conjugated bile acids in human bile using ^{1} H NMR spectroscopy. *Lipids*. 2006; 41(6): 591-603.

35. Fayad LM, Salibi N, Wang X, Machado AJ, Jacobs MA, Bluemke DA, Barker PB. Quantification of muscle choline concentrations by proton MR spectroscopy at 3 T: technical feasibility. *AJR Am J Roentgenol.* 2010; 194(1): W73-79.

36. van Erpecum KJ. Biliary lipids, water and cholesterol gallstones. *Biol Cell.* 2005; 97(11): 815-822.

37. Ijare OB, Somashekar BS, Nagana Gowda GA, Sharma A, Kapoor VK, Khetrapal CL: Quantification of glycine and taurine conjugated bile acids in human bile using ^{1}H NMR spectroscopy. *Magn. Reson. Med.* 2005; **53**(6): 1441-1446.
38. Yao X, Zeng M, Wang H, Fei S, Rao S, Ji Y. Metabolite detection of pancreatic carcinoma by in vivo proton MR spectroscopy at 3T: initial results. *Radiol Med.* 2012; 117(5): 780-788.
39. Bove KE, Heubi JE, Balistreri WF, Setchell KD. Bile acid synthetic defects and liver disease: a comprehensive review. *Pediatr. Dev. Pathol.* 2004; 7(4): 315-334.
40. Bezabeh T, Ijare OB, Mohajeri S, Lipschitz J, Smith,ICP. Magnetic resonance spectroscopy of bile in the diagnosis of chronic cholestatic diseases. In: *Advances in Medicine and Biology.* Vol. 45, Berhardt, Leon V (Ed). Hauppauge, N.Y., Nova Science Publishers (USA), 2012; p 95 – 112.

CHAPTER 5. CONCLUSION

5.1 SUMMARY

The hepatopancreatobiliary (HPB) system has a critical role in digestion, control of glucose level, and metabolic detoxification. The pathologies associated with the HPB can be life threatening. Most of the time, these are not detected until the diseases are advanced. For years, the diagnosis of HPB disorders was based on the medical history, physical examination, and blood biochemistry, and in some cases imaging. Unfortunately, most of the clinical and laboratory findings are non-specific, making it difficult to reach a definite diagnosis in a reasonably short time. Therefore, there is ongoing effort toward earlier diagnosis of HPB disorders using approaches such as cellular techniques (DIA, and FISH) and imaging methods (1).

PSC is a particularly challenging cholestatic HPB disorder. It has a long course and life threating complications, including cholangiocarcinoma. Treatment is controversial, and the only cure is orthotopic liver transplantation (OLT) which is contraindicated in the presence of CC (1). As a result, on-time diagnosis of PSC is critical in saving lives and differentiating the cases with and without CC, to help in the allocation of donated livers to those who can best benefit from transplantation. In this regard, MRS is an emerging diagnostic field that can follow the metabolic footprint of different pathologies. *In vitro* MRS of bile has demonstrated the potential of this evolving technique in the early diagnosis of HPB disorders (2-11). In particular, the simultaneous quantification of major bile metabolites from our lab by Ijare et al. (12) verified the capacity of this technique in the differentiation of HPB disorders. However, the *in vitro* analysis requires collection of bile invasively by ERCP or during surgery. Therefore, non-invasive application of MRS,

in combination with MR imaging, is considered a suitable alternative. Following the initial attempts by Prescot et al. (13) and Künnecke et al. (14) to acquire spectra from bile inside the gallbladder, we tried to overcome some of the difficulties they encountered. We improved the quality of spectra, compared to Prescot et al., by using higher magnetic field (3 T compared to 1.5 T), applying respiratory-gated sequence and aligning every single scan during data processing to decrease chemical shift drift, decreasing TE from 60 ms to 30 msec in order to reduce T_2 signal loss, and by applying spatial saturation bands around the gallbladder to reduce lipid contamination. Unlike Künnecke et al., our study was performed under clinical conditions (3T scanner and use of a receive array coil instead of a transmit/receive coil which has safety challenges). Finally, we acquired a 1D spectrum with enough resolution to detect and quantify the major bile metabolites (other than choline-containing phospholipids (chol-PLs) which were already quantified by Prescot et al. (13)). We calculated the molar concentrations of total bile acids (TBAs) + cholesterol presented by the methyl (-CH_3) group at 0.66 ppm, taurine-conjugated bile acids (TCBAs) presented by the H-26 -CH_2- group at 3.08 ppm, glycine-conjugated bile acids (GCBAs) presented by the H-25 -CH_2-group at 3.74 ppm, and amide groups of both GCBAs and TCBAs resonating in the region 7.76-8.05 ppm as well as chol-PLs presented by the trimethylammonium [$–N^+(CH_3)_3$] group at 3.22 ppm. Moreover, in order to differentiate overlapping signals in the 1D spectrum, we obtained 2D L-COSY spectrum from gallbladder bile *in vivo*, for the first time, based on the method described by Thomas et al. (15, 16).

2D L-COSY spectra were helpful in detecting amide proton [-NH] signals [diagonal peak ($\mathbf{F_2}$ = $\mathbf{F_1}$ = 7.81 ppm) and cross peak ($\mathbf{F_2}$ = 7.81, $\mathbf{F_1}$ = 3.62 ppm)], in samples with either

very low levels of conjugated bile acids (GCBAs and/or TCBAs) or low signal intensity due to chemical exchange with water (high pH). We also detected the glyceryl 2-CH signals of phosphatidylcholine (PC) (cross peak, $\mathbf{F_2}$ = 5.24, $\mathbf{F_1}$ = 4.18 ppm) which will be valuable in distinguishing PC from its hydrolysis products and other chol-PLs.

In the second phase of this project, the corrected molar concentrations of the above bile metabolites were compared between healthy volunteers and PSC patients. The corrected molar concentrations of all the above metabolites were significantly lower in PSC patients compared to controls ($P<0.05$). There were no statistically significant differences in the concentration of the above metabolites between males and females. Due to the small sample size, it was impossible to evaluate the confounding effect of age. All PSC patients except one showed a cholestatic pattern in their blood biochemistry (elevated ALP and /or GGT). Correlation analysis of the levels of ALP and GGT and the levels of each mentioned metabolite found statistically significant negative correlations between ALP and TBAs + cholesterol, GCBAs, PC, and amide groups of GCBAs + TCBAs, and between GGT and TBAs + cholesterol, GCBAs, and PC ($P<0.05$). Therefore, it seems ALP is correlated with more biliary metabolites. This finding is in agreement with the fact that the ALP is located in the canalicular membrane of hepatocytes, and its increase is more important in the diagnosis of cholestasis compared to GGT which is found in the endoplasmic reticulum of bile duct epithelial cells (17).

From our experience in *in vitro* studies, under pathologic conditions, the PC with protective effect on biliary epithelia was found to be hydrolyzed to GPC and lyso-PC. 1D spectra cannot distinguish PC, GPC, and lyso-PC based on their trimethylammonium [$-N^+(CH_3)_3$] group resonating around 3.22 ppm (18). 2D COSY spectra that have potential

to distinguish PC from other choline-PLs based on the PC-glyceryl 2-CH signals (19,20). Therefore, the absence of a cross peak ($\mathbf{F_2}$ = 5.24, $\mathbf{F_1}$ = 4.18 ppm) will be helpful in detecting pathologic conditions of the HPB system, including PSC. However, in order to make use of this finding a 2D spectrum with high SNR should be obtained. Our results showed the value of the 2D spectrum in confirming the presence of PSC based on loss of the diagonal peak ($\mathbf{F_2}$ = $\mathbf{F_1}$ = 7.81 ppm) and a cross peak ($\mathbf{F_2}$ = 7.81, $\mathbf{F_1}$ = 3.62 ppm) which represent the amide groups of conjugated bile acids. In addition, the absence of symmetric cross peaks at ($\mathbf{F_2}$= 4.3, $\mathbf{F_1}$ = 3.6 ppm) and ($\mathbf{F_2}$= 3.6, $\mathbf{F_1}$ = 4.3 ppm) due to J-coupling between the (-N-CH_2-) and the (-CH_2-O-) of chol-PLs and loss of the cross peak at ($\mathbf{F_2}$ = 3.5, $\mathbf{F_1}$ = 3.07 ppm) due to coupling between H-25 and H-26 -CH_2- protons of TCBAs indicate reduced levels of chol-PLS and TCBAs in bile respectively. These findings suggest the value of 2D COSY ^{1}H MRS in detecting the presence of pathological conditions in HPB system including PSC.

5.2 ANALYTICAL METHODS

We used the conventional peak-area analysis method to calculate the molar concentrations of metabolites (21). Then we compared these concentrations between healthy controls and patients by Student's t-tests and a non-parametric Mann-Whitney U test. With larger sample sizes a more robust, objective assessment would give even more reliable classification. MR-spectral data are rich in information with potential diagnostic and prognostic value. In order to use this information completely, the statistical classification strategy (SCS) developed in our lab (22) could be used. These methods have been successfully applied in the classification of MR spectra of various tissue specimens (23-25).

5.3 FUTURE PROSPECTIVE AND CLINICAL APPLICATIONS

In the current study, we were be able to differentiate PSC patients from healthy volunteers based on the corrected molar concentrations of major bile metabolites including chol-PLS, TCBAs, GCBAs, TBAs + cholesterol *in vivo*. In the next step, we need to compare the bile spectra acquired from PSC patients with those recorded from other cholestatic and non-cholestatic hepatobiliary patients as well as pancreatic patients. Especially, it is important to compare PSC patients with cholangiocarcinoma cases in order to show the ability of current technique in detecting the malignancy in PSC patients. This could be helpful in allocating the donated livers to the patients who can benefit from transplantation.

As noticed in my results, the bile composition is quite variable. As a result, the application of current methodology, in the clinical settings in the future might be challenging. In some cases, the level of biliary metabolites can well fit in normal and pathologic categories. Therefore, the source of variability should be determined. One of the possible explanations is the influence of different subjective and environmental factors such as age, sex, diet, medications, and environmental toxins, on the bile composition. Therefore, we need to eliminate the confounding factors as much as possible. In this regard, in a larger sample size, age and gender matching should be considered. Moreover, the subjects should be on similar diet, in order to eliminate the effect of diet on bile composition.

In the next step, the sensitivity, specificity and finally accuracy of ^{1}H MRS methodology should be determined using larger groups of patients and controls and compared with the current gold standard procedure, ERCP.

In the current study, 2D *in vivo* bile spectra showed potential in easy and rapid differentiation of PSC patients from healthy subjects, which is desirable in the clinical settings. Improving the SNR and decreasing the scanning time can help the transfer of this technique to the clinical settings.

5.4 REFERENCES

1. Shanbhogue AK, Tirumani SH, Prasad SR, Fasih N, McInnes M. Benign biliary strictures: a current comprehensive clinical and imaging review. *AJR Am J Roentgenol.* 2011; 197(2): W295-306.
2. Bezabeh T, Ijare OB, Albiin N, Bergquist A, Arnelo U, Löhr M, Hov JR, Smith ICP. Alteration in the Conjugation Pattern of Bile acids in Human Bile during Cholestasis: A ^{1}H MRS Study. *Proc. Intl. Soc. Mag. Reson. Med*. 2010; 18: 4590.
3. Ijare OB, Bezabeh T, Albiin N, Arnelo U, Bergquist A, Lindberg B, Smith ICP. Absence of glycochenodeoxycholic acid (GCDCA) in human bile is an indication of cholestasis: a ^{1}H MRS study. *NMR Biomed.* 2009; 22(5): 471-479.
4. Nagana Gowda GA, Shanaiah N, Cooper A, Maluccio M, Raftery D: Visualization of bile homeostasis using ^{1}H-NMR spectroscopy as a route for assessing liver cancer. *Lipids.* 2009; 44(1): 27-35.
5. Albiin N, Smith ICP, Arnelo U, Lindberg B, Bergquist A, Dolenko B, Bryksina N, Bezabeh T. Detection of cholangiocarcinoma with magnetic resonance spectroscopy of bile in patients with and without primary sclerosing cholangitis. *Acta Radiol.* 2008; 49(8): 855-862.
6. Hashim Abdalla MS, Taylor-Robinson SD, Sharif AW, Williams HR, Crossey MM, Badra GA, Thillainayagam AV, Bansi DS, Thomas HC, Waked IA, Khan SA.

Differences in phosphatidylcholine and bile acids in bile from Egyptian and UK patients with and without cholangiocarcinoma. *HPB (Oxford).* 2011; 13(6): 385-390.

7. Sharif AW, Williams HRT, Lampejo T, Khan SA , Bansi DS, Westaby D, Thillainayagam AV, Thomas HC, Cox IJ, Taylor-Robinson SD. Metabolic profiling of bile in cholangiocarcinoma using *in vitro* magnetic resonance spectroscopy. *HPB (Oxford).* 2010; 12(6): 396-402.
8. Bezabeh T, Ijare OB, Albiin N, Arnelo U, Lindberg B, Smith ICP. Detection and quantification of D-glucuronic acid in human bile using ^{1}H NMR spectroscopy: relevance to the diagnosis of pancreatic cancer. *MAGMA.* 2009; 22(5): 267-275.
9. Gowda GA. NMR spectroscopy for discovery and quantitation of biomarkers of disease in human bile. *Bioanalysis.* 2011; 3(16): 1877-1890.
10. Gowda GA. Human bile as a rich source of biomarkers for hepatopancreatobiliary cancers. *Biomark Med.* 2010; 4(2): 299-314.
11. Nishijima T, Nishina M, Fujiwara K. Measurement of lactate levels in serum and bile using proton nuclear magnetic resonance in patients with hepatobiliary diseases: its utility in detection of malignancies. *Jpn J Clin Oncol.* 1997; 27(1): 13-17.
12. Ijare OB, Bezabeh T, Albiin N, Bergquist A, Arnelo U, Lindberg B, Smith ICP. Simultaneous quantification of glycine- and taurine-conjugated bile acids, total bile acids, and choline-containing phospholipids in human bile using ^{1}H NMR spectroscopy. *J Pharm Biomed Anal.* 2010; 53(3): 667-673.
13. Prescot AP**,** Collins DJ, Leach MO, Dzik-Jurasz AS. Human gallbladder bile: noninvasive investigation *in vivo* with single-voxel ^{1}H MR Spectroscopy. *Radiology* 2003; 229(2): 587-592.

14. Künnecke B, Bruns A, von Kienlin M. Non-invasive analysis of gallbladder bile composition in cynomolgus monkeys using *in vivo* ^{1}H magnetic resonance spectroscopy. *Biochim. Biophys. Acta.* 2007; 1771(4): 544-549.
15. Thomas MA, Yue K, Binesh N, Davanzo P, Kumar A, Siegel B, Frye M, Curran J, Lufkin R, Martin P, Guze B. Localized two-dimensional shift-correlated MR spectroscopy of human brain. *Magn Reson Med.* 2001; 46(1): 58-67.
16. Thomas MA, Hattori N, Umeda M, Sawada T, Naruse S. Evaluation of two-dimensional L-COSY and JPRESS using a 3 T MRI scanner: from phantoms to human brain *in vivo*. *NMR Biomed.* 2003; 16(5): 245-251.
17. Longo DL, Fauci AS, Kasper DL, Hauser SL, Jameson JL, Loscalzo J (Eds). Harrison's Principles of Internal Medicine, (Harrison's online) Ed 18, McGraw-Hill (USA): New York, 2012. http://www.accessmedicine.com.proxy2.lib.umanitoba.ca/resourceTOC.aspx?resourceID=4
18. Bezabeh T, Ijare OB, Mohajeri S, Lipschitz J, Smith,ICP. Magnetic resonance spectroscopy of bile in the diagnosis of chronic cholestatic diseases. In: *Advances in Medicine and Biology.* Vol. 45, Berhardt, Leon V (Ed). Hauppauge, N.Y., Nova Science Publishers (USA), 2012; p 95 – 112.
19. Ijare OB, Bezabeh T, Albiin N, Arnelo U, Bergquist A, Lindberg B, Smith ICP. Absence of glycochenodeoxycholic acid (GCDCA) in human bile is an indication of cholestasis: a ^{1}H MRS study. *NMR Biomed.* 2009; 22(5): 471-479.

20. Ijare OB, Somashekar BS, Gowda GA, Sharma A, Kapoor VK, Khetrapal CL. Quantification of glycine and taurine conjugated bile acids in human bile using ^{1}H NMR spectroscopy. *Magn. Reson. Med.* 2005; 53(6): 1441-1446.
21. Cox IJ, Menon DK, Sargentoni J, Bryant DJ, Collins AG, Coutts GA, Iles RA, Bell JD, Benjamin IS, Gilbey S, et al. Phosphorus-31 magnetic resonance spectroscopy of the human liver using chemical shift imaging techniques. *J Hepatol. 1*992; 14(2-3): 265-275.
22. Lean CL, Somorjai RL, Smith ICP, Russell P, Mountford CE. Accurate diagnosis and prognosis of human cancers by proton MRS and a three stage classification strategy. *Ann Rep NMR Spectrosc* 2002; 48: 71-111.
23. Somorjai RL, Dolenko B, Nikulin AK, Pizzi N, Scarth G, Zhilkin P, Halliday W, Fewer D, Hill N, Ross I, West M, Smith IC, Donnelly SM, Kuesel AC, Briere KM. Classification of ^{1}H MR Spectra of human brain neoplasms: the influence of preprocessing and computerized consensus diagnosis on classification accuracy. *J Magn Reson Imaging.* 1996; 6(3): 437-444.
24. Somorjai RL, Nikulin AE, Pizzi N, Jackson D, Scarth G, Dolenko B, Gordon H, Russell P, Lean CL, Delbridge L, et al. Computerized consensus diagnosis: a classification strategy for the robust analysis of MR spectra. I. Application to ^{1}H spectra of thyroid neoplasms. *Magn Reson Med.* 1995; 33(2): 257-263.
25. Nikulin AE, Dolenko B, Bezabeh T, Somorjai RL. Near-optimal region selection for feature space reduction: novel preprocessing methods for classifying MR spectra. *NMR Biomed.* 1998; 11(4-5): 209-216.